PULSE NARROWING IN OPTICAL FIBERS WITH POLARIZATION MODE DISPERSION

by

Mauricio Yañez

Ing. Elec. Universidad de Guanajuato, 1997

A THESIS SUBMITTED IN PARTIAL FULFILMENT OF
THE REQUIREMENTS FOR THE DEGREE OF

Master of Science in Engineering

in the Department of Electrical and Computer Engineering

Supervisors: Dr. Brent R. Petersen, BEng, MASc, PhD, ECE Asst Prof
Dr. Liang Chen, BSc, MA, PhD, PHYS Asst Prof
Dr. Xiaoyi Bao, BSc, MSc, PhD, PHYS Assoc Prof

Examining Board: Dr. Eugene Lewis, BScE, PhD, PEng, ECE Prof and Chair
Dr. Philip A. Parker, BScE, MSc, PhD, PEng, ECE Prof
Dr. Bernd J. Kurz, Dipl Ing, MScE, PhD, CS Prof and Dean of Sch of Graduate Studies

This thesis is accepted.

Dean of Graduate Studies

THE UNIVERSITY OF NEW BRUNSWICK

May, 2000

This thesis is dedicated to all
the people who always trusted me.

Esta tesis está especialmente
dedicada a mis padres,...

ABSTRACT

A mathematical procedure aimed to compensate Polarization Mode Dispersion by reducing the root mean square pulsewidth of a signal through the optimization of the launching and receiving states of polarization has recently been proposed. It is the objective of this thesis to explore the nature of such compensation method. Analytically exact solutions are presented for the case in which the optical fiber consists of one, two and three segments of Highly-Birefringent (Hi-Bi) fiber. Numerical generated results are presented for a fiber consisting of an arbitrary number of segments of Hi-Bi fiber.

The solution of the mathematical procedure shows, in all cases, the existence of two sets of orthogonal input and output states of polarization which allow an output pulse to be narrower than the input pulse. The cost for obtaining a narrower pulse at the output of the fiber is a power loss.

ACKNOWLEDGEMENTS

The author wishes to thank the following people for their guidance, teachings, expertise and boundless patience during the development of this thesis:
Dr. Liang Chen, Dr. Brent R. Petersen and Dr. Xiaoyi Bao

Last but not least, I would like to thank the Canadian tax-payer for providing funding through the Natural Sciences and Engineering Research Council of Canada (NSERC) and The University of New Brunswick.

TABLE OF CONTENTS

LIST OF TABLES

LIST OF FIGURES

LIST OF SYMBOLS

a	Real number
A_x	Magnitude of the horizontally polarized component
A_y	Magnitude of the vertically polarized component
c	Speed of light in the vacuum ($3X10^8$)
c_{+}	Projection of ϕ onto ε_{a+}
c_{-}	Projection of ϕ onto ε_{a-}
$c(\chi)$	Primal function dependent on χ
$c(\phi)$	Primal function dependent on ϕ
e	Base of the natural exponential function (2.71828182845905...)
E	Electric field
E	Vector field
E_{in}	Input electric field
$\mathbf{E_{in}}$	Input vector field
$\mathbf{E_{out}}$	Output vector field
E_{out}	Output electric field
E_x	Output electric field after projection of $\mathbf{E_{out}}$ onto χ
F_1 to F_3	Real valued functions of Γ
FOM_{+}	Figure of merit for the optimization of the output state of polarization
FOM_{-}	Figure of merit for the optimization of the input state of polarization
FOM_{-+}	Figure of merit for the optimization of the input and output states of polarization
$h(\chi)$	Objective function for the constrained minimization dependent on χ
$h(\phi)$	Objective function for the constrained minimization dependent on ϕ
$h_L(t)$	Complex lowpass time impulse response of the fiber
$\mathbf{H_L}(\omega)$	Complex lowpass frequency response of the fiber
i	Integer number
j	Imaginary number equal to $\sqrt{(-1)}$
k,l,m,n	Real numbers
k_o	Free space wave number
L_B	Beat Length
$\mathbf{M_1}(\phi,\chi)$	Complex 2 by 2 matrix used in the optimization of χ
$\mathbf{M_2}(\phi,\chi)$	Complex 2 by 2 matrix used in the optimization of ϕ
$M_i(\omega)$	Jones transfer matrix of the i-th waveplate
n	Mode index
N	Number of waveplates used during simulation
$\mathbf{P_{+}}$	Power matrix as a function of the output state of polarization
$\mathbf{P_{-}}$	Power matrix as a function of the input state of polarization
P_x	Power of the signal after projection of E_{out} onto χ
R	Ninety degrees rotation matrix

$\mathbf{S}$	Stokes vector
s_0 to s_3	Elements of the stokes vector
$\mathbf{S}_{out}$	Second moment matrix as a function of the output state of polarization
$\mathbf{S}_{in}$	Second moment matrix as a function of the input state of polarization
t	Time
T	Bit period in picoseconds
$\mathbf{T}(\omega)$	Jones transfer matrix
$\mathbf{T}_{out}$	First moment matrix as a function of the output state of polarization
$\mathbf{T}_{in}$	First moment matrix as a function of the input state of polarization
$\mathbf{T_L}(\omega)$	Lowpass complex equivalent of $\mathbf{T}(\omega)$
$\mathbf{T_{PC}}$	Jones transfer matrix of a polarization controller
$\mathbf{U}(\omega)$	Jones transfer matrix
u_1,u_2	Complex numbers, elements of a Jones transfer matrix
w_1 to w_8	Complex numbers
$\mathbf{w_{1234}}$	Complex 1 by 4 vector
$\mathbf{w_{1256}}$	Complex 1 by 4 vector
$\mathbf{w_{3478}}$	Complex 1 by 4 vector
$\mathbf{w_{5678}}$	Complex 1 by 4 vector
x	Real number
$\mathbf{x}$	Jones vector of horizontal polarization
$\mathbf{y}$	Jones vector of vertical polarization
z	Transmission distance
α	Angular value in radians
α_1,α_2	Angular value in radians
β	Complex number
χ	Output state of polarization
χ_{new}	Output state of polarization in the current iteration
χ_o	Initial value of the output state of polarization
χ_{old}	Output state of polarization in the previous iteration
χ_{opt}	Optimum output state of polarization
χ_{wc}	Worst case output state of polarization
Δ	Real number
Δ_{neff}	Effective mode index
$\Delta\tau$	Differential group delay
$\Delta\tau_i$	Differential group delay introduced by the i-th waveplate
$\Delta\tau_{rms}$	Root mean square of $\Delta\tau$
$\delta\omega$	Frequency translation defined as $\omega - \omega_1$
$\Delta\omega$	Frequency translation defined as $\omega + \omega_1$
ε	Jones vector
ε_1,ε_2	Mutually orthogonal states of polarization
$\varepsilon_{a\pm}$	Input principal states of polarization
$\varepsilon_{b\pm}$	Output principal states of polarization

ε_{in}	Input state of polarization (randomly chosen for all frequencies)
ε_{out}	Output state of polarization (randomly chosen for all frequencies)
$\varepsilon_{out}(\omega)$	Output state of polarization for a given frequency, ω
ε_x	Arbitrary state of polarization
ε_y	Arbitrary state of polarization
γ	Relative phase between horizontally and vertically polarized components
Γ	Real number
γ_1, γ_2	Angular value in radians
γ_x	Absolute phase of the horizontally polarized component
γ_y	Absolute phase of the vertically polarized component
η	Lagrange multiplier used during the optimization of χ
ϕ	Input state of polarization
ϕ_{new}	Input state of polarization in the current iteration
ϕ_o	Initial value of the input state of polarization
ϕ_{old}	Input state of polarization in the previous iteration
ϕ_{opt}	Optimum input state of polarization
ϕ_{wc}	Worst case input state of polarization
λ	Wavelength
λ_c	Carrier wavelength
π	Pi, the ratio of the circumference of a circle to its diameter (3.14159265...)
θ_i	Rotation angle for the i-th waveplate or fusion angle of the i-th segment of Hi-Bi fiber
θ_{out}	Output phase
$\theta_{out,n}$	The n-th derivative of the output phase evaluated at $\omega = \omega_c$
ρ	Fiber loss
σ_{eff}	Effective rms-pulsewidth
σ_x	Root mean square pulsewidth after projection of the output signal onto χ
τ	Root mean square pulsewidth of the Gaussian-shaped input pulse
τ_+	Transmission time in the slow eigenmode
τ_-	Transmission time in the fast eigenmode
τ_i'	Differential group delay introduced by the i-th segment of Hi-Bi fiber (three segment model)
ω	Angular frequency in radians per second
ω_c	Angular carrier frequency in radians per second
ξ	Jones vector
$\Psi(\omega)$	Propagation constant
ζ	Lagrange multiplier used during the optimization of ϕ
$\mathfrak{F}$	Fourier transform
$\mathfrak{F}^{-1}$	Inverse Fourier Transform

LIST OF ABBREVIATIONS AND ACRONYMS

DGD	Differential group delay
FOM	Figure of merit
Gbps	Gigabit per second
GHz	Giga hertz
Hi-Bi	Highly birefringent
Hz	Hertz
IM/DD	Intensity modulation / Direct detection
ns	Nanoseconds
PA	Polarization analyzer
PBS	Polarization beam splitter
PC	Polarization controller
PC1	Polarization controller 1
PC2	Polarization controller 2
PDF	Probability distribution function
PDL	Polarization dependent loss
PMD	Polarization mode dispersion
ps	Picoseconds
PSP	Principal estate of polarization
PSPs	Principal estates of polarization
rad	Radians
rms	Root mean square
SM	Single mode
SOP	State of polarization
WDM	Wavelength division multiplexing
μm	Micrometers

1 INTRODUCTION

1.1 MOTIVATION

In recent years, the exponential rise in the demand for high speed optical communication systems [1] has led to the introduction of multigigabit per second communications equipment into the market [2]. The increase in the transmission rate and the possibility of using optical amplification [3] to extend the communications link over even longer distances have created new technical challenges. The bandwidth of the communication system is limited by optical and electrical components and also by the properties of the optical fiber itself.

A major limiting factor, known as Polarization Mode Dispersion (PMD), constitutes the ultimate impairment for the transmission of high speed optical signals over the already embedded optical fiber network [4].

Digital signals propagating through an optical fiber with PMD may be broadened during transmission and as a consequence spread beyond their allocated bit slot and interfere with neighbouring bits. The distortion introduced by PMD becomes relevant for systems operating at data rates of 4.8 Gbit/s or higher [5] in the absence of chromatic dispersion [3].

In this thesis we examine the dependence of the frequency response of an optical fiber with PMD on the input and output states of polarization of a signal transmitted through it. The goal of our calculations will be to prove the hitherto unnoticed fact that it is possible to achieve maximum pulsewidth compression of a signal transmitted over an optical fiber with PMD when its input and output states of polarization are adequately chosen.

1.2 THESIS CONTRIBUTIONS

This thesis solves for the first time, analytically and numerically, a mathematical formulation proposed by Chen et. al. [7] which allows the rms[1]-pulsewidth of a signal to be minimized at the output of the fiber when PMD is the only impairment.

The solution of the mathematical analysis postulated by Chen et. al. [7] shows the existence of two sets of input and output states of polarization which minimize the rms-pulsewidth of the received signal. These states of polarization depend on the shape of the transmitted signal. In general they are different from other commonly adopted [6] sets of input and output states of polarization which are used to minimize PMD induced distortion.

Here, we introduce the idea of leveraging the dependence of the frequency response of an optical fiber with PMD on the input and output states of polarization of the signal in order to minimize its rms-pulsewidth at the output. This allows us to perform the equivalent of equalization in the optical domain by only adjusting the state of polarization of the signal.

1.3 THESIS OVERVIEW

Chapter 2 gives an introduction to the concept of polarization mode dispersion. The necessary tools to represent an arbitrary state of polarization using Jones calculus and the Poincaré sphere are presented. At the end, the statistical nature of PMD is described.

Chapter 3 presents in detail the mathematical formulations introduced by Chen et al. [7] and the fundamental eigenvalue equations required to minimize the rms-pulsewidth of a signal at the output of an optical fiber with PMD. Algorithms which can recursively

---

[1] root mean square.

solve those eigenvalue equations are illustrated at the end.

Chapter 4 briefly describes the analytical model of an optical fiber with PMD. Through simulation, the probability distribution function of the envelope of its complex lowpass time impulse response [8] is shown to be Rayleigh.

Chapter 5 outlines the mathematical analysis followed in order to obtain the exact solutions to the eigenvalue equations introduced in chapter three when a Gaussian-shaped pulse is used as the input signal. The solution of the eigenvalue equations is obtained through exhaustive computer simulation using analytic formulas for the case in which the optical fiber consists of 1, 2 and 3 segments of highly-birefringent fiber. Finally, the more generic case of an optical fiber made up by a large number (500) of sections of highly-birefringent fiber is considered. The solution to the eigenvalue equations for such a fiber is numerically calculated and presented.

Chapter 6 studies the special case in which only the input or output state of polarization is allowed to vary in order to minimize the rms-pulsewidth of the output signal. The final performance of varying both, input and output states of polarization, is compared through computer simulation with the case in which only one of them is varied.

Chapter 7 gives a summary of the thesis work and indicates future lines of research.

The appendices contain the proof of mathematical expressions used throughout the thesis as well as the analytic formulas used in chapter 5. The simulation of a five channel wavelength division multiplexing (WDM) system is presented and the Matlab code needed to numerically solve the pulsewidth eigenvalue equations when the optical fiber consists of an arbitrary large number of sections of highly-birefringent fiber is given.

2 BACKGROUND

Polarization Mode Dispersion, PMD, has increasingly attracted the attention of researchers, fiber manufacturers and system planners due to several reasons. Different techniques have recently succeeded in keeping chromatic dispersion under control [3] and chromatic dispersion compensation modules have become commercially available, making the previously neglected effects of PMD a dominating factor. The introduction of optical amplifiers has allowed a considerable increase in the length of the communications link before electronic regeneration of the signal is required. This however, also allowed PMD effects to accumulate over even longer distances. Researchers in the late 1980's and early 1990's realized [9,10] that PMD would have to be addressed because of its significant impact on the performance of multi-gigabit per second optical communication systems operating over the embedded optical fiber network. The purpose of the present chapter is to explain the phenomenon known as *PMD* and to provide readers with some of the key concepts and tools used throughout the rest of this thesis.

2.1 JONES CALCULUS

The state of polarization of a signal at any given frequency can be uniquely represented by two parameters. Those parameters account for the relative magnitude of the horizontally and vertically polarized components of the electric field and the phase lag between them [11]. In general, a signal with a given electric field, E(t), polarized along a particular state of polarization has a total vector field, **E**, given by

$$\mathbf{E} = \left(A_x e^{j\gamma_x}\mathbf{x} + A_y e^{j\gamma_y}\mathbf{y}\right)E(t)\,, \tag{2.1a}$$

where

$$\sqrt{A_x^2 + A_y^2} = 1 \tag{2.2b}$$

and γ_x and γ_y are the absolute phases of each component. The vectors **x** and **y** representing horizontal and vertical states of polarization in eq 2.1 are in general, "Jones vectors" [11,12].

A Jones vector is essentially a 2 by 1 unitary vector with complex components. Each complex component accounts for the magnitude and absolute phase of the electric field polarized in either the horizontal or vertical directions. Thus, a Jones vector, ξ, representing some arbitrary state of polarization is given by

$$\xi = \begin{bmatrix} A_x e^{j\gamma_x} \\ A_y e^{j\gamma_y} \end{bmatrix} . \tag{2.2}$$

As only the relative phase between components is needed to define a state of polarization, eq. 2.2 can be slightly modified and re-expressed as

$$\xi = e^{j\left(\frac{\gamma_x + \gamma_y}{2}\right)} \begin{bmatrix} e^{-j\gamma} \cos(\alpha) \\ e^{j\gamma} \sin(\alpha) \end{bmatrix} , \tag{2.3}$$

where $\gamma = (\gamma_y - \gamma_x)/2$ and the magnitude components (A_x and A_y) are now a function of the angle α. The absolute phase term in the right hand side of eq. 2.3 can be neglected as the phase difference between the horizontal and vertical components is given by γ. Throughout this thesis, the Jones vector representing an arbitrary state of polarization, ε, will be given by

$$\varepsilon = \begin{bmatrix} e^{-j\gamma} \cos(\alpha) \\ e^{j\gamma} \sin(\alpha) \end{bmatrix}, \tag{2.4}$$

where both γ and α are real numbers. The signal in eq. 2.1a can be more compactly

expressed in terms of the Jones vector ε as

$$\mathbf{E} = \varepsilon E(t) \quad . \tag{2.5}$$

The use of Jones vectors to represent states of polarization provides a simple way of mathematically manipulating signals with a particular state of polarization. However, it becomes difficult to directly appreciate the changes in the state of polarization of a signal when the complex elements of a Jones vector change. An alternative way of representing a state of polarization is through the use of Stokes vectors.

2.2 Stokes Vectors And The Poincaré Sphere

The Stokes vectors offer a qualitative way of representing a state of polarization, [12]. A Stokes vector is a 4 by 1 vector with real elements,

$$\mathbf{S} = \begin{bmatrix} s_0 \\ s_1 \\ s_2 \\ s_3 \end{bmatrix} \quad . \tag{2.6}$$

In eq. 2.6, s_0 represents the total normalized power of the signal, s_1 is the difference in the intensities of the horizontally and vertically polarized components of the signal, s_2 is the difference between the intensities of the components polarized with tilt angles [12] of $\pi/4$ and $3\pi/4$ rad. and s_3 is the difference between the left and right circularly polarized components.

Any arbitrary state of polarization can be represented as a point in a Cartesian three-dimensional space with axes s_1, s_2 and s_3. Each axis corresponding to one of the stokes parameters s_1, s_2 and s_3 and ranging from -1 to +1. The Poincaré sphere [11] is a powerful

tool for the visualization of any state of polarization. The center of the Poincaré sphere coincides with the origin of the three dimensional Cartesian space with axes s_1, s_2 and s_3 and its radius is equal to s_0. Any fully polarized signal [12,13] can be represented as a point on the surface of the Poincaré sphere as indicated in fig. 2.1. All the linear states of polarization lie on the equator of the sphere and all the left (right) [12,13] elliptical and circular states of polarization are located in the upper (lower) hemisphere. The states of polarization where the $\pi/4$ ($3\pi/4$) tilt angle dominates over the $3\pi/4$ ($\pi/4$) tilt angle fall in the right (left) half of the Poincaré sphere. Finally, all the points between the equator and the poles on the sphere represent elliptical states of polarization and the north (south) pole represents left (right) circularly polarized light [11-13]. It is possible to obtain the Stokes vector components for a given state of polarization from its corresponding Jones vector [11-13] by using

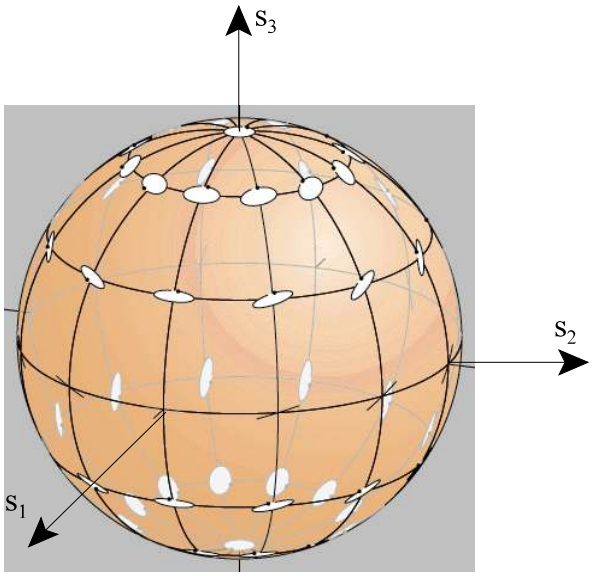

Fig 2.1 The Poincaré sphere [14].

$$\left.\begin{aligned} s_1 &= \cos^2(\alpha) - \sin^2(\alpha) \\ s_2 &= 2\cos(\alpha)\sin(\alpha)\cos(2\gamma) \\ s_3 &= 2\cos(\alpha)\sin(\alpha)\sin(2\gamma) \end{aligned}\right\} , \qquad (2.7)$$

where α and γ are the parameters of the Jones vector in eq. 2.4. Throughout this thesis, the Jones vector representation of a state of polarization is used for quantitative calculations whilst the equivalent Stokes vector and the Poincaré sphere are used for the qualitative

representation of the state of polarization.

2.3 BIREFRINGENCE IN OPTICAL FIBERS

A single mode fiber operating in the HE_{11} mode, actually supports two degenerate modes which are orthogonally polarized [3]. These degenerate modes will have the same mode index, n[1], only when the core of the fiber is perfectly cylindrical, (i.e. it has a uniform diameter) refer to fig. 2.2.

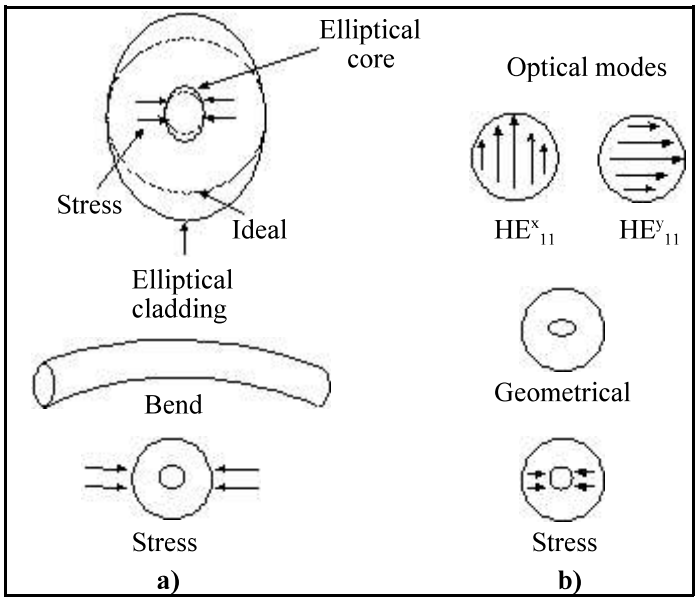

Fig. 2.2 a) Extrinsic and b) Intrinsic mechanisms of fiber birefringence.

The degeneracy is broken if the core exhibits some degree of asymmetry. The causes of ellipticity in the core can be intrinsic (non uniform stress introduced during the drawing or cooling stage of fabrication) or extrinsic (stress introduced by cabling, micro or macro-bending, twisting side pressure, etc.) [15].

The former cause is more common with older fiber which was made with less geometrical control than nowadays, while the latter one can occur due to environmental

---

[1]A particular mode propagates within a fiber with an effective refractive index : $n = \psi(\omega)/k_o$, where $\psi(\omega)$ is the propagation constant, $k_o = \omega/c$ is the free space wave number, ω is the angular optical frequency and "c" is the speed of light [3].

factors (temperature changes for example, [16-18]) or during the cabling process. Once the symmetry of the core has been altered, the two degenerate supported modes will experience a different mode index, i.e. the fiber will become *Birefringent*. The difference between these two indexes is known as the *degree of birefringence*, $\Delta n_{eff} = |n_x - n_y|$. As a result of Birefringence, a signal launched into the fiber at a particular state of polarization, ε, will be split into two identical, linearly polarized signals having their electric field vectors aligned with the symmetry axes of the fiber.

At each frequency, a phase lag is introduced between those two components due to the fact that each one propagates through the fiber experiencing different mode indexes. This progressive slippage of the two orthogonally polarized modes will, in turn, cause the overall state of polarization of the signal to evolve with distance (refer to fig. 2.3), effectively tracing out a circle on the surface of the Poincaré sphere.

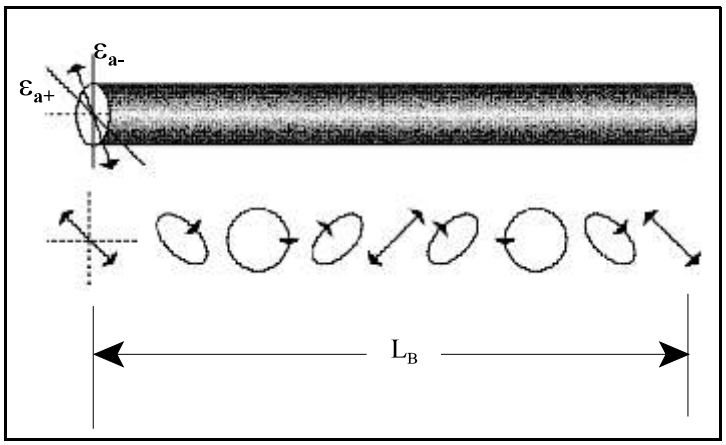

Fig. 2.3 Beat length, L_B [14].

The distance over which the state of polarization undergoes a full rotation on the Poincaré sphere (i.e. experiences a phase shift of 2π between its components) is called the *Beat Length* and it is defined as: $L_B = \lambda/\Delta n_{eff}$. Fibers for which Δn_{eff} is large ($\sim 10^{-4}$) are called *Highly-Birefringent* (Hi-Bi) fibers. In general, the net effect of launching a signal with an arbitrary state of polarization into a piece of Hi-Bi fiber will

be that of obtaining two replicas of the input signal, polarized at different orthogonal states of polarization and with a relative time shift between them. The input state of polarization which yields the lowest value of n is called the *fast input state of polarization* and it is customarily represented as ε_{a-}. Likewise the input state of polarization which yields the highest value of n is known as the *slow input state of polarization*, ε_{a+}.

In general, a signal with a state of polarization ε_{a+} (ε_{a-}), launched into a birefringent optical fiber will come out of it polarized along ε_{b+} (ε_{b-}). For the special case of a Hi-Bi fiber, $\varepsilon_{a+} = \varepsilon_{b+}$, $\varepsilon_{a-} = \varepsilon_{b-}$ and both coincide with the symmetric axes of the fiber.

This signal splitting and time delaying phenomenon is known as *Polarization Mode Dispersion, PMD* and to date, represents the ultimate hurdle for the massive deployment of multi-gigabit per second optical communication systems.

2.4 First Order Polarization Mode Dispersion

During the mid 1980's [6] the necessary concepts and analytical tools required to describe PMD were introduced. In a real optical fiber, the degree of birefringence, Δn_{eff}, does not remain constant throughout its length but changes randomly as a result of fluctuations in the core shape and non-uniform stress acting on it [20]. In fact, a real optical fiber can be thought as being a "special" Hi-Bi fiber which has been cleaved into segments of random length and then fusion spliced back with random fusion angles in between each segment.

There exists, however, at any given frequency ω two input, $\varepsilon_{a+}(\omega)$ and $\varepsilon_{a-}(\omega)$, and

two corresponding output, $\varepsilon_{b+}(\omega)$ and $\varepsilon_{b-}(\omega)$, states of polarization which render the shortest and the longest propagation time through the fiber. The difference in the transmission time of two signals polarized along the states of polarization producing the shortest and longest propagation times is known as the *Differential Group Delay (DGD)* and it is usually represented [6] as $\Delta\tau = \tau_+ - \tau_-$. Where τ_+ (τ_-) represents the longest (shortest) transmission time.

In the absence of polarization dependent losses, the input (output) states of polarization $\varepsilon_{a+}(\omega)$ and $\varepsilon_{a-}(\omega)$, ($\varepsilon_{b+}(\omega)$ and $\varepsilon_{b-}(\omega)$) are mutually orthogonal[2], i.e., $<\varepsilon_{a+}(\omega), \varepsilon_{a-}(\omega)> = 0$, ($<\varepsilon_{b+}(\omega), \varepsilon_{b-}(\omega)> = 0$). These states of polarization are commonly [6] referred to as *Principal States of Polarization (PSPs).* The differential transmission time of two undistorted signals polarized along mutually orthogonal states of polarization constitutes what it is known as the *first order effect* of PMD.

Both the PSPs and the DGD are assumed to be independent of frequency if only first order PMD effects are being considered. When a signal with an electric field $E_{in}(t)$ and polarized along a state of polarization ϕ is launched into a birefringent optical fiber which exhibits only first order PMD effects, the vector field of the signal at the output of the fiber, $\mathbf{E_{out}}$, [20], is given by

$$\mathbf{E_{out}} = c_+ E_{in}(t + \tau_+)\varepsilon_{b+} + c_- E_{in}(t + \tau_-)\varepsilon_{b-} \qquad (2.8)$$

where the input state of polarization, ϕ, was expressed in terms of the orthonormal basis of the input PSPs according to

---

[2] The inner product of two complex vectors **u** and **v** is defined as $<\mathbf{u},\mathbf{v}> = \mathbf{u}^+\mathbf{v}$ and "+" represents the transpose complex conjugate (Hermitian) of a vector or a matrix.

$$\begin{aligned} \varphi &= (\varphi^{+}\varepsilon_{a+})\varepsilon_{a+} + (\varphi^{+}\varepsilon_{a-})\varepsilon_{a-} \\ &= c_{+}\varepsilon_{a+} + c_{-}\varepsilon_{a-} \end{aligned} \quad . \tag{2.9}$$

The constants c_+ and c_- represent the projection of ϕ onto ε_{a+} and ε_{a-} respectively, i.e., $c_+ = \phi^{+}\varepsilon_{a+}$ and $c_- = \phi^{+}\varepsilon_{a-}$. From eq. 2.8 it is clear that unless, $c_+ = 0$ or $c_- = 0$ or $\tau_+ = \tau_-$, the receiver will "see" two signals with different magnitudes arriving at different times. The latter will cause intersymbol interference (ISI) when $\Delta\tau$ is roughly equal to or greater than one tenth of the bit period [21], refer to fig. 2.4. Eqs. 2.8 and 2.9 also tell us that, for a given $\Delta\tau$, the worst interference will be introduced when ϕ falls between ε_{a+} and ε_{a-}.

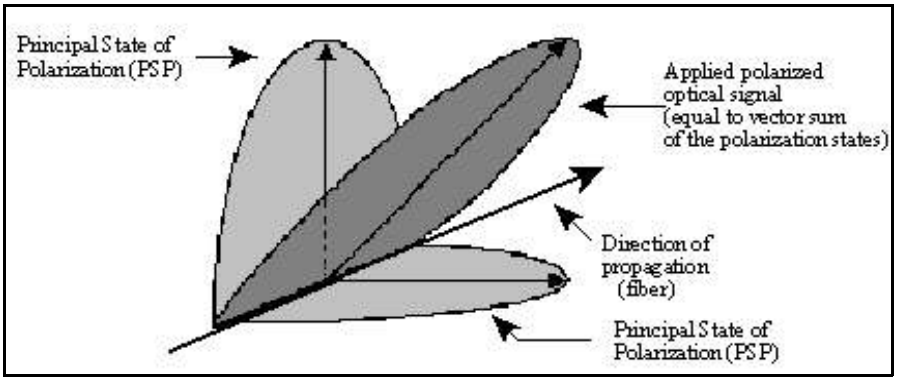

Fig. 2.4a Signal at the input of an optical fiber with first order PMD

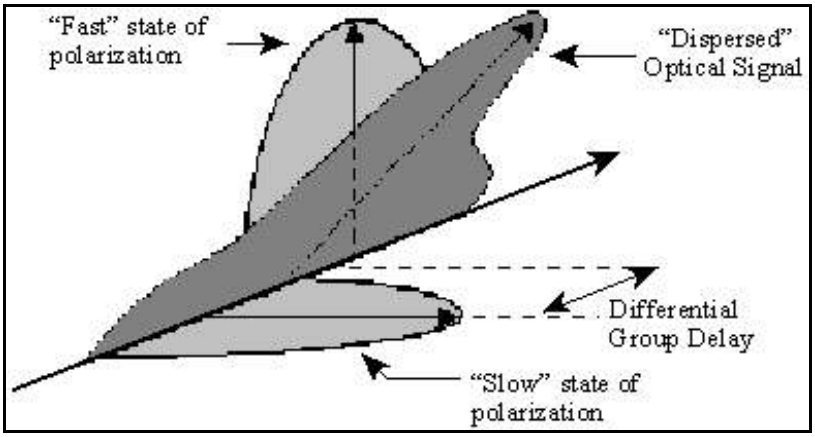

Fig. 2.4b Signal at the output of an optical fiber with first order PMD.

The time duration of $E_{in}(t)$ will also influence the amount of interference generated. A return to zero (RZ) coding scheme is for example, more resistant to first order PMD impairments than a non return to zero (NRZ) coding [22]. In fact, the bit error rate (BER) in an Intensity Modulated / Direct Detection (IM/DD) system has been shown to strongly depend on the input state of polarization and $\Delta\tau$, [21]. A conservative design guideline for a 10 Gbps system with first order PMD allows for a maximum value of only eight ps for $\Delta\tau$ in order to permit a power penalty of only 1dBm during 20 mn every year while maintaining a BER of 10^{-9} [21].

The next important concept to be introduced before describing second order PMD effects is that of *mode coupling*. As mentioned before, a real fiber can be modelled by a large number of segments of Hi-Bi fiber of random length and with random fusion angles between them. Each one of those segments has its own PSPs and a portion of the signal propagates on each of them. At the boundary between the sections, the signal will be resolved into new pairs of local PSPs belonging to the next segment. The process of rotating the optical field into the new PSPs of the following segment is known as *mode coupling* and it does not introduce any loss in the power of the signal whenever polarization dependent losses (PDL) are negligible.

It is the mode coupling phenomenon which makes the DGD and the PSPs of the fiber to be frequency dependent [19]. The mode coupling process also allows the DGD to grow proportionally to the square root of the length of the link [23]. The DGD does not grow linearly with length in highly mode coupled fibers because occasionally, the coupling between segments reduces the accumulated DGD, i.e., when the slow PSP of one segment

is very nearly aligned with the fast PSP of the next or previous segment the DGD of both segments will cancel each other out.

2.5 SECOND ORDER POLARIZATION MODE DISPERSION

As indicated in the previous section, both the DGD and the PSPs are assumed to be independent of frequency (at least within the spectral range of the signal) when only first order PMD effects are considered. In reality however, the DGD and the PSP are frequency dependent to some extent. The linear frequency dependence of the DGD and the PSPs constitutes what it is known as *second order* PMD effects [6,24-26]. The implications [24], systems impact [9,27-30] and pulsewidth effects [24,30,31] due to second and higher order PMD have been thoroughly studied.

According to Poole et al. [6,24], an optical fiber exhibiting PMD can be treated as a linear medium described by a complex 2 by 2 transfer matrix $\mathbf{T}(\omega)$, and in the absence of polarization dependent losses that matrix is given [6] by

$$\mathbf{T}(\omega) = e^{\beta(\omega)}\mathbf{U}(\omega), \tag{2.10}$$

where $\beta(\omega)$ is in general a complex number given by

$$\beta(\omega) = -z\left[\rho + j\psi(\omega)\right], \tag{2.11}$$

z is the transmission distance, ρ represents the fiber loss and $\psi(\omega)$ is the propagation constant. In eq. 2.10, $\mathbf{U}(\omega)$ is a unitary matrix defined [6] as

$$\mathbf{U} = \begin{bmatrix} u_1(\omega) & u_2(\omega) \\ -u_2^*(\omega) & u_1^*(\omega) \end{bmatrix}, \tag{2.12}$$

where $|u_1(\omega)|^2 + |u_2(\omega)|^2 = 1$. The Jones vector notation can be used to represent the vector field $\mathbf{E_{in}}$ of a real lowpass signal [8], $E_{in}(\omega)$, polarized along ϕ at the input of an optical

fiber,

$$\mathbf{E_{in}} = E_{in}(\omega)\boldsymbol{\varphi} \quad . \tag{2.13}$$

As we are treating the fiber as a linear medium, the complex lowpass vector signal [79] at the output of the fiber can be expressed by

$$\mathbf{E_{out}} = \mathbf{T}(\Delta\omega)\mathbf{E_{in}} = e^{j\beta(\Delta\omega)}\mathbf{U}(\Delta\omega)\mathbf{E_{in}} \quad , \tag{2.14}$$

where $\Delta\omega = \omega + \omega_o$ and ω_o is the optical angular carrier frequency.

According to the phenomenological approach introduced by Poole and Wagner [6], a signal of a given frequency ω, launched into a birefringent optical fiber on one of its input PSPs at the frequency, $\varepsilon_{a\pm}(\omega)$, will come out at the other end polarized on one of the output PSPs at that frequency, $\varepsilon_{b\pm}(\omega)$, and with a given phase $\theta_{b\pm}(\omega)$.

Let us, for the sake of simplicity, assume that, ϕ corresponds to one of the input PSPs at the carrier frequency, i.e., $\phi = \varepsilon_{a\pm}(\omega_o)$. With the use of eq. 2.13, eq. 2.14 can be expressed as

$$\mathbf{E_{out\pm}} = e^{j\beta(\Delta\omega)}\mathbf{U}(\Delta\omega)E_{in}(\omega)\boldsymbol{\varepsilon}_{a\pm}(\omega_o) \tag{2.15a}$$

or alternatively,

$$\mathbf{E_{out\pm}} = \left|E_{out\pm}(\omega)\right| e^{j\theta_{out\pm}(\omega)}\varepsilon_{b\pm}(\omega), \tag{2.15b}$$

where $|E_{out\pm}(\omega)|$ is the magnitude of the complex lowpass output signal. The output phase, $\theta_{out\pm}(\omega)$ can be expanded in a Taylor series around the carrier frequency and approximated by the first three terms as

$$\theta_{out\pm}(\omega) = \theta_{out,0\pm} + \theta_{out,1\pm}\delta\omega + \frac{1}{2}\theta_{out,2\pm}\delta\omega^2 \tag{2.16}$$

where $\delta\omega = \omega - \omega_o$ and $\theta_{out,n\pm} = d^n\,\theta_{out\pm}(\omega)/d\omega^n\big|_{\omega=\omega_o}$, n=0,1,2. The first term in the right

hand side of eq. 2.16 is an arbitrary phase and can be neglected, the second term represents the transmission time of the signal and the third term represents the frequency dependence of the transmission time, commonly known as *chromatic dispersion*[3] [3]. Thus, a signal of a given frequency transmitted along the slow input PSP, $\varepsilon_{a+}(\omega)$, will experience a transmission time of $\tau_{\cdot} = \theta_{out,1+}$ and will be polarized along $\varepsilon_{b+}(\omega)$ at the output of the fiber. Likewise, a signal of a given frequency transmitted along the fast input PSP, $\varepsilon_{a-}(\omega)$, will experience a transmission time of $\tau_{\cdot} = \theta_{out,1\cdot}$ and will be polarized along $\varepsilon_{b-}(\omega)$ at the output of the fiber.

Therefore, if $\theta_{out,2\cdot} \neq 0$ then the differential group delay will depend on frequency, which is one of the *second order effects* of PMD. The other effect being the frequency dependence of the input and output PSPs.

Both second order effects are actually correlated [29] in such a way that when $<\Delta\tau>$ is high[4], the rate of change of $\varepsilon_{b\cdot}(\omega)$ with frequency is low and vice versa [28,29]. The impact of second order PMD on the pulsewidth of the signal at the output of the fiber has recently been studied in both, the frequency [30-33] and the time domain [34]. It has generally been concluded that, whenever $<\Delta\tau>$ is less than one tenth of the bit period, second order PMD effect can be neglected [28]. However, second order PMD effects may also interact with the chromatic dispersion of the fiber and introduce fluctuations on the transmission performance of the system [33]. When second order PMD is not negligible,

---

[3]When the chromatic dispersion is exclusively owed to PMD it is known as *polarization dependent chromatic dispersion.*

[4]Where $<\bullet>$ means the average of "$\bullet$" over frequency.

the frequency content of the signal becomes a concern [35,36] and low chirp[5] modulation techniques (such as the use of external modulators) are required.

An analysis of the probability of experiencing a "performance outage" (when the bit error rate increases beyond 10^{-9}) due to first and second order PMD effects [37] shows however, that if $<\Delta\tau> \leq T/10$ (where "T" is the bit period), a relatively high laser chirp will not cause additional system degradation due to second order PMD.

Nevertheless, it is the frequency dependence of the input and output PSPs which causes most of the harmful effects for an IM/DD system, [27,29,33,38] and can even render a coherent system useless [3] or considerably diminish the effectiveness of several recently proposed first order compensation schemes [31,39-51].

2.6 The Statistical Nature Of Polarization Mode Dispersion

The intersymbol interference caused by pulse spreading due to PMD has a different origin from the ISI caused by the chromatic dispersion in the fiber [52]. The latter one is deterministic, grows linearly with distance and can be compensated by using dispersion compensating fiber [53] or any other commercially available dispersion compensation technique [3].

PMD however, is a stochastic process [54]. The random configuration of birefringence which causes PMD depends on the stress induced by spooling, cabling, temperature changes and any other environmental factor that may cause the core of the fiber

[5]A highly coherent laser source [3] is said to be "chirped" if the carrier frequency produced by it drifts over time.

to deviate from being perfectly cylindrical. The statistical properties of PMD have been experimentally and theoretically studied [54-57]. It was found, [58], that the evolution of DGD at a particular frequency over time yields a Maxwellian probability density function [54] given by

$$\mathrm{PDF}(\Delta\tau) = 3\sqrt{\frac{6}{\pi}}\,\frac{\Delta\tau^2}{\Delta\tau_{rms}^3}\exp\left(-\frac{3\Delta\tau^2}{2\Delta\tau_{rms}^2}\right), \tag{2.17}$$

where $\Delta\tau_{rms} = \langle\Delta\tau^2\rangle^{1/2}$.

Interestingly, as a result of the multiple factors which contribute to the randomly varying birefringence along the fiber, the statistics of PMD at a given frequency over time are the same as the statistics of PMD at a given time over a broad enough frequency range [54]. Even more interesting is the fact that the statistics of PMD over either time or frequency for a single fiber are the same as the statistics of PMD over an ensemble of fibers [58]. This makes PMD an ergodic process of course.

It is this highly statistical nature of PMD which makes it difficult to compensate. The PMD dependence on environmental factors [17,36,58,60,61] introduces a time variation in the frequency response of the fiber, which in turn implies the need for an adaptive compensation technique. Not only does the frequency response of the fiber evolve with time but also with the input and output [33,50,52] states of polarization. A successful PMD compensation scheme should therefore, be capable of tracking relatively fast variations [19,62] in the frequency response of the fiber.

3 PULSEWIDTH NARROWING

This chapter will present, in detail, the mathematical derivation, first introduced by Chen et al. [7], which establishes the theoretical framework necessary in order to minimize the rms-pulsewidth of a signal transmitted through an optical fiber with PMD. It is noteworthy to mention that the theoretical work by Chen et al. does not make any simplifying assumption about the orders of PMD in the fiber or the shape of the transmitted signal. The system under consideration is also presented and mathematically described. At the end of this chapter a set of algorithms is introduced, the purpose of which is to vary the input and output states of polarization in order to minimize the rms-pulsewidth of a signal before it reaches the detector. The latter is equivalent to searching for an absolute minimum in a four dimensional space.

3.1 THE SYSTEM CONSIDERED

In order to clearly appreciate the dependence of the frequency response of the fiber on the input and output states of polarization of the signal being transmitted, eq. 2.14 can be rewritten as

$$\mathbf{E}_{out} = \mathbf{T}_L(\omega) \cdot \mathbf{E}_{in}(\omega) \tag{3.1}$$

where $\mathbf{T}_L(\omega) = \mathbf{T}(\omega+\omega_o) = \mathbf{T}(\Delta\omega)$ is the complex lowpass equivalent of $\mathbf{T}(\omega)$ [8].

Signals can be launched into a fiber on any state of polarization with the help of a *Polarization Controller, (PC)*[63,64]. A PC is essentially a set of waveplates with different retardation values [65], each of which can be rotated in such a way that the complex Jones transfer matrix resultant, $\mathbf{T}_{PC}$, maps an input state of polarization, ε_x, into any desired output

state of polarization on the surface of the Poincaré Sphere, ε_y, according to

$$\varepsilon_y = \mathbf{T}_{PC}\varepsilon_x . \tag{3.2}$$

Receiving the signal at the output of the fiber along a particular state of polarization, χ, means projecting the signal polarized along $\varepsilon_{out}(\omega)$ onto χ at every frequency, i.e., $<\chi^+, \varepsilon_{out}(\omega)>$ for all ω. To that end, a *Polarization Analyser, (PA)* is required. A PA can be built by cascading a PC and a *Polarization Beam Splitter, (PBS).*

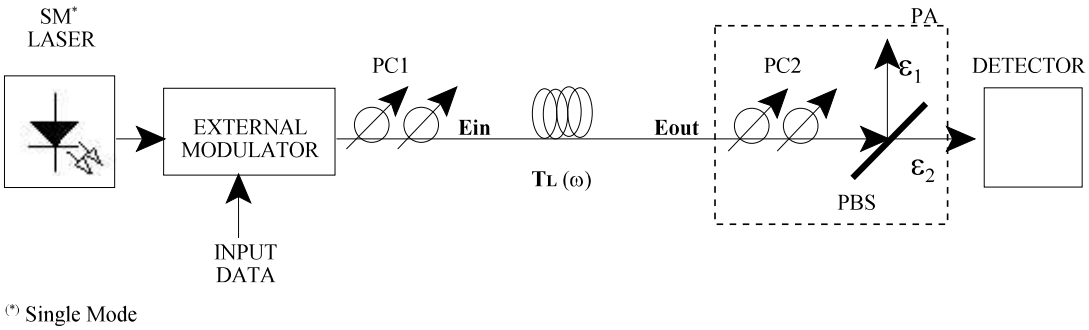

Fig. 3.1 A system with a polarization analyzer at the end.

In fig. 3.1, ε_1 and ε_2 represent two mutually orthogonal states of polarization respectively.

The purpose of the latter is to spatially separate two orthogonal states of polarization incident on it. The PC will transform those frequency components of $\mathbf{E}_{out}$ polarized along χ into a particular state of polarization (ε_2 for example), which can be extracted by the PBS and subsequently detected. Refer to fig. 3.1. The overall effect will be the extraction of those frequency components polarized along χ in such a way that the receiver only "sees" that portion of $\mathbf{E}_{out}$. This can be mathematically expressed as

$$E_x(\omega) = \chi^{+}\mathbf{E}_{out} = \chi^{+}\mathbf{T}_L(\omega)\varphi E_{in}(\omega) = H_L(\omega)E_{in}(\omega) \tag{3.3}$$

Where $E_x(\omega)$ is the signal seen by the detector and we made use of eq. 3.1. In eq. 3.3, $\mathbf{H_L}(\omega)$ represents the complex lowpass frequency response of the fiber and is given by

$$\mathbf{H_L}(\omega) = \mathbf{\chi}^{+}\mathbf{T_L}(\omega)\mathbf{\varphi}. \tag{3.4}$$

3.2 BASIC DEFINITIONS

This section gives some of the fundamental definitions required for the pulsewidth analysis presented in the next sections. The Fourier transform definitions used here are

$$E(\omega) = \Im\{E(t)\} = \frac{1}{\sqrt{2\pi}}\int_{-\infty}^{\infty} E(t)e^{-j\omega t}dt \tag{3.5a}$$

$$E(t) = \Im^{-1}\{E(\omega)\} = \frac{1}{\sqrt{2\pi}}\int_{-\infty}^{\infty} E(\omega)e^{j\omega t}d\omega \tag{3.5b}$$

The rms-pulsewidth of the signal seen by the detector is defined [7,32,33,66] as

$$\sigma_x = \sqrt{< t^2 > - < t >^2}, \tag{3.6}$$

where the n-th moment of *t*, [32], is given by

$$< t^n > = \frac{\int_{-\infty}^{\infty} E_x^*(t)t^n E_x(t)dt}{\int_{-\infty}^{\infty} |E_x(t)|^2 dt}. \tag{3.7}$$

and the asterisk ,"*", denotes complex conjugate.

It is straightforward to prove[1] that the first two moments of *t* can be expressed in the frequency domain [32] as

[1]Refer to appendix "A"

$$\langle t \rangle = \frac{j\int_{-\infty}^{\infty} E_x^*(\omega)\frac{dE_x(\omega)}{d\omega}d\omega}{\int_{-\infty}^{\infty}\left|E_x(\omega)\right|^2 d\omega} \tag{3.8a}$$

$$\langle t^2 \rangle = \frac{\int_{-\infty}^{\infty}\left|\frac{dE_x(\omega)}{d\omega}\right|^2 d\omega}{\int_{-\infty}^{\infty}\left|E_x(\omega)\right|^2 d\omega}. \tag{3.8b}$$

The complex lowpass time impulse response of the optical fiber can be obtained by taking the inverse Fourier transform of eq. 3.4 as

$$\mathbf{h_L(t) = \mathfrak{F}^{-1}\{H_L(\omega)\} = \mathfrak{F}^{-1}\{\chi^+ T_L(\omega)\varphi\}} \tag{3.9}$$

Therefore, for a given optical fiber exhibiting PMD, described by a complex Jones transfer matrix $\mathbf{T_L}(\omega)$ in a system like that from fig. 3.1, the time impulse response seen by any signal propagating through it will depend on the state of polarization at which the signal is launched and received [50].

3.3 PULSEWIDTH EQUATIONS

In this section, the mathematical expressions for the rms-pulsewidth as a function of the input and output states of polarization are presented [7]. From equations 3.3 and 3.8, the first and second moments of *t* can be expressed as

$$\langle t \rangle = \frac{j\int_{-\infty}^{\infty}\chi^+\left(\frac{dE_{out}}{d\omega}\right)E_{out}^+\chi d\omega}{\int_{-\infty}^{\infty}\chi^+ E_{out}E_{out}^+\chi d\omega} \tag{3.10a}$$

$$\langle t^2 \rangle = \frac{\int_{-\infty}^{\infty} \chi^+ \left(\frac{dE_{out}}{d\omega} \right) \left(\frac{dE_{out}^+}{d\omega} \right) \chi d\omega}{\int_{-\infty}^{\infty} \chi^+ E_{out} E_{out}^+ \chi d\omega}. \tag{3.10b}$$

The input, ϕ, and output, χ, states of polarization are degrees of freedom of the system and they are assumed to be independent of frequency. Therefore, by using eq. 3.1, we can rewrite eq. 3.10 as

$$\langle t \rangle = \frac{\chi^+ \left\{ \int_{-\infty}^{\infty} j \left[\frac{d}{d\omega} T_L(\omega) E_{in}(\omega) \right] \varphi\varphi^+ T_L^+(\omega) E_{in}^*(\omega) d\omega \right\} \chi}{\chi^+ \left\{ \int_{-\infty}^{\infty} T_L(\omega) \varphi\varphi^+ T_L^+(\omega) \left| E_{in}(\omega) \right|^2 d\omega \right\} \chi} \tag{3.11a}$$

$$\langle t^2 \rangle = \frac{\chi^+ \left\{ \int_{-\infty}^{\infty} \left[\frac{d}{d\omega} T_L(\omega) E_{in}(\omega) \right] \varphi\varphi^+ \left[\frac{d}{d\omega} T_L^+(\omega) E_{in}^*(\omega) \right] d\omega \right\} \chi}{\chi^+ \left\{ \int_{-\infty}^{\infty} T_L(\omega) \varphi\varphi^+ T_L^+(\omega) \left| E_{in}(\omega) \right|^2 d\omega \right\} \chi}. \tag{3.11b}$$

The expressions within the braces in eq. 3.11 are not a function of frequency, but a function of the input state of polarization, ϕ. For that reason, the notation can be simplified [7] by defining

$$T_\varphi = \int_{-\infty}^{\infty} j \left[\frac{d}{d\omega} T_L(\omega) E_{in}(\omega) \right] \varphi\varphi^+ T_L^+(\omega) E_{in}^*(\omega) d\omega \tag{3.12a}$$

$$S_\varphi = \int_{-\infty}^{\infty} \left[\frac{d}{d\omega} T_L(\omega) E_{in}(\omega) \right] \varphi\varphi^+ \left[\frac{d}{d\omega} T_L^+(\omega) E_{in}^*(\omega) \right] d\omega \tag{3.12b}$$

$$P_\varphi = \int_{-\infty}^{\infty} T_L(\omega) \varphi\varphi^+ T_L^+(\omega) \left| E_{in}(\omega) \right|^2 d\omega \tag{3.12c}$$

where $\mathbf{T}_3$, $\mathbf{S}_3$ and $\mathbf{P}_3$ are complex 2 by 2 matrices. Equation 3.11 is now reexpressed as

$$< t > = \frac{\chi^{+}\mathbf{T}_{\varphi}\chi}{\chi^{+}\mathbf{P}_{\varphi}\chi} \tag{3.13a}$$

$$< t^2 > = \frac{\chi^{+}\mathbf{S}_{\varphi}\chi}{\chi^{+}\mathbf{P}_{\varphi}\chi}. \tag{3.13b}$$

For a given value of the input state of polarization, ϕ, eq. 3.6 can be expressed as a function of the output state of polarization, χ, by using eq. 3.13

$$\sigma_x^2(\chi) = \frac{\chi^{+}\mathbf{S}_{\varphi}\chi}{\chi^{+}\mathbf{P}_{\varphi}\chi} - \left(\frac{\chi^{+}\mathbf{T}_{\varphi}\chi}{\chi^{+}\mathbf{P}_{\varphi}\chi}\right)^2. \tag{3.14}$$

Had we changed the order of the terms within the integrals of eq. 3.10, we would have obtained the following result

$$< t > = \frac{j\int_{-\omega}^{\omega} \mathbf{E}_{out}^{+}\chi\chi^{+}\left(\frac{d\mathbf{E}_{out}}{d\omega}\right)d\omega}{\int_{-\omega}^{\omega} \mathbf{E}_{out}^{+}\chi\chi^{+}\mathbf{E}_{out}d\omega} \tag{3.15a}$$

$$< t^2 > = \frac{\int_{-\omega}^{\omega}\left(\frac{d\mathbf{E}_{out}^{+}}{d\omega}\right)\chi\chi^{+}\left(\frac{d\mathbf{E}_{out}}{d\omega}\right)d\omega}{\int_{-\omega}^{\omega} \mathbf{E}_{out}^{+}\chi\chi^{+}\mathbf{E}_{out}d\omega}. \tag{3.15b}$$

Eq. 3.15 can also be arranged in a way similar to eq. 3.10 by using eq. 3.1, yielding the following result

$$< t > = \frac{\varphi^{+}\left\{j\int_{-\omega}^{\omega}\mathbf{T}_L^{+}(\omega)\mathbf{E}_{in}^{*}(\omega)\chi\chi^{+}\left[\frac{d}{d\omega}\mathbf{T}_L(\omega)\mathbf{E}_{in}(\omega)\right]d\omega\right\}\varphi}{\varphi^{+}\left\{\int_{-\omega}^{\omega}\mathbf{T}_L^{+}(\omega)\chi\chi^{+}\mathbf{T}_L(\omega)\left|\mathbf{E}_{in}(\omega)\right|^2 d\omega\right\}\varphi} \tag{3.16}$$

$$\langle t^2 \rangle = \frac{\varphi^+ \left\{ \int_{-\infty}^{\infty} \left[\frac{d}{d\omega} \mathbf{T}_L^+(\omega) \mathbf{E}_{in}^*(\omega) \right] \boldsymbol{\chi}\boldsymbol{\chi}^+ \left[\frac{d}{d\omega} \mathbf{T}_L(\omega) \mathbf{E}_{in}(\omega) \right] d\omega \right\} \varphi}{\varphi^+ \left\{ \int_{-\infty}^{\infty} \mathbf{T}_L^+(\omega) \boldsymbol{\chi}\boldsymbol{\chi}^+ \mathbf{T}_L(\omega) \left| \mathbf{E}_{in}(\omega) \right|^2 d\omega \right\} \varphi} . \quad (3.16b)$$

In this case, similar to eq. 3.11, neither of the expressions within the braces in eq. 3.16 is a function of frequency but a function of the output state of polarization, χ. Therefore the notation can be further simplified, [7], by defining

$$\mathbf{T}_\gamma = \int_{-\infty}^{\infty} j \mathbf{T}_L^+(\omega) \mathbf{E}_{in}^*(\omega) \boldsymbol{\chi}\boldsymbol{\chi}^+ \left[\frac{d}{d\omega} \mathbf{T}_L(\omega) \mathbf{E}_{in}(\omega) \right] d\omega \quad (3.17a)$$

$$\mathbf{S}_\gamma = \int_{-\infty}^{\infty} \left[\frac{d}{d\omega} \mathbf{T}_L^+(\omega) \mathbf{E}_{in}^*(\omega) \right] \boldsymbol{\chi}\boldsymbol{\chi}^+ \left[\frac{d}{d\omega} \mathbf{T}_L(\omega) \mathbf{E}_{in}(\omega) \right] d\omega \quad (3.17b)$$

$$\mathbf{P}_\gamma = \int_{-\infty}^{\infty} \mathbf{T}_L^+(\omega) \boldsymbol{\chi}\boldsymbol{\chi}^+ \mathbf{T}_L(\omega) \left| \mathbf{E}_{in}(\omega) \right|^2 d\omega \quad (3.17c)$$

where $\mathbf{T}_\gamma$, $\mathbf{S}_\gamma$ and $\mathbf{P}_\gamma$ are 2 by 2 complex matrices. Thus, eq. 3.15 will now be given by

$$\langle t \rangle = \frac{\varphi^+ \mathbf{T}_\gamma \varphi}{\varphi^+ \mathbf{P}_\gamma \varphi} \quad (3.18a)$$

$$\langle t^2 \rangle = \frac{\varphi^+ \mathbf{S}_\gamma \varphi}{\varphi^+ \mathbf{P}_\gamma \varphi} . \quad (3.18b)$$

For a given output state of polarization, χ, eq. 3.6 can be expressed as a function of the input state of polarization, ϕ, by using eq. 3.18, to give

$$\sigma_x^2(\varphi) = \frac{\varphi^+ \mathbf{S}_\gamma \varphi}{\varphi^+ \mathbf{P}_\gamma \varphi} - \left(\frac{\varphi^+ \mathbf{T}_\gamma \varphi}{\varphi^+ \mathbf{P}_\gamma \varphi} \right)^2 \quad (3.19)$$

3.4 CONSTRAINED MINIMIZATION

Eq. 3.14 (or eq. 3.19) represents the case in which the objective function, σ_x^2, is expressed as a function of the output (input) state of polarization while the input (output) state of polarization is held fixed. A constrained minimization using Lagrange multipliers will be carried out in eq. 3.14 and 3.19. In both cases the minimization constraint, will be that the 2 by 1 complex vectors ϕ and χ represent a Jones vector state of polarization, i.e. $\phi^+\phi = 1$, $\chi^+\chi = 1$, respectively. The primal equation [67] for the constrained minimization of eq. 3.14 is given by

$$c(\chi) = 1 - \chi^+\chi \quad . \tag{3.20}$$

We can define a new function, h(χ), needed for the minimization procedure,

$$h(\chi) = \sigma_x^2(\chi) + \eta c(\chi) \tag{3.21a}$$

$$h(\chi) = \frac{\chi^+ S_\varphi \chi}{\chi^+ P_\varphi \chi} - \left(\frac{\chi^+ T_\varphi \chi}{\chi^+ P_\varphi \chi}\right)^2 + \eta(1 - \chi^+\chi) \ , \tag{3.21b}$$

where eqs. 3.14 and 3.20 were used and η is the Lagrange multiplier [85]. Differentiating eq. 3.21 with respect to χ^+, we will obtain the adjoint [67] equation,

$$\frac{\partial h(\chi)}{\partial \chi^+} = 0 \tag{3.22a}$$

$$\frac{\partial h(\chi)}{\partial \chi^+} = \frac{(\chi^+ P_\varphi \chi) S_\varphi \chi - P_\varphi \chi (\chi^+ S_\varphi \chi)}{(\chi^+ P_\varphi \chi)^2}$$
$$-2\left[\frac{(\chi^+ P_\varphi \chi) T_\varphi \chi - P_\varphi \chi (\chi^+ T_\varphi \chi)}{(\chi^+ P_\varphi \chi)^2}\right]\left(\frac{\chi^+ T_\varphi \chi}{\chi^+ P_\varphi \chi}\right) - \eta \chi = 0. \tag{3.22b}$$

The notation can be further simplified by defining

$$\overline{P} = \chi^{+} P_{\varphi} \chi \tag{3.23a}$$

$$\overline{T} = \chi^{+} T_{\varphi} \chi. \tag{3.23b}$$

Substituting eq. 3.23 into eq. 3.22b will produce the following eigenvalue equation, (after reordering terms)

$$\left(\frac{1}{\overline{P}} S_{\varphi} - \frac{1}{\overline{P}^2} P_{\varphi} \chi \chi^{+} S_{\varphi} - \frac{2}{\overline{P}^2} T_{\varphi} \chi \chi^{+} T_{\varphi} + \frac{2\overline{T}}{\overline{P}^3} P_{\varphi} \chi \chi^{+} T_{\varphi} \right) \chi = \eta \chi \tag{3.24a}$$

or

$$\left[M_1(\varphi, \chi) \right] \chi = \eta \chi. \tag{3.24b}$$

It is possible to follow a similar procedure but starting from $c(\phi) = 1 - \phi^{+}\phi$ and $h(\phi) = \sigma_x^2(\phi) + \zeta c(\phi)$, where σ_x^2 is obtained from eq. 3.19 and ζ is the Lagrange multiplier in this case. The eigenvalue equations produced will be

$$\left(\frac{1}{\overline{P}} S_{\gamma} - \frac{1}{\overline{P}^2} P_{\gamma} \varphi \varphi^{+} S_{\gamma} - \frac{2}{\overline{P}^2} T_{\gamma} \varphi \varphi^{+} T_{\gamma} + \frac{2\overline{T}}{\overline{P}^3} P_{\gamma} \varphi \varphi^{+} S_{\gamma} \right) \varphi = \zeta \varphi \tag{3.25a}$$

or

$$\left[M_2(\varphi, \chi) \right] \varphi = \zeta \varphi. \tag{3.25b}$$

The eigenvalue equations 3.24 and 3.25 are the fundamental results presented by Chen et al. [7]. The next sections will discuss how to use them in order to find the input and output states of polarization which produce the minimum rms-pulsewidth.

3.5 METHOD OF SOLUTION

Both eigenvalue equations, 3.24b and 3.25b are derived independently. Each one, however, tries to minimize σ_x^2 by adjusting only one state of polarization while the other is held fixed. It must be pointed out that $\mathbf{M_1}(\phi,\chi)$ in eq. 3.24b and $\mathbf{M_2}(\phi,\chi)$ in eq. 3.25b are functions of both the input and the output states of polarization. Therefore the solution to eq. 3.24b and 3.25b will require a set of initial values for ϕ and χ.

3.6 OPTIMIZATION OF THE RECEPTION STATE OF POLARIZATION

If the input state of polarization is held fixed, eq. 3.24b can be solved recursively by assuming an initial value for χ, χ_o. If a value close to the optimum value of χ, χ_{opt}, is not known beforehand (which is usually the case), an arbitrary initial value of χ_o, is chosen. Every time that the eigenvalue equation 3.24b is solved, it will produce two eigenvectors, χ_1 and χ_2. Each of those values of χ can be used along with ϕ in eq. 3.14 to calculate $\sigma_x(\chi_1)$ and $\sigma_x(\chi_2)$. The output state of polarization yielding the smallest value of σ_x will become the new value of χ_o. The process is repeated until a figure of merit (FOM) reaches certain limit. At that point, it is assumed that the search for χ_{opt} has converged and σ_x^2 has the smallest possible value for the given input state of polarization, ϕ. The figure of merit used here is defined as

$$\mathrm{FOM}_\chi = 1 - \chi_{old}^{+}\chi_{new} , \tag{3.26}$$

where χ_{new} (χ_{old}) represents the value of χ which minimized σ_x in the current (previous) iteration. The convergence limits used here were empirically chosen and range from 10^{-6}

to 10^{-14}. The search for χ_{opt} will thus stop when χ_{new} is almost the same as χ_{old} . Fig. 3.2 shows a flowchart of the procedure described.

3.7 Optimization Of The Transmission State Of Polarization

The procedure for optimizing the input state of polarization, ϕ, and the convergence limits are similar to those described in the previous section, but this time assuming that the output state of polarization is held fixed. Figure 3.3 shows the flowchart corresponding to the search for ϕ_{opt}. The figure of merit, FOMϕ, in this case is given by

$$FOM_{\phi} = 1 - \varphi_{old}^{+}\varphi_{new} , \tag{3.27}$$

where ϕ_{new} (ϕ_{old}) corresponds to the value of ϕ which minimized σ_x in the current (previous) iteration.

3.8 Optimization of the Transmission and Reception States of Polarization

The procedure for optimizing the transmission and reception states of polarization, ϕ and χ is, in essence, the same as that presented in the two previous section. Here, however, we will combine the two individual searches. Initial arbitrary values of ϕ and χ are chosen, and a new figure of merit, FOM$_{\phi,\chi}$, will simply be defined as: FOM$_{\phi,\chi}$ = FOM$_{\phi}$ + FOM$_{\chi}$. The convergence limit for the new figure of merit also falls in the same range as that from the previous cases.

Fig. 3.4 shows the flowchart for the search of ϕ_{opt} and χ_{opt}. In all the optimization

procedures described, the search for ϕ_{opt} and χ_{opt} is repeated a number of times, each time using different, randomly chosen values of ϕ_o and χ_o. This is done with the purpose of avoiding convergence to possible local minimum points. The results of the searches are presented in chapters five and six.

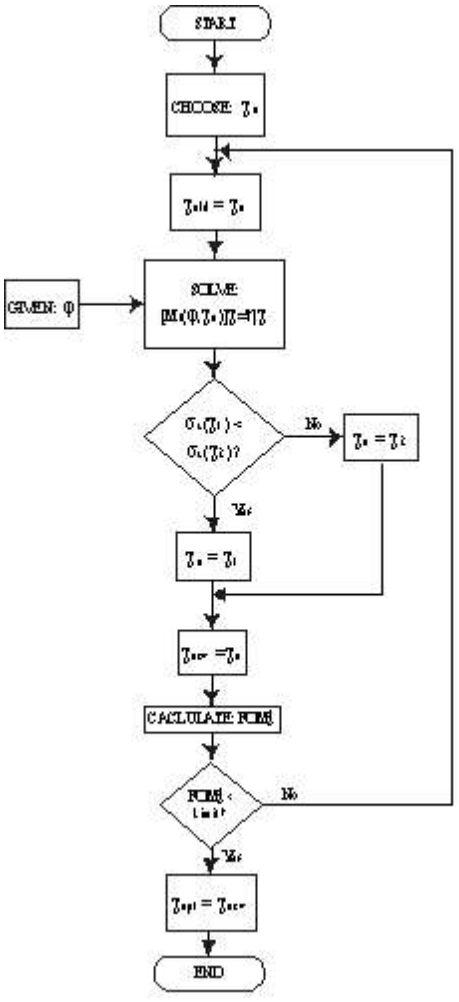

Fig. 3.2 Flowchart for the optimization of the output state of polarization, χ.

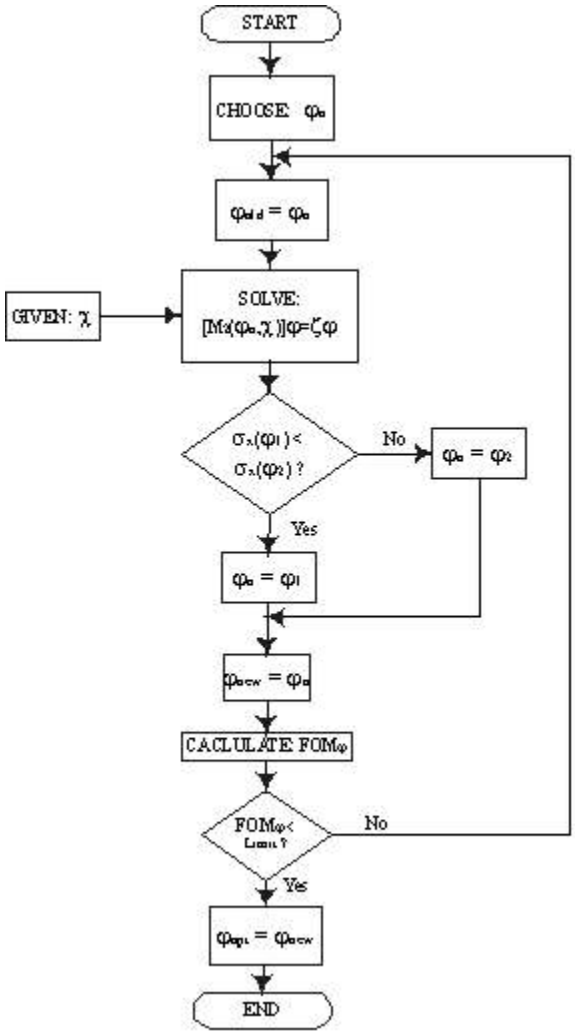

Fig. 3.3 Flowchart for the optimization of the input state of polarization, ϕ.

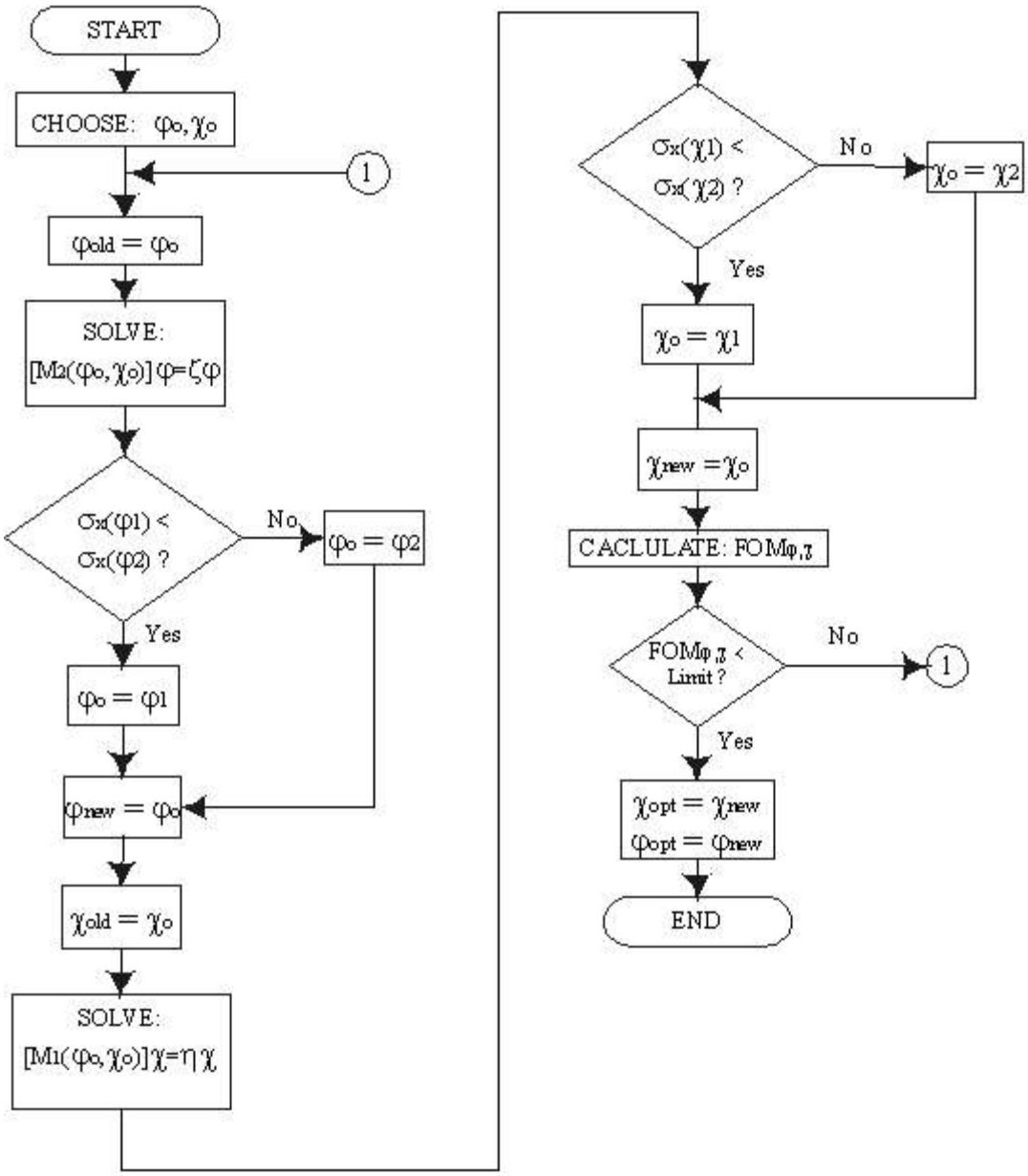

Fig. 3.4 Flowchart for the optimization of the input, ϕ, and output, χ, states of polarization.

4 FIBER SIMULATION

Due to its highly statistical nature, PMD research relies to an unusual extent on computer simulations. The purpose of this chapter is to introduce the mathematical model of an optical fiber exhibiting PMD. The model is used throughout the rest of the thesis and in this chapter is utilized to explore the statistical nature of the time impulse response owed to PMD.

4.1 THE WAVEPLATE MODEL

A waveplate can be thought[1] as being a short section of highly birefringent fiber which strongly guides light along two states of linear polarization, coincident with the symmetry axes of the fiber. The waveplate introduces a phase shift between the orthogonally polarized components of a signal propagating through it. Fig. 4.1 shows the simplest case of a pulse being transmitted through a single waveplate with fast and slow axes corresponding to the lower and higher values of the refractive index respectively.

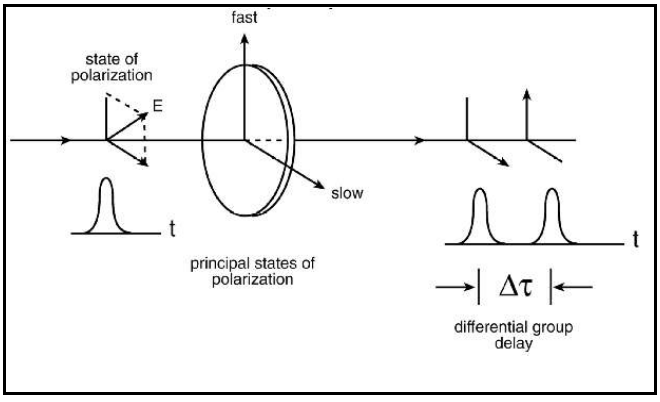

Fig 4.1 Single waveplate [12].

Fig. 4.2 illustrates the dephasing of the two orthogonally polarized components at the output of a waveplate at a particular frequency.

[1]In reality a waveplate is a birefringent crystal with well defines optical axes [12].

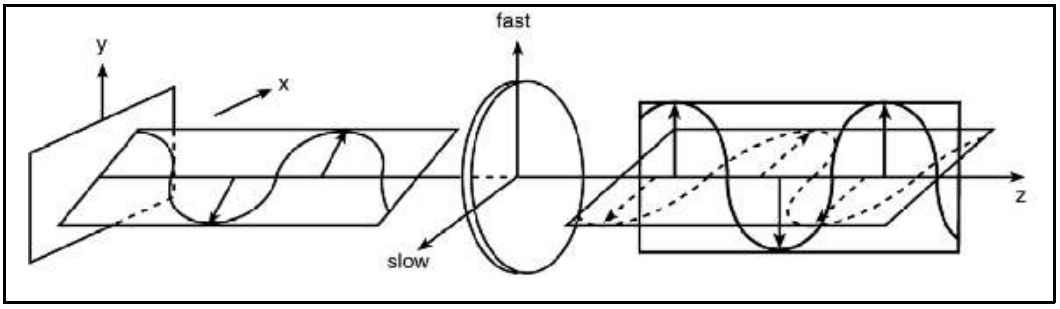

Fig. 4.2 A Single frequency component delayed by a waveplate [14].

The widely used approach [50,65,66,68-70,74] for modelling an optical fiber with some given mean DGD, $<\Delta\tau>$ consists of cascading a large number, N, of waveplates, each one introducing a random delay, $\Delta\tau_i$, and with their fast and slow axis randomly rotated as shown in fig. 4.3 .

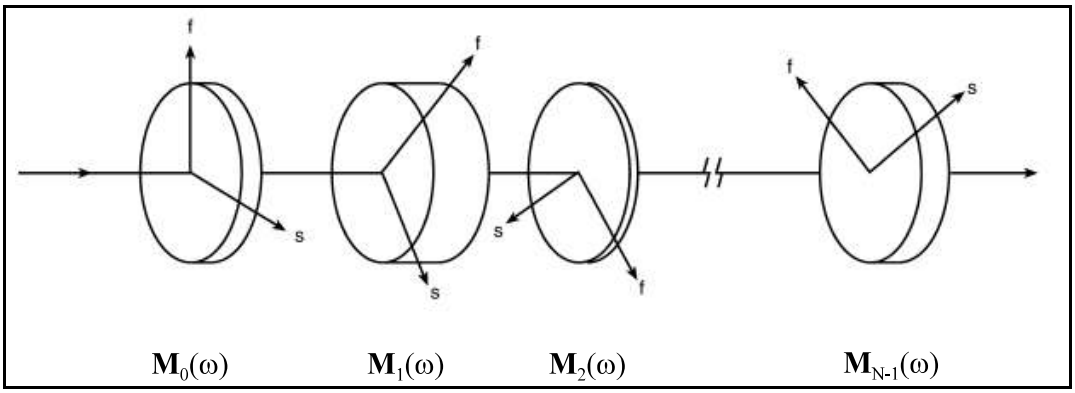

Fig. 4.3 PMD modelled by a series of cascaded waveplates [14].

Each of the waveplates in fig. 4.3 is characterized by a complex 2 by 2 Jones matrix given by

$$\mathbf{M}_i(\omega) = \begin{bmatrix} \cos\theta_i & \sin\theta_i \\ -\sin\theta_i & \cos\theta_i \end{bmatrix} \begin{bmatrix} e^{j\omega\frac{\Delta\tau_i}{2}} & 0 \\ 0 & e^{-j\omega\frac{\Delta\tau_i}{2}} \end{bmatrix}, \qquad (4.1)$$

where the first matrix introduces a rotation of the optical field into the frame of reference of the local principal states of polarization and the second one accounts for the DGD on each of the orthogonally polarized components. The rotation angles of every segment, θ_i, are random with a uniform distribution from 0 to 2π radians; the values of $\Delta\tau_i$ (in picoseconds, ps) are also drawn from a uniform distribution between 0 and a maximum value of DGD, $\Delta\tau_{max}$. Under these conditions, $\mathbf{U}(\omega)$ in eq.2.12 can be obtained as the successive multiplication [50,66,69] of the Jones matrices of each individual waveplate,

$$\mathbf{U}(\omega) = \prod_{i=0}^{N-1} \mathbf{M}_i(\omega) \quad . \tag{4.2}$$

The use of eq. 4.2 produces an optical fiber [65] with a mean DGD[2], $<\Delta\tau>$ given by

$$<\Delta\tau> \;=\; \sqrt{\frac{8N}{3\pi}} \cdot \frac{\Delta\tau_{max}}{\sqrt{3}} \quad . \tag{4.3}$$

As we wish to focus on the nature of the changes introduced solely by PMD on a single optical pulse, we will neglect the effect introduced by the fiber chromatic dispersion and fiber loss unless it is indicated otherwise. Using numerical approximation methods, [71-72], it is possible to calculate the DGD as shown in fig. 4.4a) for an optical fiber made up of 700 different waveplates and with $<\Delta\tau>$ = 20 ps. Fig 4.4b) depicts the principal output states of polarization on the Poincaré sphere for the same wavelength range as in 4.4a). Second order PMD effects are present in this case, the differential group delay depends on the frequency, $\Delta\tau = \Delta\tau(\omega)$, and so do the principal output states of polarization, $\varepsilon_{b\_\hat{u}} = \varepsilon_{b\_\hat{u}}(\omega)$.

---

[2] Throughout this thesis the notations $<\Delta\tau>$ and <DGD> are used interchangeably, as it often appears in the literature, to represent the mean differential group delay over wavelength or frequency.

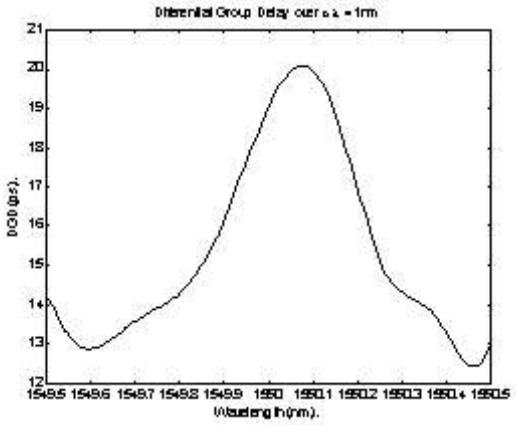

Fig. 4.4a Variation of DGD over 1 nm.

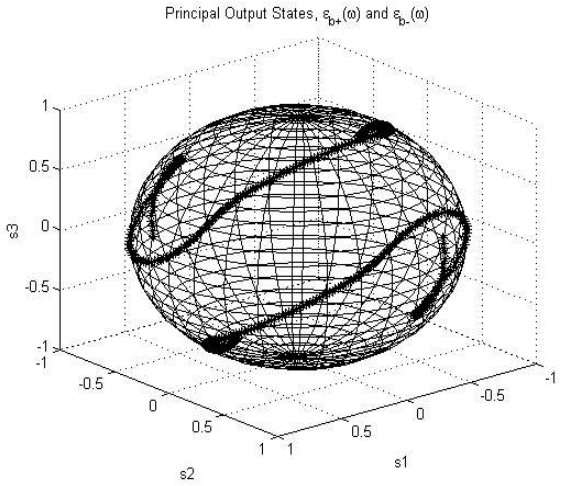

Fig. 4.4b Variation of the output PSPs over 1 nm.

4.2 THE STATISTICAL NATURE OF THE TIME IMPULSE RESPONSE

The envelope of the complex lowpass time impulse response [8] of an optical fiber with PMD given by eq. 3.9 can be expressed[3] as

$$|h_L(t)| = \sqrt{Re^2[h_L(t)] + Im^2[h_L(t)]}\ . \qquad (4.4)$$

As indicated in chapter two, the multiple birefringence along the fiber will change randomly over time. These changes will in turn, make $h_L(t)$ a stochastic quantity. In order to explore the statistical nature of $h_L(t)$, the probability distribution function of $|h_L(t)|$ was estimated through simulation.

The time varying characteristics of the fiber were accounted for by using an ensemble of 10,000 statistically independent fibers, each one consisting of 500 waveplates with a mean DGD of 20 ps. The input (output) state of polarization, ϕ (χ), was randomly chosen at the beginning of the simulation and held fixed thereafter.

---

[3] The notation Re[•] and Im[•] represent the Real and Imaginary parts of the complex number "•" respectively.

For each fiber, $|h_L(t_1)|$ was numerically calculated from eq. 4.4 for some arbitrary time instant, t_1. $\mathbf{U}(\omega)$ was calculated from eq. 4.2. The histogram for the frequency of occurrence of the different values of $|h_L(t_1)|$ is shown in fig. 4.5 along with Rayleigh and Maxwellian fits.

From fig. 4.5 we can see that a Rayleigh probability distribution is a good approximation to the distribution of the data rendered by the simulation.

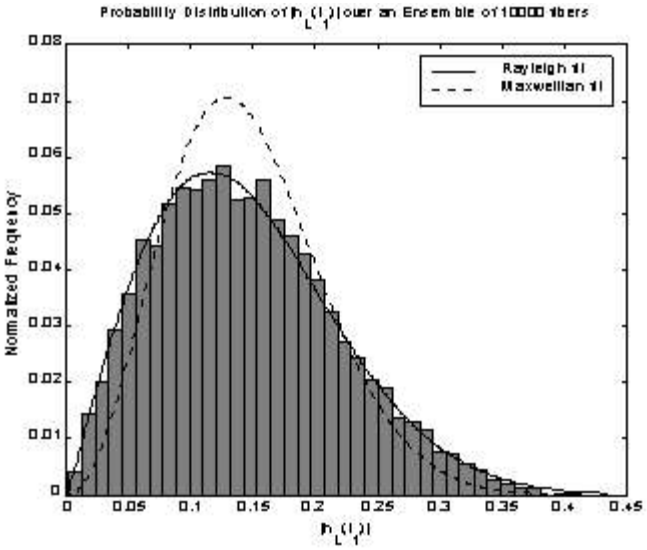

Fig. 4.5 Probability distribution of $|h_L(t_1)|$.

This hitherto unnoticed fact implies that at least from the linear time variant system point of view, a system as that from fig. 3.1 subject to time varying PMD will be equivalent to a wireless communications channel exhibiting multipath propagation on a signal transmitted through it [73]. The analogy with a wireless channel suggests the possibility of introducing a relationship between the DGD and figures of merit such as the *rms Delay Spread* [73] in order to study the system limitations imposed by PMD. This however, is beyond of the scope of this thesis and should be considered a topic for future research.

5 SOLUTION TO THE NARROWING EIGENVALUE EQUATIONS

This chapter will make use of the waveplate model previously introduced in order to analytically and numerically solve the eigenvalue equations presented in chapter three. The analytically exact solution will be calculated for the case in which the optical fiber consists of one, two and three segments of Highly-Birefringent fiber, each one having a different DGD, τ_0, τ_1 and τ_2 and with different fusion angles in between them. The solution for the more general case of a fiber made up of "n" segments of Hi-Bi fiber is numerically obtained. The existence is revealed, of two orthogonal input states of polarization, ϕ_+, ϕ_-, and two orthogonal output states of polarization, χ_+, χ_-, under which the rms-pulsewidth of the output signal is the smallest possible.

5.1 BASIC DEFINITIONS

In order to simplify the calculations and as a good approximation to a real system, a Gaussian shape of the transmitted optical power[1], $P_{in}(t)$, is assumed such that the input lowpass electric field is given by

$$E_{in}(t) = \sqrt{P_{in}(t)} = \frac{1}{\sqrt{\tau}(2\pi)^{\frac{1}{4}}} e^{\left(-\frac{t^2}{4\tau^2}\right)}, \qquad (5.1)$$

where "τ" is the rms-pulsewidth of $P_{in}(t)$. Unless indicated otherwise, τ = 25ps, which is appropriate for a 10 Gigabit per second, Gbps, system and the carrier frequency will be

[1]The electrical signal at the receiver is proportional to the optical power incident on it for an IM/DD system [8] as the one considered here.

ω_0 = 1216.1 rad/ps which corresponds to a carrier wavelength, λ_c of 1.55μm. The input electric field can be expressed in the frequency domain by using eq. 3.5 as

$$E_{in}(\omega) = \Im\{E_{in}(t)\} = \sqrt{\tau}\left(\frac{2}{\pi}\right)^{\frac{1}{4}} e^{-(\tau\omega)^2} \tag{5.2a}$$

and

$$\left|E_{in}\right|^2 = \sqrt{\frac{2}{\pi}}\tau e^{-2(\tau\omega)^2} \tag{5.2b}$$

For the sake of simplifying the calculations in the following sections, we will define the following set of functions (the proof can be found in appendix "A")

$$F_1(\Gamma) = \tau\sqrt{\frac{2}{\pi}}\int_{-\infty}^{\infty} e^{-2\tau^2\omega^2 + j\omega\Gamma} d\omega = e^{-\Gamma^2/8\tau^2} \tag{5.3a}$$

$$F_2(\Gamma) = 2\tau^3\sqrt{\frac{2}{\pi}}\int_{-\infty}^{\infty} \omega\, e^{-2\tau^2\omega^2 + j\omega\Gamma} d\omega = \frac{j\Gamma}{2} e^{-\Gamma^2/8\tau^2} \tag{5.3b}$$

$$F_3(\Gamma) = 4\tau^5\sqrt{\frac{2}{\pi}}\int_{-\infty}^{\infty} \omega^2 e^{-2\tau^2\omega^2 + j\omega\Gamma} d\omega = e^{-\Gamma^2/8\tau^2}\left(\tau^2 - \frac{\Gamma^2}{4}\right) \tag{5.3c}$$

In general, the normalized Jones vectors representing the input, ϕ, and output, χ, states of polarization will be represented [12] as

$$\varphi = \begin{bmatrix} e^{-j\gamma_1}\cos\alpha_1 \\ e^{j\gamma_1}\sin\alpha_1 \end{bmatrix}; \qquad \varphi^+ = \begin{bmatrix} e^{j\gamma_1}\cos\alpha_1 & e^{-j\gamma_1}\sin\alpha_1 \end{bmatrix} \tag{5.4a}$$

$$\chi = \begin{bmatrix} e^{-j\gamma_2}\cos\alpha_2 \\ e^{j\gamma_2}\sin\alpha_2 \end{bmatrix}; \qquad \chi^+ = \begin{bmatrix} e^{j\gamma_2}\cos\alpha_2 & e^{-j\gamma_2}\sin\alpha_2 \end{bmatrix}, \tag{5.4b}$$

with γ_1,γ_2,α_1 and α_2 being real. Fig. 5.1 shows a schematic system in which the optical fiber in fig 3.1 consists of three segments of Hi-Bi fiber with different DGDs, τ_0, τ_1 and τ_2 and fusion angles, θ_1 and θ_2, between them. Here, θ_2 is measured with respect to θ_1.

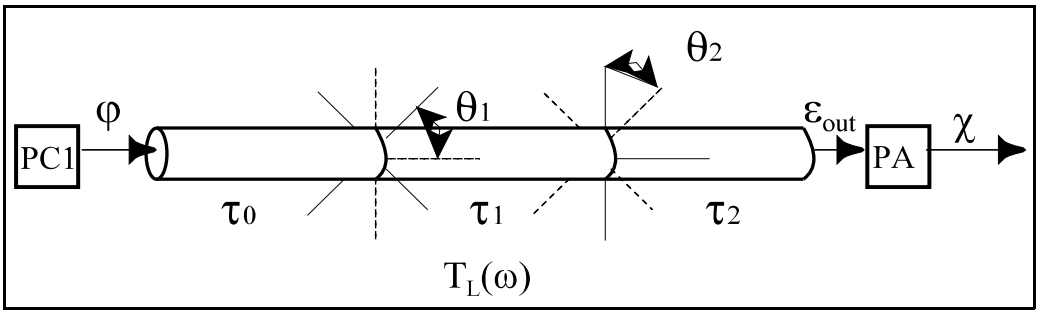

Fig. 5.1 Three segment system.

The one segment case can be obtained by aligning the three segments together, $\theta_1 = \theta_2 = 0^o$. Then the total DGD introduced will simply be the sum of the individual DGDs, $\tau_{tot} = \tau_0 + \tau_1 + \tau_2$, [25]. The two segment case can also be retrieved by aligning the first two or the last two segments, i.e. $\theta_1 = 0^o$ or $\theta_2 = \theta_1$. Without loss of generality, the analysis for the three segment case will be presented in detail and the other two cases will then be derived by setting the appropriate values of θ_1 and θ_2.

According to the waveplate model introduced in the previous chapter and eq.4.2, the complex Jones transfer matrix of the 3-segment fiber in fig.5.1 is given by

$$\mathbf{T}(\omega) = \mathbf{U}(\omega) = \prod_{i=0}^{2} \begin{bmatrix} \cos\theta_i & \sin\theta_i \\ -\sin\theta_i & \cos\theta_i \end{bmatrix} \begin{bmatrix} e^{\frac{j\omega\tau_i}{2}} & 0 \\ 0 & e^{-\frac{j\omega\tau_i}{2}} \end{bmatrix}, \qquad (5.5)$$

where we have neglected the chromatic dispersion and fiber losses. For the sake of simplicity we choose $\theta_0 = 0^o$. After multiplying out all the terms indicated in eq. 5.5 and having simplified the notation, the complex lowpass Jones transfer matrix, $\mathbf{T_L}(\omega)$ is obtained from $\mathbf{T}(\omega)$ by a simple frequency shifting [25], $\mathbf{T_L}(\omega) = \mathbf{T}(\omega+\omega_c)$ and is given by

$$T_L(\omega) = \begin{bmatrix} e^{j\omega k}w_1 + e^{j\omega l}w_2 & e^{-j\omega m}w_3 + e^{-j\omega n}w_4 \\ e^{j\omega n}w_5 + e^{j\omega m}w_6 & e^{-j\omega l}w_7 + e^{-j\omega k}w_8 \end{bmatrix} \tag{5.6a}$$

and its corresponding Hermitian is,

$$T_L^+(\omega) = \begin{bmatrix} e^{-j\omega k}w_1^* + e^{-j\omega l}w_2^* & e^{-j\omega n}w_5^* + e^{-j\omega m}w_6^* \\ e^{j\omega m}w_3^* + e^{j\omega n}w_4^* & e^{j\omega l}w_7^* + e^{j\omega k}w_8^* \end{bmatrix} . \tag{5.6b}$$

The newly introduced set of variables is defined as follows

$$\left.\begin{aligned} w_1 &= e^{j\omega_o k}\cos\theta_1\cos\theta_2\,; & w_5 &= -e^{j\omega_o n}\sin\theta_1\cos\theta_2 \\ w_2 &= -e^{j\omega_o l}\sin\theta_1\sin\theta_2\,; & w_6 &= -e^{j\omega_o m}\cos\theta_1\sin\theta_2 \\ w_3 &= e^{-j\omega_o m}\cos\theta_1\sin\theta_2\,; & w_7 &= -e^{-j\omega_o l}\sin\theta_1\sin\theta_2 \\ w_4 &= e^{-j\omega_o n}\sin\theta_1\cos\theta_2\,; & w_8 &= e^{-j\omega_o k}\cos\theta_1\cos\theta_2 \\ k &= \frac{\tau_0+\tau_1+\tau_2}{2}\,; & m &= \frac{-\tau_0-\tau_1+\tau_2}{2} \\ l &= \frac{\tau_0-\tau_1+\tau_2}{2}\,; & n &= \frac{-\tau_0+\tau_1+\tau_2}{2} \end{aligned}\right\} . \tag{5.7}$$

The final results can be further simplified by introducing the following vectors,

$$\left.\begin{aligned} w_{1234} &= \begin{bmatrix} w_1\cos\alpha_1 & w_2\cos\alpha_1 & w_3\sin\alpha_1 & w_4\sin\alpha_1 \end{bmatrix} \\ w_{5678} &= \begin{bmatrix} w_5\cos\alpha_1 & w_6\cos\alpha_1 & w_7\sin\alpha_1 & w_8\sin\alpha_1 \end{bmatrix} \\ w_{1256} &= \begin{bmatrix} w_1\cos\alpha_2 & w_2\cos\alpha_2 & w_5\sin\alpha_2 & w_6\sin\alpha_2 \end{bmatrix} \\ w_{3478} &= \begin{bmatrix} w_3\cos\alpha_2 & w_4\cos\alpha_2 & w_7\sin\alpha_2 & w_8\sin\alpha_2 \end{bmatrix} \end{aligned}\right\} . \tag{5.8}$$

In order to assess the difference between the signal rms-pulsewidths and power levels at the output of PC1 and PA in figures 3.1 and 5.1 we will make use of the *effective rms-pulsewidth* defined here as

$$\sigma_{eff} = \sigma_x - \tau \tag{5.9a}$$

where the rms-pulsewidth of the output signal, σ_x, is given by eq. 3.6.

The power of the input signal is normalized to one due to the Gaussian shape of the transmitted signal and the power of the signal at the output of the PA will be

$$P_x = \int_{-\infty}^{\infty} |E_x(\omega)|^2 d\omega = \chi^+ P_\varphi \chi = \varphi^+ P_\gamma \varphi \tag{5.9b}$$

where we made use of eq. 3.3. $\mathbf{P}_\varphi$ and $\mathbf{P}_\gamma$ are given by equations 3.12c and 3.17c respectively.

The following sections, will outline the mathematical procedure required to derive the analytically exact expressions for $\mathbf{T}_\varphi$, $\mathbf{S}_\varphi$, $\mathbf{P}_\varphi$, $\mathbf{T}_\gamma$, $\mathbf{S}_\gamma$ and $\mathbf{P}_\gamma$ as functions of the variables and functions defined in this section. The actual results are presented in Appendix B.

5.2 Power Calculations, P_ϕ

From eq. 5.2, 5.4 and 5.6 we can see that the term within the integral of eq. 3.12c is a complex 2 by 2 matrix.

$$\mathbf{T_L}(\omega)\varphi\varphi^+\mathbf{T_L^+}(\omega)|E_{in}(\omega)|^2 = \begin{bmatrix} a_1(\omega) & a_2(\omega) \\ a_3(\omega) & a_4(\omega) \end{bmatrix}. \tag{5.10}$$

Thus, $\mathbf{P}_\varphi$ will in turn be a complex 2 by 2 matrix given by

$$\mathbf{P}_\varphi = \int_{-\infty}^{\infty} \begin{bmatrix} a_1(\omega) & a_2(\omega) \\ a_3(\omega) & a_4(\omega) \end{bmatrix} d\omega = \begin{bmatrix} P_{\varphi 1} & P_{\varphi 2} \\ P_{\varphi 3} & P_{\varphi 4} \end{bmatrix} \tag{5.11a}$$

where

$$P_{\varphi_i} = \int_{-\infty}^{\infty} a_i(\omega) d\omega \; ; \qquad i = 1,\ldots,4 \quad . \tag{5.11b}$$

By making use of eqs. 5.2-4, 5.6, 5.10 and 5.11 we obtain, after considerable mathematical manipulations the results presented in eq. B.1.

5.3 POWER CALCULATIONS, P_χ

As in the previous case, the term within the integral in eq. 3.17c will be a 2 by 2 complex matrix given bv

$$\mathbf{T}_L^+(\omega)\boldsymbol{\chi}\boldsymbol{\chi}^+\mathbf{T}_L\left|E_{in}(\omega)\right|^2 = \begin{bmatrix} a_5(\omega) & a_6(\omega) \\ a_7(\omega) & a_8(\omega) \end{bmatrix} \tag{5.12}$$

Therefore, $\mathbf{P}_{\chi}$ in eq. 3.21c will also be a complex 2 by 2 matrix,

$$P_\chi = \int_{-\infty}^{\infty}\begin{bmatrix} a_5(\omega) & a_6(\omega) \\ a_7(\omega) & a_8(\omega) \end{bmatrix}d\omega = \begin{bmatrix} P_{\chi_1} & P_{\chi_2} \\ P_{\chi_3} & P_{\chi_4} \end{bmatrix} \tag{5.13a}$$

where

$$P_{\chi_i} = \int_{-\infty}^{\infty} a_{i+4}(\omega)d\omega \;; \qquad i = 1,\ldots,4 \quad . \tag{5.13b}$$

The components of $\mathbf{P}_{\chi}$ in eq. 5.13 are obtained from equations 5.2-4, 5.6 and 5.13. The final expressions for $\mathbf{P}_{\chi_1}$ to $\mathbf{P}_{\chi_4}$ are given in eq. B.2.

5.4 FIRST MOMENT CALCULATIONS, T_ϕ

Here, the procedure is essentially the same as that for the power calculations, except for the intermediate algebraic steps (not shown) which become increasingly more elaborated. The terms within the integral in eq. 3.12a will make up a 2 by 2 complex matrix.

$$j\left[\frac{d}{d\omega}\mathbf{T}_L(\omega)E_{in}(\omega)\right]\boldsymbol{\varphi}\boldsymbol{\varphi}^+\mathbf{T}_L^+(\omega)E_{in}^*(\omega) = j\begin{bmatrix} a_9(\omega) & a_{10}(\omega) \\ a_{11}(\omega) & a_{12}(\omega) \end{bmatrix}. \tag{5.14}$$

Accordingly, eq. 3.12a can be reexpressed as a 2 by 2 complex matrix given by

$$\mathbf{T}_\varphi = j\int_{-\infty}^{\infty}\begin{bmatrix} a_9(\omega) & a_{10}(\omega) \\ a_{11}(\omega) & a_{12}(\omega) \end{bmatrix}d\omega = \begin{bmatrix} T_{\varphi_1} & T_{\varphi_2} \\ T_{\varphi_3} & T_{\varphi_4} \end{bmatrix} \tag{5.15a}$$

where

$$T_{\varphi_i} = j\int_{-\infty}^{\infty} a_{8+i}(\omega)d\omega \;; \qquad i = 1,\ldots,4 \quad . \tag{5.15b}$$

The set of analytical expressions for $\mathbf{T}_{3,*}$ to $\mathbf{T}_{3,.}$ can be found in eq. B.3. Equation B.3 was obtained by using equations 5.2-4, 5.6 and 5.15.

5.5 First Moment Calculations, Tχ

The calculations for $\mathbf{T}_{\ddagger}$ are as elaborated as those for $\mathbf{T}_{3}$ and only the final results are shown in appendix B. The terms within the integral of eq. 3.17a will produce the following matrix

$$j\mathbf{T}_{\mathbf{L}}^{+}(\omega)\mathbf{E}_{in}^{*}(\omega)\chi\chi^{+}\left[\frac{d}{d\omega}\mathbf{T}_{\mathbf{L}}(\omega)\mathbf{E}_{in}(\omega)\right] = j\begin{bmatrix} a_{13}(\omega) & a_{14}(\omega) \\ a_{15}(\omega) & a_{16}(\omega) \end{bmatrix} \qquad (5.16)$$

Substituting eq. 5.16 back into eq. 3.17a gives

$$\mathbf{T}_{\chi} = j\int_{-\infty}^{\infty}\begin{bmatrix} a_{13}(\omega) & a_{14}(\omega) \\ a_{15}(\omega) & a_{16}(\omega) \end{bmatrix} = j\begin{bmatrix} T_{\chi_1} & T_{\chi_2} \\ T_{\chi_3} & T_{\chi_4} \end{bmatrix} \qquad (5.17a)$$

where

$$T_{\chi_i} = j\int_{-\infty}^{\infty} a_{12+i}(\omega)\,d\omega \qquad ; \qquad i = 1,..,4\,. \qquad (5.17b)$$

Equation B.4 is finally obtained by using eqs. 5.2-4, 5.6 and eq. 5.17.

5.6 Second Moment Calculations, Sϕ

Although the mathematical procedure required to derive the analytically exact expressions for the second moment terms, $\mathbf{S}_{3}$ and $\mathbf{S}_{\ddagger}$ is essentially the same as that from preceding sections, the algebraic manipulations are in general more intricate. Here, all the intermediate steps are skipped. Only the initial steps are illustrated and the final results are included in appendix B. After multiplying out the terms within the integral of eq. 3.12b, a 2 by 2 complex matrix results.

$$\left[\frac{d}{d\omega}\mathbf{T_L}(\omega)\mathbf{E_{in}}(\omega)\right]\boldsymbol{\varphi}\boldsymbol{\varphi}^{+}\left[\frac{d}{d\omega}\mathbf{T_L^{+}}(\omega)\mathbf{E_{in}^{*}}(\omega)\right]=\begin{bmatrix}a_{17}(\omega) & a_{18}(\omega)\\ a_{19}(\omega) & a_{20}(\omega)\end{bmatrix}. \quad (5.18)$$

Substituting eq. 5.18 back into eq. 3.12b yields

$$\mathbf{S}_{\varphi}=\int_{-\infty}^{\infty}\begin{bmatrix}a_{17}(\omega) & a_{18}(\omega)\\ a_{19}(\omega) & a_{20}(\omega)\end{bmatrix}d\omega=\begin{bmatrix}S_{\varphi_1} & S_{\varphi_2}\\ S_{\varphi_3} & S_{\varphi_4}\end{bmatrix} \quad (5.19a)$$

where

$$S_{\varphi_i}=\int_{-\infty}^{\infty}a_{16+i}(\omega)\,d\omega\ ;\qquad i=1,\ldots,4\quad . \quad (5.19b)$$

The final result in eq. B.5 makes use of equations 5.2-4, 5.6 and 5.19.

5.7 Second Moment Calculations, S_χ

Finally, the expression for the second moment factor, $\mathbf{S}_{\chi}$, is calculated by applying the same procedure. We begin by multiplying all the terms within the integral of eq. 3.17b.

$$\left[\frac{d}{d\omega}\mathbf{T_L^{+}}(\omega)\mathbf{E_{in}^{*}}(\omega)\right]\boldsymbol{\chi}\boldsymbol{\chi}^{+}\left[\frac{d}{d\omega}\mathbf{T_L}(\omega)\mathbf{E_{in}}(\omega)\right]=\begin{bmatrix}a_{21}(\omega) & a_{22}(\omega)\\ a_{23}(\omega) & a_{24}(\omega)\end{bmatrix}. \quad (5.20)$$

Substituting back eq. 5.20 into eq. 3.17b will result in another 2 by 2 complex matrix,

$$\mathbf{S}_{\chi}=\int_{-\infty}^{\infty}\begin{bmatrix}a_{21}(\omega) & a_{22}(\omega)\\ a_{23}(\omega) & a_{24}(\omega)\end{bmatrix}d\omega=\begin{bmatrix}S_{\chi_1} & S_{\chi_2}\\ S_{\chi_3} & S_{\chi_4}\end{bmatrix} \quad (5.21a)$$

where

$$S_{\chi_i}=\int_{-\infty}^{\infty}a_{20+i}(\omega)\,d\omega\quad ;\quad i=1,\ldots,4\ . \quad (5.21b)$$

The use of equations 5.2-4, 5.6 and 5.21 along with lengthy algebraic manipulations renders the result for $\mathbf{S}_{\varphi\varphi}$ to $\mathbf{S}_{\chi\chi}$ which can be found in eq. B.6.

To this point we have derived the necessary mathematical expressions for the evaluation of the eigenvalue equations presented in chapter three. In the following sections, we will gradually incorporate those results into the searching procedure depicted in fig.3.4

in order to explore the possibility of obtaining an output signal with an rms-pulsewidth smaller than the rms-pulsewidth of the input signal.

5.8 THE ONE SEGMENT CASE

In this section, we investigate the effect of varying the input and output states of polarization in a single segment of Hi-Bi fiber. To that end we resort to our three segment model and align all the segments, i.e. $\theta_1 = \theta_2 = 0^o$. We also choose a typical value of 20ps (τ_{tot}=20ps) for the DGD introduced by the fiber. As all the segments are aligned, the total DGD is equal to the sum of the DGDs of each individual segment [25]. Without loss of generality we can select $\tau_1 = \tau_2 = \tau_3 = 20/3$ ps.

The mathematical expressions for $\mathbf{T}_{\perp}$, $\mathbf{S}_{\perp}$, $\mathbf{P}_{\perp}$, $\mathbf{T}_{\parallel}$, $\mathbf{S}_{\parallel}$ and $\mathbf{P}_{\parallel}$ contained in appendix B were evaluated for the chosen values of θ_1, θ_2, τ_0, τ_1 and τ_2 and used in the searching procedure illustrated in fig. 3.4. In order to find the values ϕ_{opt} and χ_{opt} which minimize σ_x^2, the search was repeated 100 times, each time with different initial values ϕ_o and $\chi_{\perp}$. In all cases a convergence limit of 10^{-10} was used. The reason for choosing such limit was simply that neither an increase nor a decrease seemed to have any effects on the final results. The Poincaré sphere is used in fig. 5.2 to represent the initial and final values of the input state of polarization.

Figure 5.2a shows the randomly selected initial search points for ϕ and fig. 5.2b shows the final values of ϕ rendered by the search after it reached the convergence limit. The results for the output state of polarization, χ, were similar and are omitted. It seems

apparent that at least for the case of a single segment of Hi-Bi fiber, no unique solution exists.

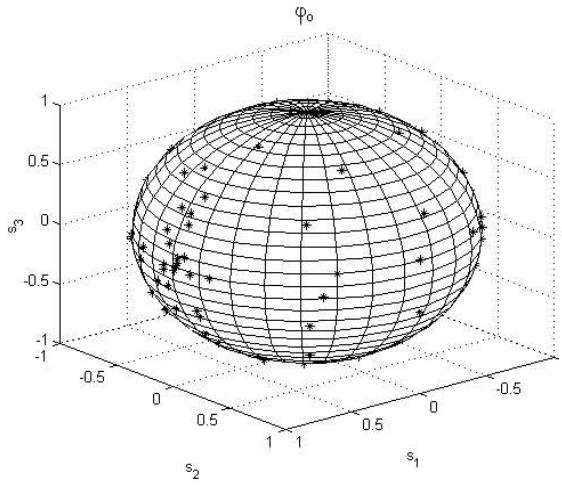

Fig. 5.2a Initial ϕ values.

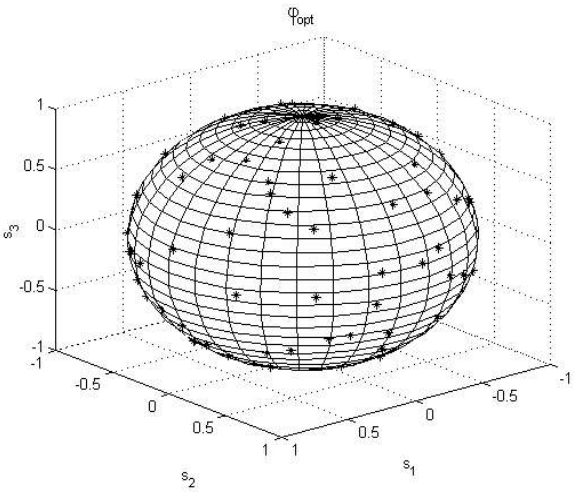

Fig. 5.2b Final ϕ values.

To show an example of one of the solutions reached, we randomly picked one set of final input and output states of polarization and used it to transmit and receive our Gaussian shaped signal of eq. 5.2. The time domain output signal, $E_x(t)$, can be obtained by taking the inverse Fourier transform of eq. 3.3. Figure 5.3 depicts that result.

Although we have been able to achieve an effective rms-pulsewidth reduction of 3.07 ps, (σ_{eff} = -3.07ps), the narrower pulse obtained contains only 6.69% of the original power. This power reduction will, in general, become the price to be paid for the improvement obtained of not only avoiding PMD induced distortion

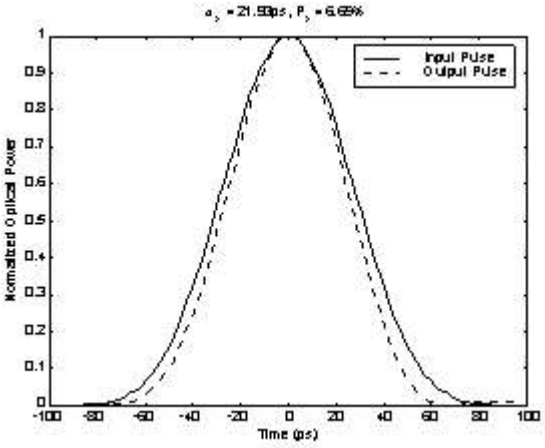

Fig. 5.3 Input and output pulses for one segment of Hi-Bi fiber.

but producing a narrower output pulse. In this section, we have analytically shown, for the first time to our knowledge, that is possible to obtain an output pulse which is narrower than the input pulse when only one segment of Hi-Bi fiber is used by appropriately adjusting the input and output states of polarization. The narrowing effect observed here cannot be credited to the influence of second or higher order PMD effects, [24,30,34,75], as these are absent for the case of a single segment of Hi-Bi fiber. From the linear systems point of view, the dependence of the time impulse response on the input and output states of polarization in eq. 3.9 is responsible for the narrowing effect. It all reduces to finding the appropriate values of χ and ϕ which produce a time impulse response (frequency response) capable of minimizing the figure of merit under study, in this case the rms-pulsewidth. A microscopic analysis of the phenomenon [76] reveals that the narrowed pulse is obtained as a result of the constructive interference of two pulses.

5.9 The Two Segment Case

Here we allow one additional degree of freedom with respect to the previous case. Our three segment model of fig.5.1 will reduce to the two segment case by setting $\theta_1 = 0^o$ and by allowing θ_2 to move freely. Although additional simulations revealed that the amount of rms-pulsewidth narrowing achievable ultimately depends on the DGD introduced by each segment of birefringent fiber and the rms-pulsewidth of the input signal, the exact correlation between those parameters was not further investigated. We will therefore confine ourselves to the use of relatively small values of DGD. For the two segment case we somewhat arbitrarily choose, $\tau_1 = \tau_2 = \tau_3 = 15$ps.

The analysis begins by setting $\theta_2 = 45^o$. The search procedure of fig. 3.4 was repeated 60 times with a convergence limit of 10^{-13} and 60 different, randomly selected, initial values of χ and ϕ. The convergence limit was chosen empirically by looking at the quality of the obtained results. Figures 5.4a through 5.4d show the initial and final values of χ and ϕ .

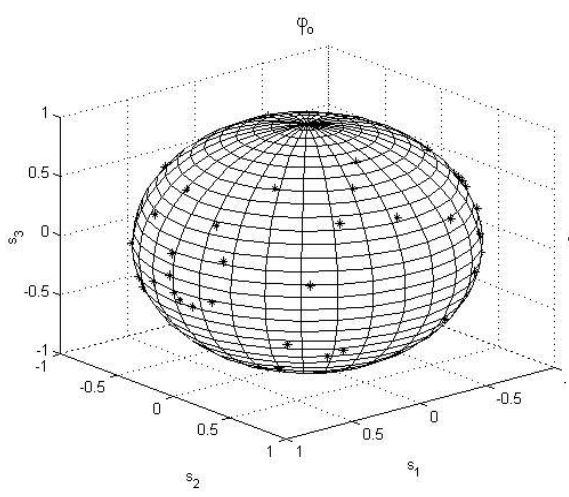

Fig. 5.4a Initial ϕ values.

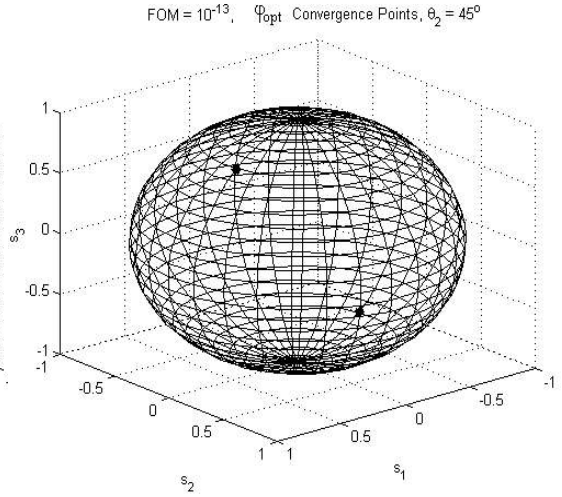

Fig. 5.4b Final ϕ values .

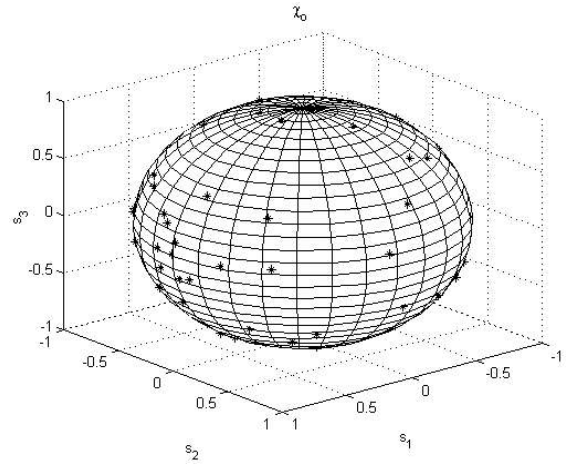

Fig. 5.4c Initial χ values .

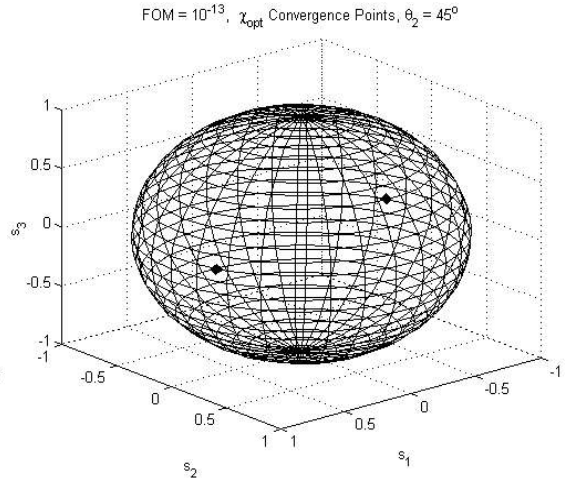

Fig. 5.4d Final χ values.

Unlike the previous single segment case, we can see from fig. 5.4 that all the original values of χ and ϕ have migrated to two diametrically opposite locations on the surface of the

Poincaré sphere.

From here on, the diametrically opposite solutions for the input (output) state of polarization will be referred as ϕ_+ and ϕ_- (χ_+ and χ_-). As ϕ_+ and ϕ_- (χ_+ and χ_-) lie on opposite points on the Poincaré sphere, then it must be true that $\phi_+^+\phi_- = 0$ ($\chi_+^+\chi_-=0$) [12]. Fig. 5.5 shows the normalized input and output pulses for a signal transmitted along ϕ_+ and received along χ_+. It can be seen that a pulse reduction of 5.85 ps with respect to the input pulse has been achieved. However the output pulse contains only a very small fraction of the power of the input pulse.

The influence of the fusion angle θ_2 on the minimum rms-pulsewidth reachable and the power level of the output signal was also studied through simulation. Fig. 5.6 shows the dependence of σ_{eff} and P_x on θ_2 when the fusion angle is rotated from 10^o to 80^o in 1^o increments. For each value of θ_2, 60 different initial values of ϕ_o and χ_o were used along with a convergence limit of 10^{-14}.

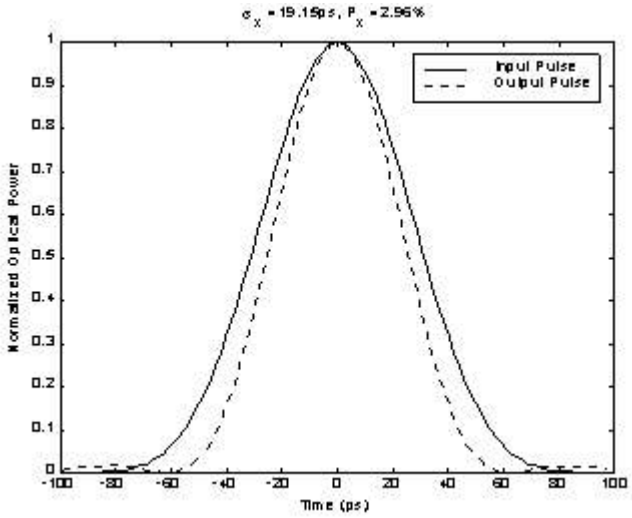

Fig 5.5 Best σ_{eff} when $\theta_1 = 0^0$ and $\theta_2 = 45^0$.

A somewhat surprising result from fig. 5.6 is the small scale of the variations of σ_{eff} with changes on θ_2. This can be explained by looking at eq. 3.4. In order to maintain a similar value of σ_{eff} when θ_2 changes, the frequency response of the two segments of Hi-Bi

fiber must remain relatively unchanged. If $\mathbf{T_L}(\omega)$ is changed in eq. 3.4 by varying θ_2, then it will be up to the input and output states of polarization to compensate that change so that $H_L(\omega)$ remains nearly the same. In fact, ϕ and χ will act like a constrained equalizer [77] in the optical domain.

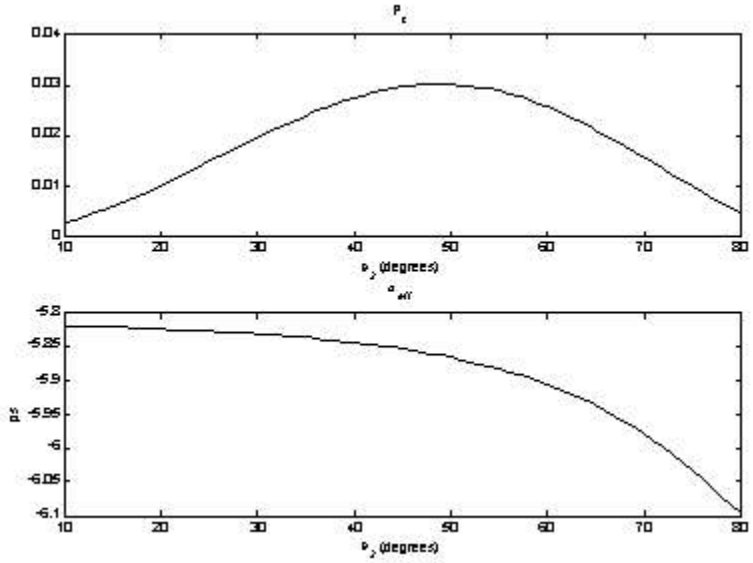

Fig. 5.6 Dependence of σ_{eff} and P_x on the fusion angle, θ_2.

Fig. 5.7 shows the expected evolution[2] of $\phi_{\pm}(\theta_2)$ and $\chi_{\pm}(\theta_2)$.

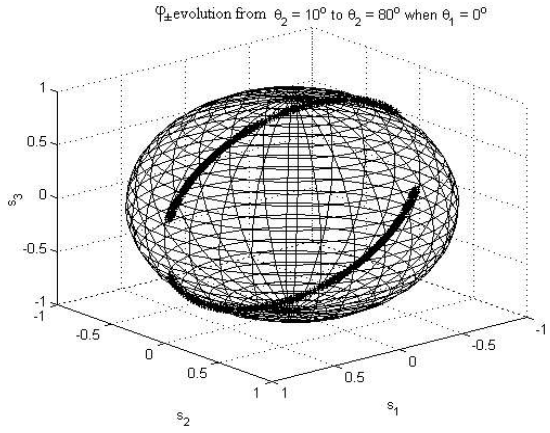

Fig. 5.7a $\phi_{\pm}$ Evolution with θ_2.

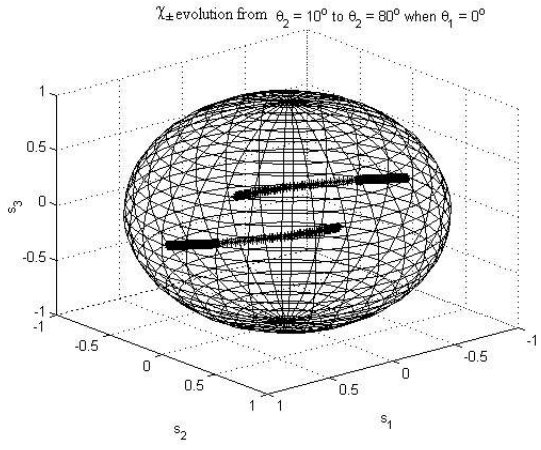

Figure 5.7b $\chi_{\pm}$ Evolution with θ_2.

[2] The "±" notation, makes reference to both orthogonal states of polarization "+" and "-".

It must be pointed out here, that in fig. 5.5, every time that θ_2 is incremented, $\phi_{\pm}$ ($\chi_{\pm}$) will move over diametrically opposite trajectories, thus maintaining its orthogonality.

We now know that σ_{eff} will have the smallest possible value when a signal is transmitted on ϕ_+ (ϕ_-) and received on χ_- (χ_+). In order to investigate the consequences of receiving a signal along χ_- and transmitting it on any other state of polarization, ϕ, we varied α_1 and γ_1 from 0 to π in eq. 5.4a and made use of equations. 3.19, 5.9a and the equations in appendix B to calculate σ_{eff}. The results for our previously analysed case of $\theta_1 = 0^o$, $\theta_2 = 45^o$, $\tau_1 = \tau_- = \tau_+ = 15$ps are shown in fig. 5.8 for the case of χ_+ reception.

Fig. 5.8a presents the change in the effective pulsewidth when α_1 and γ_+ vary from 0 to 2π in eq. 5.5a and fig. 5.8b shows its top[3] view. In reality however, it is only necessary to vary γ_+ from 0 to $\pi/2$ [16]. For that reason every input state of polarization, ϕ, will repeat twice.

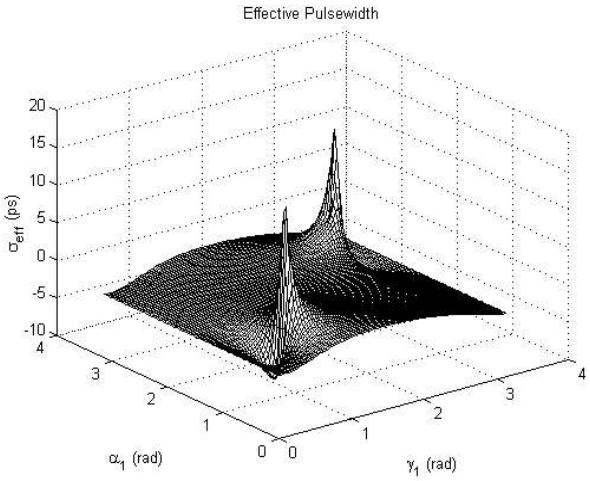

Fig. 5.8a Effective pulsewidth with χ_+ reception, $\theta_1 = 0^o$ and $\theta_2 = 45^o$.

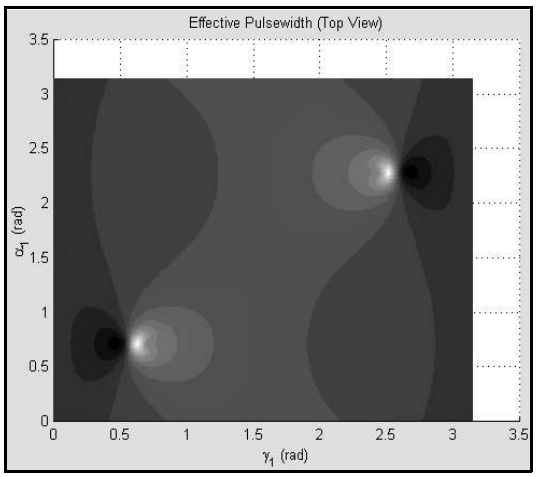

Fig. 5.8b Effective pulsewidth with χ_+ reception, $\theta_1 = 0^o$ and $\theta_2 = 45^o$ (top view).

[3]In all the top views presented in this section, light regions represent positive high numerical values whilst dark regions represent small positive or negative numerical values.

As can be seen from fig. 5.8a the value of ϕ which produces the minimum σ_{eff} ϕ_{+}, is adjacent to an input state of polarization which produces a very large positive value of σ_{eff}. The latter implies that the output signal will be broader than the input signal, which is not desirable. The behaviour of P_x for the same set of values of ϕ was obtained from eq. 5.9b by making $\chi = \chi_{-}$ and calculating $\mathbf{P}_{-}$ for multiple values of ϕ, the results are shown in fig. 5.9.

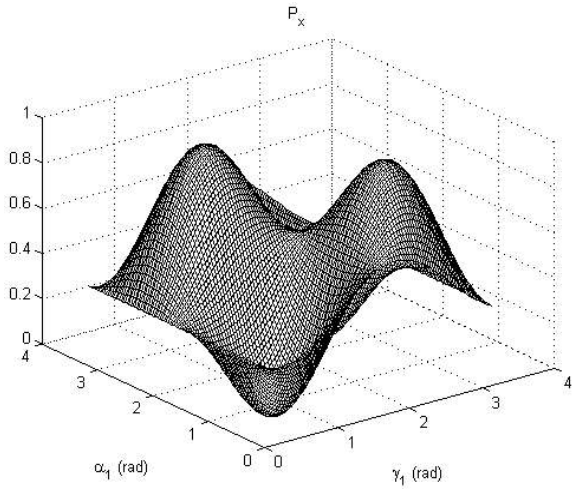

Fig. 5.9a Power of the output signal with χ_{-} reception, $\theta_1 = 0^o$ and $\theta_{-} = 45^o$.

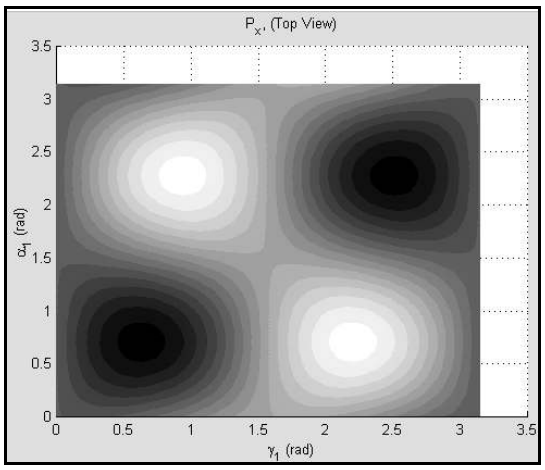

Fig. 5.9b Power of the output signal with χ_{-} reception, $\theta_1 = 0^o$ and $\theta_{-} = 45^o$ (top view).

If we overlay the two top views presented in figs. 5.8b and 5.9b we find that the region of signal narrowing / broadening falls in a very low power section of P_x. This behaviour of σ_{eff} agrees well with previously empirically obtained results, [75]. The low power levels imply that significant amplification would be required before re-transmitting or detecting the narrowed pulse. Fig. 5.10 shows the broadened output signal (obtained by transmitting on the value of ϕ which produces the maximum σ_{eff} and receiving the signal on χ_{-}) along with its power level.

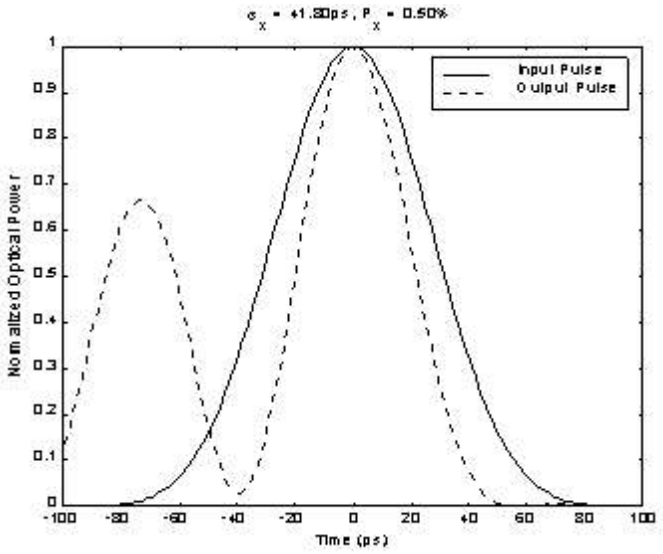

Fig. 5.10 Worst σ_{eff} when $\theta_1 = 0^0$ and $\theta_2 = 45^0$.

Fig. 5.10 helps to understand the abrupt nature of the change from best (minimum) σ_{eff} to worst (maximum) σ_{eff}. The signal with the worst value of σ_{eff} is not a single Gaussian pulse broadened, but two narrowed time-delayed pulses. A detailed analysis [76] of the output signal when ϕ is varied within the narrowing / broadening region reveals that, when ϕ is varied from the value with worst σ_{eff} to the value with best σ_{eff}, one of the two narrowed pulses shown in fig. 5.8b will quickly die out leaving only a single pulse with negative σ_{eff}.

The opposite is also true, when ϕ varies from the best σ_{eff} to the worst σ_{eff}, a second narrowed pulse will appear delayed in time with respect to the first one, thus rendering a high rms-pulsewidth of the output signal. The next section will explore the influence of ϕ and χ on the minimum rms-pulsewidth achievable for three segments of Hi-Bi fiber.

5.10 The Three Segments Case

We will now make full use of the analytical expressions contained in appendix B for the 3-segment system shown in fig. 5.1. We somewhat arbitrarily chose $\theta_1 = \theta_2 = 45^o$ and $\tau_0 = \tau_1 = \tau_2 = 15$ ps. The searching algorithm illustrated in fig 3.4 was used in order to find

ϕ_{opt} and χ_{opt}. Sixty initial random values of ϕ_o and χ_+ where used to prevent falling into a possible local minimum. The convergence limit used was 10^{-14}.

After converging, all the initial values of ϕ and χ moved to opposite points on the surface of the Poincaré sphere like in the two segment case. These two sets of orthogonal solutions[4], $\phi_\pm$ and $\chi_\pm$ produced the minimum possible value of σ_{eff}. To reach such a minimum value of σ_{eff} it is necessary to transmit the signal on ϕ_+ (ϕ_-) and receive[5] it on χ_- (χ_+).

Fig. 5.11 illustrates the behaviour of σ_{eff} when the parameters of ϕ in eq. 5.4a are varied from $-\pi$ to π and the signal is received in χ_+. The $-\pi$ to π range was chosen only for plotting purposes and as a result of that, each value of ϕ repeats several times as shown in fig. 5.11.

In fig.5.11 we can see the same coexistence of the best and worst values of σ_{eff} next to each other. This is a rather unfortunate and undesirable coincidence, as any small change in the input state of polarization from its

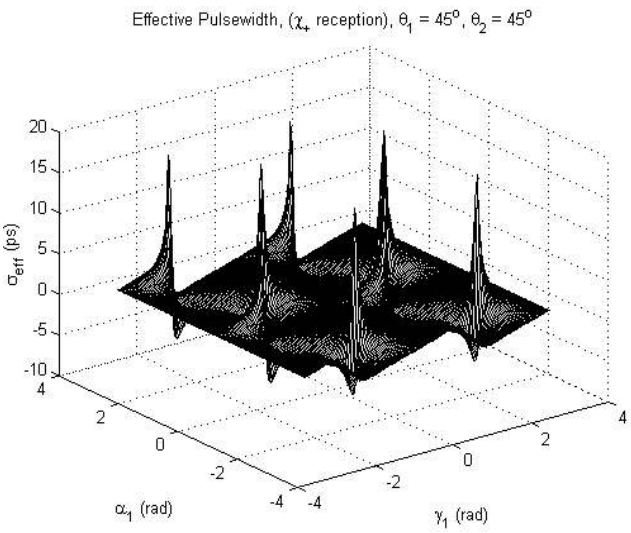

Fig. 5.11a Effective pulsewidth with χ_+ reception, $\theta_1 = 45^o$ and $\theta_2 = 45^o$.

[4] The assignment of "+" and "-" is completely arbitrary.

[5] This is true regardless of the number of segments which makes up the fiber as will be shown in the next section.

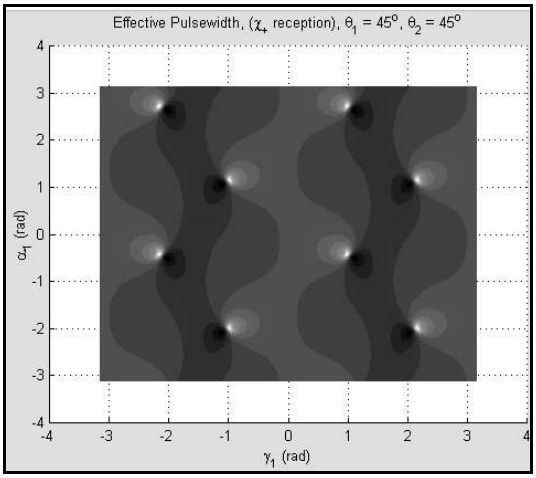

Fig. 5.11b Effective pulsewidth with χ_+ reception, $\theta_1 = 45^o$ and $\theta_2 = 45^o$ (top view).

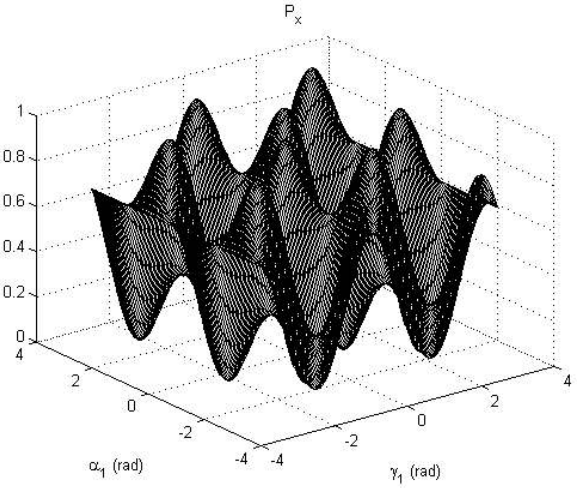

Fig. 5.12a Power of the output signal with χ_+ reception, $\theta_1 = 45^o$ & $\theta_2 = 45^o$.

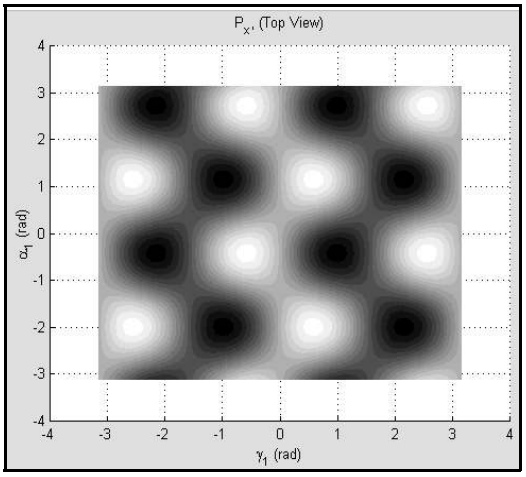

Fig. 5.12b Power of the output signal with χ_+ reception, $\theta_1 = 45^o$ & $\theta_2 = 45^o$ (top view).

optimum value, will quickly introduce the worst possible degradation in the output signal.

If we overlay figs. 5.11b and 5.12b we can see that the region of signal narrowing /broadening falls again in a low power section of P_x. This is in general the price to be paid for obtaining a narrower signal at the output[5].

Finally, figs. 5.13 and 5.14 show the narrower and broader signals obtained for the best and worst cases of σ_{eff}. As in the two segment case, a small variation of ϕ (in the wrong direction) from its optimum value will create two different, time delayed, pulses which will increase σ_{eff}.

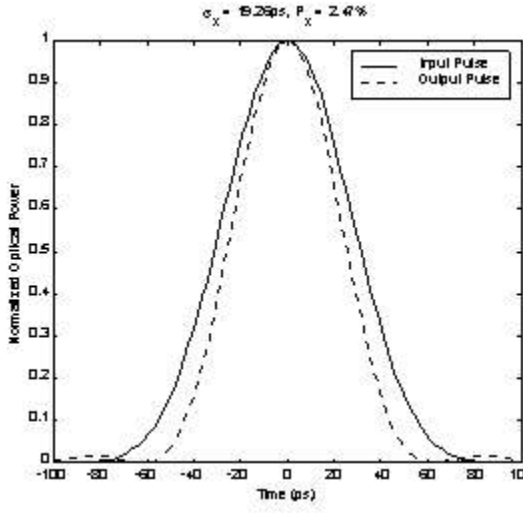

Fig 5.13 Best σ_{eff} when $\theta_1 = \theta_2 = 45^0$.

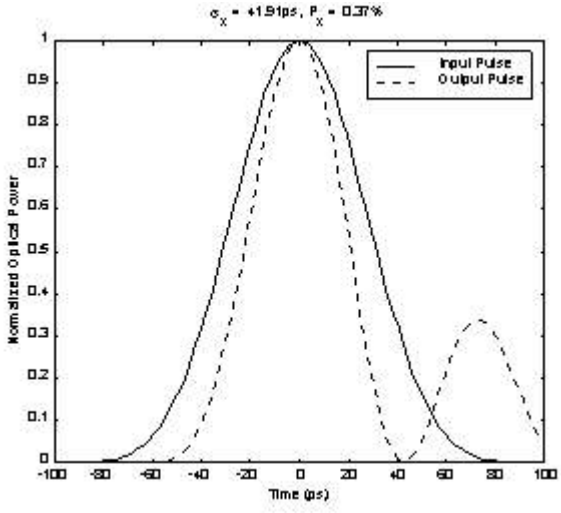

Fig 5.14 Worst σ_{eff} when $\theta_1 = \theta_2 = 45^0$.

5.11 THE n SEGMENT CASE

Until this point we have been using the analytically exact formulas from appendix B to study the rms-pulsewidth narrowing effects introduced by properly adjusting the input and output states of polarization in the system depicted in fig. 5.1. However, as mentioned in chapter two, a real fiber would consist of the concatenation of a large number of segments of Hi-Bi fiber. Each of those segments introducing a different DGD and being rotated by a different angle.

In this section we make use of the waveplate model to numerically simulate the complex lowpass Jones transfer matrix, $\mathbf{T}_L(\omega)$, of an optical fiber made up by 500, [66,78], different sections. The integrals and derivatives necessary to calculate $\mathbf{T}_1$, $\mathbf{S}_1$, $\mathbf{P}_1$, $\mathbf{T}_2$, $\mathbf{S}_2$ and $\mathbf{P}_2$ were obtained by using numerical methods [79]. The optical fiber simulated had a mean DGD of 20 ps. given by eq. 4.3.

The search procedure illustrated in fig. 3.4 was repeated 60 times, every time starting from randomly chosen values of ϕ_o and χ_o. The convergence limit used was empirically fixed at 10^{-14}. After reaching convergence, two sets of orthogonal input and output states of polarization, $\phi_{\pm}$ and $\chi_{\pm}$ were obtained. The minimum value of σ_x attained was 16.73 ps. with a power of $P_x = 0.66$ %. That was the case when transmitting the signal on ϕ_+ (ϕ_-) and receiving it on χ_- (χ_+).

Multiple searches were conducted with different simulated fibers and in each case, the existence of two sets of orthogonal input and output states of polarization, $\phi_{\pm}$ and $\chi_{\pm}$, under which an output pulse narrower than the input pulse can be obtained, was revealed. This hitherto unnoticed fact has been apparently overlooked by all the optical PMD compensation techniques proposed so far [40-50,80-88].

We now proceed to examine the changes in σ_{eff} when the output state of polarization is fixed at χ_- and the input state of polarization, ϕ, is varied. Figs. 5.15 and 5.16 show the changes in σ_{eff} and P_x with ϕ. By comparing figs. 5.8, 5.9, 5.11, 5.12, 5.15 and 5.16 we can see that the nature of the changes induced on σ_{eff} and P_x by variations of ϕ is always the same, i.e. the point of maximum pulse narrowing is always close to the point of sharp signal broadening and both fall in a region

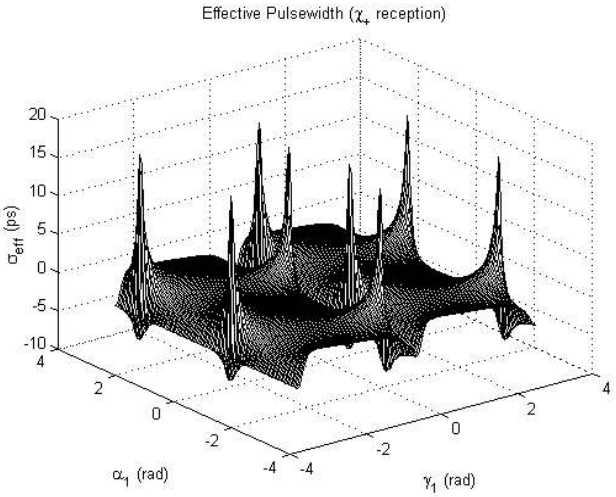

Fig. 5.15a Effective pulsewidth with χ_+ reception for a 500 segment fiber.

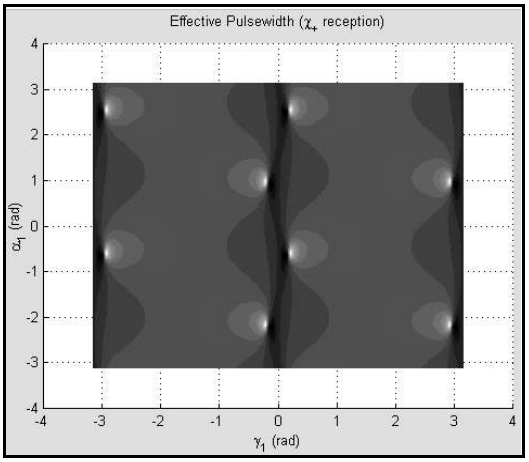

Fig. 5.15b Effective pulsewidth with χ_+ reception for a 500 segment fiber (top view).

of low power. This in fact, seems to be the case for optical fibers consisting of two, three, five hundred or any number of segments. The existence of the orthogonal polarization states $\phi_\pm$ and $\chi_\pm$ which allow us to obtain output pulses which are narrower than the input pulses in optical fibers with PMD is the main result of this chapter and indeed of this thesis.

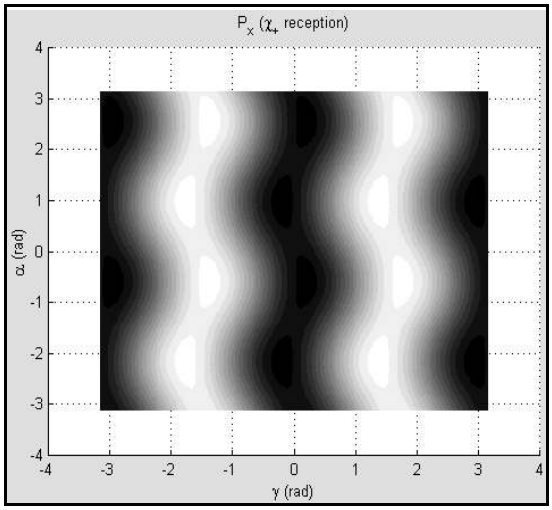

Fig. 5.16a Power of the output signal with χ_- reception for a 500 segment fiber (top view).

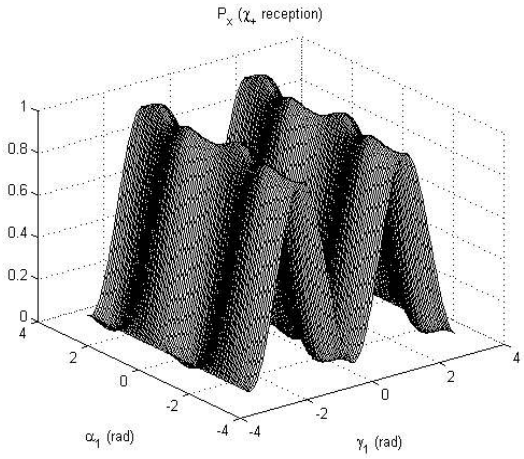

Fig. 5.16b Power of the output signal with χ_+ reception for a 500 segment fiber.

Figures 5.17 and 5.18 show the time domain output signals obtained for the best and worst values of σ_{eff}. The pulse narrowing achieved in this case, comes at the expense of an extreme loss in power. As in the previous sections, the point of maximum rms-pulsewidth corresponds to the coexistence of two narrowed pulses.

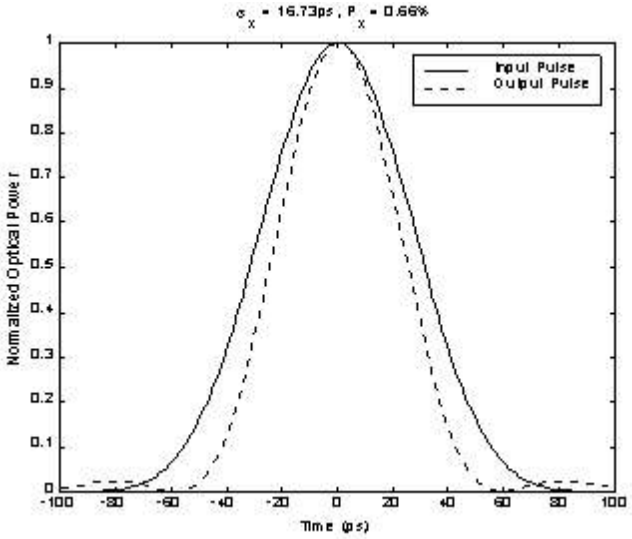

Fig. 5.17 Best σ_{eff} in an optical fiber with a mean DGD of 20 ps and made up of 500 segments of Hi-Bi fiber

All the results in this chapter confirm that, although it is possible to obtain output pulses which are narrower, [75], than input pulses by adequately choosing the launching and reception states of polarization in an optical fiber with PMD, a small drift (in the wrong direction) in the input state of polarization, ϕ, from its optimum value, $\phi_{opt,}$ will abruptly increase the rms-pulsewidth of the output signal to its worst case.

Our simulations also indicated that, regardless of the number of segments that make up the optical fiber, a sharp power loss is experienced whenever a narrower pulse is obtained at the output. In the next chapter, we look at the optimization of only one state of polarization at the time and compare the rms-pulsewidth obtained in each case.

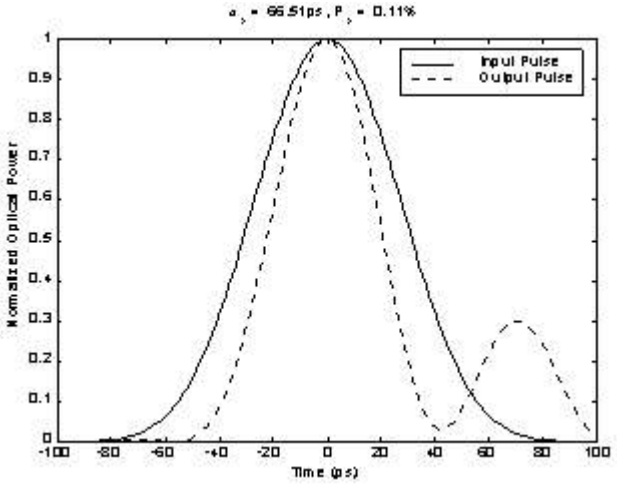

Fig. 5.18 Worst σ_{eff} in an optical fiber with a mean DGD of 20 ps and made up of 500 segments of Hi-Bi fiber

6 OPTIMIZATION PERFORMANCE

In this chapter, the optimization procedures for the input and output states of polarization introduced in figures 3.2 and 3.3 are used and their results compared with the optimization procedure of fig. 3.4, which takes into account both, the input and the output states of polarization. The benefits of properly adjusting the launching and reception states of polarization are studied by comparing the pulse shapes at the output of an optical fiber with high and low PMD when the principal input and output states of polarization, [6], are used and when the input and output states of polarization obtained through our optimization algorithms are used. Throughout this chapter, the optical fibers simulated consisted of 500 sections of Hi-Bi fiber and all the calculations needed were carried out numerically, [79].

6.1 OPTIMIZATION CONVERGENCE

In this section, the results of optimizing either the input state of polarization or the output state of polarization are compared with the case in which both input and output states of polarization are optimized to reduce the rms-pulsewidth of the output signal. Although definitive conclusions about the convergence speed of the algorithms presented in figures 3.2, 3.3 and 3.4 are difficult to draw from the simulation of a small number of optical fibers, it is hoped that the results presented in this section will shed some light into the evolution of the optimization algorithms introduced in chapter three.

In order to reach a final conclusion on the convergence speed and the quality of the results rendered by the optimization algorithms, their dependence on the initial values of ϕ and χ, (ϕ_o and χ_o), and on the mean DGD of the fiber has to be eliminated through statistical

average. This could be done by averaging the results produced by the use of multiple values of ϕ_o and χ_o along with a large enough population of fibers (~500). Such statistical average, however, would require exhaustive computer simulation and it is beyond of the scope of this thesis.

We begin by using the waveplate model presented in chapter four to simulate an optical fiber with a mean DGD of 30 ps. Next, the optimization algorithm of fig. 3.4 is used and the values of ϕ_{opt} and χ_{opt} are found. As mentioned in the previous chapter, there are actually, two solutions for ϕ_{opt} and χ_{opt}, namely $\phi_{ث}$ and $\chi_{ث}$. Knowing one solution, ϕ_+ per say, allow us to find the other soltion, ϕ_-, due to their mutually orthogonal nature, $\phi_+^+\phi_- = 0$. The worst case[1] for choosing the input (output) state of polarization would be to select a value of ϕ (χ) which is as far from ϕ_+ (χ_+) as it is from ϕ_- (χ_-). We will call such a state of polarization, the *worst case* input (output) state of polarization, and it will be represented as ϕ_{wc} (χ_{wc}).

The worst case input (output) state of polarization can easily be found (when one of the solutions is known) from $\phi_{wc}^{\wedge}\phi_{ث} = \cos(45^o)$ ($\chi_{wc}^{\wedge}\chi_{ث} = \cos(45^o)$). Once ϕ_{opt} and χ_{opt} have been found, the worst case launching and reception states of polarization, ϕ_{wc} and χ_{wc} respectively, are calculated. The input (output) worst case state of polarization, ϕ_{wc} (χ_{wc}), is then used as the given input (output) state of polarization in the optimization procedure of fig. 3.2 (fig. 3.3). This is done to ensure that the number of iterations required for the convergence of the algorithms in figs. 3.2 and 3.3 can be compared on an equal basis.

---

[1] From the point of view of minimizing the rms-pulsewidth of the output signal.

After reaching the convergence limit, the optimum output (input) state of polarization, χ_{opt} (ϕ_{opt}) is found for a given worst case input (output) state of polarization, ϕ_{wc} (χ_{wc}). It must be pointed out here that in general, the values of χ_{opt} and ϕ_{opt} obtained by the optimization algorithms in figures 3.2 and 3.3 will differ from those found by using the algorithm in fig. 3.4.

The process of using the algorithm in fig. 3.4 to find χ_{opt} and ϕ_{opt}, calculating the worst case values of ϕ and χ and applying those values to the optimization procedures of figs. 3.2 and 3.3 was repeated 78 times. Each time, a new fiber with a mean DGD of 30 ps was used. The average evolution of σ_x and P_x is shown in figures 6.1a and 6.1b respectively for the cases in which χ, ϕ and both χ and ϕ are optimized.

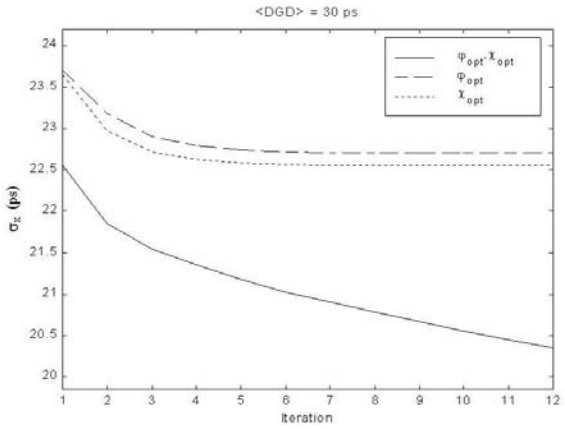

Fig. 6.1a Output pulsewidth evolution for different optimizations.

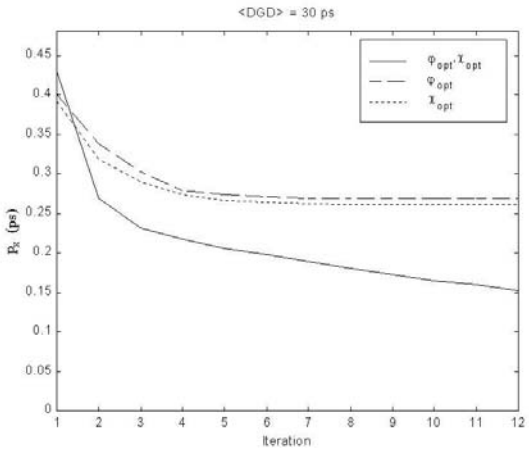

Fig. 6.1b Output power evolution for different optimizations.

Fig. 6.2 shows the average output pulses obtained by optimizing χ, ϕ and both χ and ϕ along with the input pulse and table 6.1 gives the average final values of σ_x and P_x. During each simulation, an empirically chosen convergence limit of 10^{-11} was used.

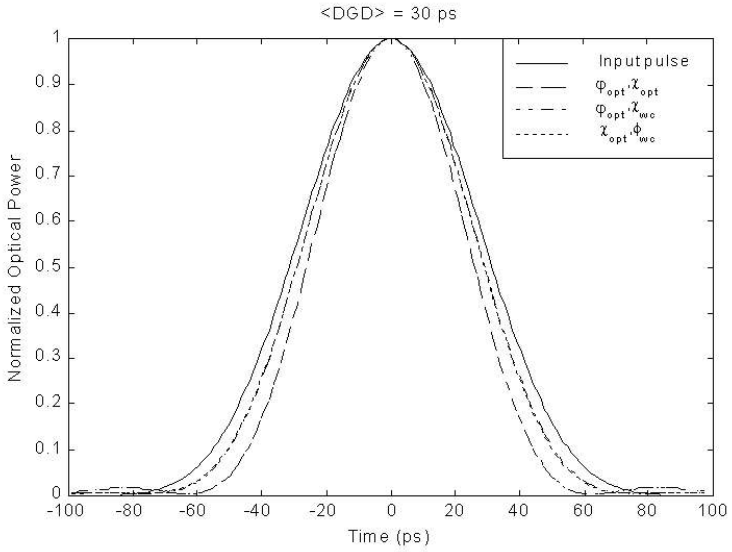

Fig. 6.2 Average output pulses for different optimizations.

Optimization:	ϕ_{opt}, χ_{opt}	ϕ_{opt}, χ_{wc}	ϕ_{wc}, χ_{opt}
σ_x **(ps)**	18.5	22.7	22.5
$\mathbf{P_x}$ **(%)**	4.1	26.9	27.2

Table 6.1 Output pulsewidths and normalized powers for different optimizations.

From figures 6.1, 6.2 and table 6.1 we can confirm what could have been intuitively assumed, the output signal will have the smallest rms-pulsewidth (and as a result the lowest power) when both degrees of freedom, ϕ and χ are jointly optimized. Our simulation results summarized in table 6.1 also seem to indicate that, on average, there is not a significant advantage in optimizing only the input state of polarization as opposed to optimizing only the output state of polarization. In both cases the minimum pulsewidth and power level of the output pulse are similar. However, such a conclusion should not be laid down without considering a larger population of fibers.

6.2 Optimum Input State Of Polarization

Several PMD compensation methods [45,51] are based on the idea of polarizing the signal at the input of the fiber along one of the principal input states of polarization, PSPs, [6]. This will produce an undistorted output signal when first order PMD dominates. However, if higher order PMD effects are relevant [24] (i.e., when the mean DGD is high or the fiber is highly mode coupled [29]) the signal at the output of the fiber will be distorted. This comes as a result of the frequency dependence of the PSPs and the DGD.

In this section, we compare the average output pulses obtained by transmitting the signal on one of the input PSPs at the carrier frequency, $\varepsilon_{a+}(\omega_c)$, and on one of the optimum input states of polarization obtained from the algorithm in fig. 3.3. The output state of polarization (ε_{out}) used for both cases, is randomly chosen. To prevent any bias[2] in the election of ε_{out}, it is initially chosen and used as the output state of polarization throughout the simulation of 100 optical fibers.

For each simulated fiber, the input principal state of polarization producing the highest power of the output signal was used as the input PSP. The algorithm of fig. 3.3 was then used to find the input state of polarization, ϕ_+, which would minimize the rms-pulsewidth of the output signal given that ε_{out} was the output state of polarization.

The comparison is made for two different scenarios, one in which all the fibers simulated had a mean DGD of 30 ps and the other where the mean DGD of the fibers was 150 ps. The normalized average input and output pulses are shown in fig. 6.3.

---

[2] Ideally, ε_{out} should be as far to any of the output PSPs as it would be from any of the output states of polarization $\chi_{\pm}$ which minimize the rms-pulsewidth of the output signal.

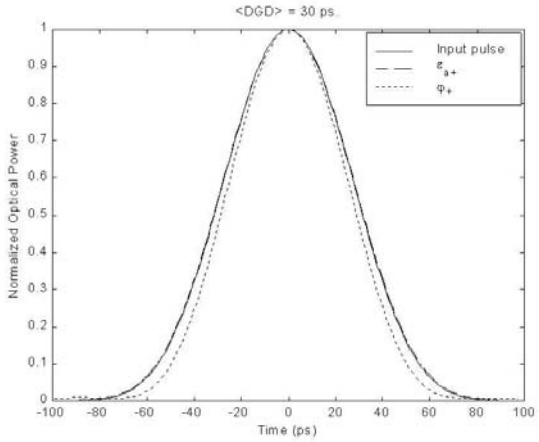

Fig. 6.3a Average output pulses for 100 fibers, low PMD (input SOP variation).

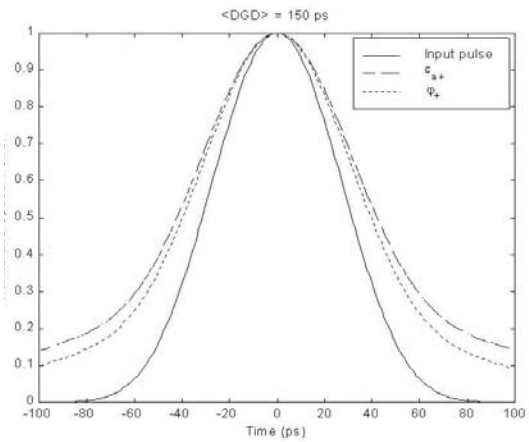

Fig. 6.3b Average output pulses for 100 fibers, high PMD (input SOP variation).

Table 6.2 summarizes the results obtained,

<DGD>	30 ps.		150 ps.	
Input SOP	$\varepsilon_{a+}(\omega_c)$	ϕ_+	$\varepsilon_{a+}(\omega_c)$	ϕ_+
σ_x **(ps)**	25.1	22.2	61.7	54.9
$\mathbf{P_x}$ **(%)**	75.4	22.2	64.7	62.7

Table 6.2 Variation of the input state of polarization (SOP).

Figure 6.3 shows that the integrity of the pulse is well preserved when fibers with low mean DGD are used. This is due to the predominance of first order PMD, i.e., $\varepsilon_{a+}(\omega_c)$ remains almost the same within the spectral range of the pulse. However the use of ϕ_+ as an input state of polarization allows the output pulse to be "compressed" with respect to the input pulse. This, despite of using a fixed output state of polarization. Pulse compression is a desirable effect when the signal is to be re-transmitted into a dispersive medium, such as an optical fiber with high chromatic or polarization dispersion at the carrier frequency.

Further simulation work is required in order to determine the exact relation between the minimum pulsewidth of the output signal, the mean DGD of the fiber and the pulsewidth of the input signal.

Interestingly, when the mean DGD of the fiber is high (fig. 6.3b), adjusting only the input state of polarization according to the algorithm of fig. 3.3 will produce a marginal improvement over the case in which the signal is transmitted on one of the input PSPs at the carrier frequency. In long-haul optical communication systems however, it is not practical to control the input state of polarization in order to improve the quality of the signal at the other end. The next section presents the situation in which the input state of polarization is fixed and the output state of polarization is varied.

6.3 Optimum Output State Of Polarization

Similar to the idea of compensating PMD induced distortion by polarizing the transmitted signal on one of the input PSPs, it is also possible to compensate PMD by receiving the signal on one of the output PSPs, [31,45]. The effectiveness of that kind of compensation will depend on the fact that the output PSPs remain the same over at least the spectral range of the signal, i.e. only first order PMD can be compensated. In this section we compare the results of compensating PMD by receiving the signal on one of the output PSPs and on one of the output states of polarization which minimize the pulsewidth of the output signal.

Throughout the calculations in this section, the input state of polarization (ε_{in}) is assumed to be known and the same for every fiber simulated. After randomly choosing ε_{in},

the algorithm from fig. 3.2 is used to find the output state of polarization χ_+ which minimizes the rms-pulsewidth of the output signal. The output PSP which produces the signal with the highest power is also calculated by using a numerical approximation [5,6]. The process is repeated for 100 different optical fibers so that any possible bias in the value of ε_{in} is averaged out.

As in the previous section, the calculations were carried out under two different scenarios. First, 100 fibers with a mean DGD of 30 ps were simulated and then 100 fibers with a mean DGD value of 150 ps were simulated. Figure 6.4 shows the output pulse obtained by averaging the output pulses from the simulated fibers with mean DGDs of 30 and 150 ps.

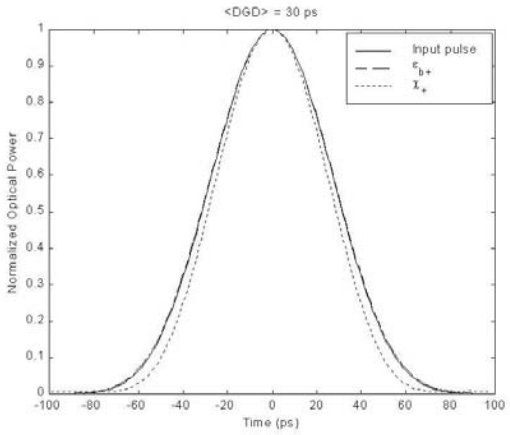

Fig. 6.4a Average output pulses for 100 fibers, low PMD (output SOP variation).

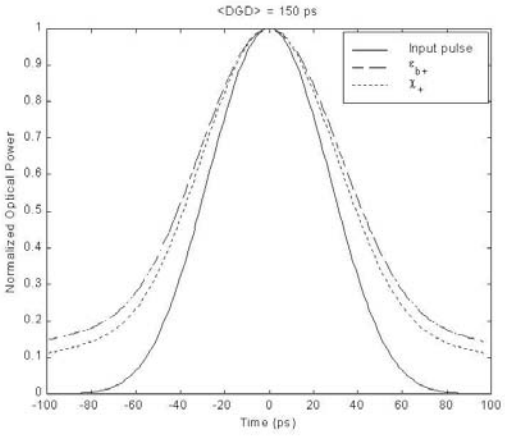

Fig. 6.4b Average output pulses for 100 fibers, high PMD (output SOP variation).

<DGD>	30 ps.		150 ps.	
Output SOP	$\varepsilon_{b+}(\omega_c)$	χ_+	$\varepsilon_{b+}(\omega_c)$	χ_+
σ_x (ps)	25.2	22.2	63.6	54.9
P_x (%)	73.3	20.9	64.9	60.4

Table 6.3 Variation of the output state of polarization.

Table 6.3 summarizes the simulation results by presenting the average output rms-pulsewidth and output pulse power for each case.

The results for the mean DGD of 30 ps presented in fig. 6.4a and table 6.3 indicate that although the input state of polarization has been fixed to an arbitrary value, it is still possible to obtain output pulses which are narrower than the input pulses when the algorithm of fig. 3.2 is used to select the output state of polarization.

In agreement with the results presented in the previous chapter, the narrowed output pulse is obtained at the expense of a reduction in its power with respect to the input pulse. Additional simulations revealed that, when the mean DGD of the fiber progressively increases, it becomes more and more difficult (and eventually impossible) to obtain output pulses which are narrower than the input pulses. Determining the exact relation between the mean DGD of the fiber and the minimum pulsewidth of the output signal is beyond of the scope of this thesis and should therefore be a topic of future research.

If the mean DGD of the fiber is high (fig. 6.4b and table 6.3), the use of the output state of polarization rendered by the optimizing algorithm of fig. 3.2 produces only a small improvement over the case in which the signal is received on one of the output PSPs.

It can be concluded from this and previous section that, when the mean DGD of the fiber is high, controlling only the input or only the output state of polarization is not sufficient to avoid pulse degradation introduced by higher order PMD effects. In a real system (where it is not practical to adjust the input state of polarization), additional optical equalization [89] would be needed along with an appropriate selection of the output state of polarization in order to obtain narrowed pulses at the output of the fiber.

7 CONCLUSIONS

7.1 SUMMARY

This thesis has presented, for the first time, the solution to a recently proposed mathematical formulation [7] which allowed us to adjust the input and output states of polarization of a signal propagating through an optical fiber with PMD in order to minimize its rms-pulsewidth at the output. This is equivalent to conducting a search for an absolute minimum in a four dimensional space.

Through numerical simulation, we studied the model of a realistic optical fiber with PMD. We have found, for the first time to our knowledge, that the statistics of the envelope of the complex lowpass time impulse response of an optical fiber with PMD are Rayleigh.

We have thus proved through simulation the previously unknown fact that for a given signal, there exist two orthogonal input and two orthogonal output states of polarization which minimize its rms-pulsewidth when it is transmitted through an optical fiber with PMD. The price to be paid for the improvement in the received signal is two fold. A reduction on the power of the output signal is introduced and a precise knowledge of the shape of the transmitted signal is required before we can calculate the optimized input and output states of polarization.

Moreover, a small misadjustment (in the wrong direction) in the optimum value of the input state of polarization will cause the rms-pulsewidth of the output signal to increase abruptly to a value considerably greater than the rms-pulsewidth of the input signal.

We also studied the benefits of using the mathematical treatment proposed by Chen

et al. [7] for the case in which only the input or the output state of polarization is varied in order to minimize the rms-pulsewidth of the output signal. We found that although it is possible to achieve pulsewidth reduction when the PMD is low, additional optical equalization would be needed if the PMD is high.

7.2 Future Research

Throughout this thesis we have neglected the influence of the chromatic dispersion introduced by the fiber and assumed no polarization dependent losses. The influence of these factors should be incorporated in a more thorough analysis.

We also confined ourselves to specific values in the mean DGD of the fibers simulated and to a particular Gaussian-shaped input signal. The impact of a change in these factors over the minimum rms-pulsewidth attainable by using the formulation proposed by Chen et al. [7] has yet to be fully assessed.

The selection of an adequate value for the convergence limit used is another point that should be further investigated. We also chose to look at the evolution of the states of polarization throughout the search and assumed that an optimum value had been reached when there was nearly no change in their value with respect to the previous iteration.

Finally, although Chen et al. [7] chose the rms-pulsewidth of the output signal as a figure of merit in his calculus of variations analysis, nothing would prevent us from trying to minimize a different figure of merit (like the mean square error, the mean absolute error or the probability of error for example) when varying the input and output states of polarization of the signal.

REFERENCES

[1] R. Castelli and T. Krause, "Market trends and evolution for optical transmission systems," *Alcatel Telecommunications Review*, pp. 165-175, 3rd Quarter 1998

[2] Nortel Networks Report, "Nortel's technology perspectives," pp. 1-6, Monday October 19, 1998

[3] G.P. Agrawal, *Fiber-Optic Communication Systems,* Second Edition, New York, NY, USA, John Wiley & Sons Inc. 1997

[4] K. Brown, X. Bao, J. Cameron, L. Chen, J. Stears, W. Hickey and R. Cormier, "Testing of fibers in an existing network for high speed system (10 Gb/s or greater) compatibility," *Proc. Photonics North, International Conference on the Application of Photonic Technology*, Quebec City, Canada, June 12 to16, 2000

[5] M. O'Sullivan, Nortel Networks, *Internal Technical Report on the tolerance of OC-192 and OC-48 equipment to PMD,* Private Communication December 15, 1998

[6] C.D. Poole and R.E. Wagner, "Phenomenological approach to polarisation mode dispersion in long single mode fibers," *Electronics Letters*, Vol. 22, No. 19, pp. 1029-1030, September 11, 1986

[7] L. Chen, "Minimum pulse broadening by optimizing by launch and receiver polarization in single mode fiber with polarization mode dispersion," *Internal Technical Report, Department of Physics, The University of New Brunswick,* Unpublished, 1999

[8] J.G. Proakis, *Digital Communications*, Third Edition, New York, NY, USA: McGraw-Hill, 1995

[9] C.D. Poole, R.W. Tkach, A.R. Chraplyvy and D.A. Fishman, "Fading in lightwave systems due to polarization mode dispersion," *IEEE Photonics Technology Letters*, Vol. 3, No.1, pp. 68-70, January 1991

[10] R.E. Wagner and A.F. Elrefaie, "Polarization dispersion limitations in lightwave systems," *Tech. Dig. Optical Fiber Communication Conference OFC'88*, p. 37, New Orleans, LA., January 25-28, 1988

[11] E. Udd, *Fiber Optic Sensors: An Introduction for Engineers and Scientists,* NewYork, NY, USA, John Wiley & Sons Inc. 1991

[12] E. Hecht *Optics,* Second Edition, Addison-Wesley, 1988

[13] J.D. Kraus, Electromagnetics, Third Edition, McGraw-Hill, New York, NY, USA, 1984

[14] G.W. Schinn, "Polarized light in so-called "single-mode" fiber: not as simple as you may think," http://www.lark.ieee.ca/library/9801shinn/shinn.htm, last accessed on May 1st of 2000

[15] F. Kapron, A. Dori, J. Peters and H. Knehr, "Polarization mode disperion: should you be concerned ?," *Proc. NFOEC'96*, pp. 1-12

[16] J. Cameron, X. Bao and J. Stears, "Field measurements of polarization mode dispersion," *Fiber and Integrated Optics,* Vol.18, No.1, pp. 49-59

[17] J. Cameron, L. Chen, X. Bao and J. Stears, "Time evolution of polarization mode dispersion in optical fibers," *IEEE Photonics Technology Letters,* Vol. 10, No. 9, pp.

1265-1267, September 1998

[18] B.W. Hakki, "Polarization mode dispersion in a single mode fiber," *IEEE Journal of Lightwave Technology*, Vol. 14, No. 10, pp. 2202-2208, October 1996

[19] Hernday Paul, "Polarization mode dispersion measurement by the Jones matrix eigenanalysis and wavelength scanning methods", *Hewlett Packard Lightwave Operations Technical Report*., Santa Rosa, CA, USA, January 1997

[20] I.P. Kaminow and T.L. Koch, *Optical Fiber Telecommunications, IIIA*, San Diego CA, USA, Academic Press, 1997

[21] B. Clesca, J.-P. Thiery, L. Pierre, V. Havard and F. Bruyère, "Bit rate degradation related to differential group delay and input polarisation for 10-Gbit/s terrestrial systems in the presence of chromatic dispersion and polarisation mode dispersion," *Proc. 21st European Conference on optical Communications, ECOC'95*, pp. 581-584, Brussels, Belgium, Sept 1995

[22] H. Taga, Msuzuki and Y. Namihira, "Polarisation mode dispersion tolerance of 10Gbit/s NRZ and RZ optical signals," *Electronics Letters*, Vol. 34, No. 22 pp. 2098-2100, October 1998

[23] F. Curti, B. Daino, Q. Mao and F. Matera, "Concatenation of polarisation dispersion in single-mode fibers," *Electronics Letters*, Vol. 25, No. 4, pp. 290-292, February 1989

[24] C.D. Poole and R.C. Giles, "Polarization-dependent pulse compression and broadening due to polarization dispersion in dispersion-shifted fiber," *Optics Letters*, Vol. 13, No. 2, pp. 155-157, February 1988

[25] N. Gisin and J.P. Pellaux, "Polarization mode dispersion: time versus frequency domains," *Optics Communications*, Vol. 89, pp. 316-323, May 1992

[26] C.D. Poole, J.H. Winters and J.A. Nagel, "Dynamical equation for polarization dispersion," *Optics Letters*, Vol. 16, No. 6, pp. 372-374, March 1991

[27] P. Ciprut, B. Gisin, and R. Passy, "Second-order polarization mode dispersion impact on analog and digital transmissions," *IEEE Journal of Lightwave Technology*, Vol. 16, No. 5, pp. 757-771, May 1998

[28] LM. Gleeson, ESR. Sikora and MJ. Mahoney, "Experimental and numerical investigation into the penalties induced by second order polarisation mode dispersion at 10 Gb/s," *IEE International Conference on Integrated Optics and Optical Fiber Communications*, pp.15-18, Stevenage, UK, September 22-25, 1997

[29] D. Penninckx and F. Bruyère, "Impact of the statistics of second-order polarization mode dispersion on system performance," *Tech. Dig. Optical Fiber Communication Conference OFC'98*, pp.340-342, San Jose, CA, US, February 22-27, 1998

[30] C. Vasallo, "PMD pulse deformation," *Electronics Letters*, Vol. 31, No. 18, pp.1597-1598, August 1995

[31] H. Sunnerud, M. Karlsson and P.A. Anderkson, "Analytic theory for PMD-compensation," *IEEE Photonics Technology Letters*, Vol. 12, No. 1, pp.50-52, January 2000

[32] M. Karlsson, "Polarization mode dispersion-induced pulse broadening in optical fibers," *Optics Letters*, Vol. 23, No. 9, pp. 688-690, May 1998

[33] F. Bruyère, "Impact of first and second order PMD in optical digital transmission systems," *Optical Fiber Technology,* Vol. 2, No. 3, pp. 269-280, July 1996

[34] C. Francia, F. Bruyère, D. Penninckx and M. Chbat, "PMD second order effects on pulse propagation in single-mode optical fibers," *IEEE Photonics Technology Letters,* Vol. 10, No. 12, pp. 1739-1741, December 1992

[35] S. Betti, F. Curti, B. Daino, G. De Marchis, E. Iannone and F. Matera, "Evolution of the bandwidth of the principal states of polarization in single-mode fibers," *Optics Letters,* Vol. 16, No. 7, pp. 467-469, April 1991

[36] M. Shtaif, A. Mecozzi and J.A. Nagel, "Mean-square magnitude of all orders of polarization mode dispersion and the relation with the bandwidth of the principal states," *IEEE Photonics Technology Letters,* Vol. 12, No. 1, pp. 53-55, January 2000

[37] H. Bülow, "System outage probability due to first and second order PMD," *IEEE Photonics Technology Letters,* Vol. 10, No. 5, May 1998

[38] F. Bruyère, L. Pierre, J.P. Thiery and B. Clesca, "Penalties induced by higher-order PMD at 10 Gbit/s in nondispersion-shifted fibers," *Tech. Dig. Optical Fiber Communication Conference OFC'97,* pp.113-114, Dallas, TX, US, February 16-21, 1997

[39] D. Mahgerefteh and C.R. Menyuk, "Effect of first order PMD compensation on the statistics of pulse broadening in a fiber with randomly varying birefringence," *IEEE Photonics Technology Letters,* Vol. 11, No. 3, pp. 340-342, March 1999

[40] D. Watley, K. Farley, B. Shaw, W. Lee, G. Bordogna, A. Hadjifotiou and R. Epworth, "Compensation of polarisation-mode dispersion exceeding one bit period using single high-birefringent fiber," *Electronics Letters,* Vol. 35, No. 13, pp. 1094-1095, June 1999

[41] F. Roy, C. Francia, F. Bruyère and D. Penninckx, "A simple dynamic polarization mode dispersion compensator ," *Proc. Optical Fiber Communications Conference, OFC'99,* pp. TuS4-1/275 - TuS4-4/278, SanDiego, CA, US, February 1999

[42] T. Takahashi, T. Imai and M. Aiki, "Automatic compensation for timewise fluctuating polarisation mode dispersion in in-line amplifier systems," *Electronics Letters,* Vol. 30, No. 4, pp. 348-349, February 1994

[43] F. Heismann, D.A. Fishman and D.L. Wilson, "Automatic compensation of first-order polarization mode dispersion in a 10 Gb/s transmission system," *Proc. European Conference on Optical Communications, ECOC'98,* pp. 529-530, Madrid, Spain, September 1998

[44] B.W. Hakki, "Polarization mode dispersion compensation by phase diversity detection," *IEEE Photonics Technology Letters,* Vol. 9, No. 1, pp. 121-123, January 1997

[45] Z. Haas, C.D. Poole, M. Santoro and J.H. Winters, "Fiber-optic polarization dependent distortion compensation," *United States Patent,* patent number: 5,311,346 May 10, 1994

[46] R. Noé, D. Sandel, M. Yoshid-Dierolf, S. Hinz, V. Mirvoda, A. Schöpflin and C. Glingener, "Polarization mode dispersion compensation at 10, 20 and 40 Gb/s with various optical equalizers," *IEEE Journal of Lightwave Technology,* Vol. 17, No.

9, pp. 1602-1616, September 1999

[47] H. Rosenfeldt, R. Ulrich, U. Feiste, R. Ludwig, H.G. weber and A. Ehrhardt, "First order PMD-compensation in a 10 Gbit/s NRZ field experiment using a polarimetric feedback-signal," *Proc. European Conference on Optical Communications, ECOC'99,* pp. II-134 to II-135, Nice, France, September 1999

[48] M.W. Chbat, J-P. Soigné, T. Fuerst, J.T. Anthony and D. Penninckx, "Long term field demonstration of optical PMD compensation on an installed OC-192 link," *Post- Deadline Papers, Optical Fiber Communications Conference, OFC'99,* pp. PD12-1 to PD29-3, SanDiego, CA, US, February 1999

[49] C. Francia, F. Bruyère, J. Thiéry and D. Penninckx, "Simple dynamic polarisation mode dispersion compensator," *Electronics Letters,* Vol. 35, No. 5 pp. 414-415, March 1999

[50] J. Winters, Z. Haas, M. Santoro and A. Ganuck, "Optical equalization of polarization dispersion," in *Proceedings, Multigigabit Fiber Communications, SPIE,* Vol. 1787, pp. 346-357, 1992

[51] T. Ono, S. Yamazaki, H. Shimizu and K. Emura, "Polarization control method for suppressing polarization mode dispersion influence in optical transmission systems," IEEE Journal of Lightwave Technology, Vol. 12, No. 5, pp. 891-898, May 1994

[52] A.F. Elrefaie and R.E. Wagner, "Chromatic dispersion limitations in coherent optical fiber transmission systems," *Electronics Letters,* Vol. 23, No. 14, pp. 756-758, July 1987

[53] P. Nouchi, H.Laklalech, P. Sansonetti, J. Von Wirth, J. Ramos, F. Bruyère, C. Brehm, J.Y. Boniort and B. Perrin, "Low-PMD dispersion compensating fibers," *Proc. 21st European Conference on optical Communications, ECOC'95,* pp. 389-392, Brussels, Belgium, Sept 1995

[54] G.J. Foschini and C.D. Poole, "Statistical theory of polarization dispersion in single mode fibers," *IEEE Journal of Lightwave Technology,* Vol. 9, No. 11, pp. 1439-1456, November 1991

[55] F. Curti, B. Daino, G. De Marchis and F. Matera, "Statistical treatment of the evolution of the principal states of polarization in single-mode fibers," *IEEE Journal of Lightwave Technology,* Vol. 8, No. 8, pp. 1162-1165, August 1990

[56] C.D. Poole, "Statistical treatment of polarization dispersion in single-mode fiber," *Optics Letters,* Vol. 13, No. 8, pp. 687-689, August 1988

[57] N. Gisin, R. Passy, J.C. Bishoff, and B. Perny, "Experimental Investigation of the Statistical Properties of Polarization Mode Dispersion in Single Mode Fibers," *IEEE Photonics Technology Letters,* Vol. 5, No. 7, pp. 819-821, July 1993

[58] C. De Angelis, A. Galtarossa, G. Gianello, F. Matera and M. Schiano, "Time evolution of polarization mode dispersion in long terrestrial links," *IEEE Journal of Lightwave Technology,* Vol. 10, No. 5, pp. 552-555, May 1995

[59] T. Takahashi, T. Imai and M. Aiki, "Time evolution of polarization mode dispersion in 120 km installed optical submarine cable," *Electronics Letters,* Vol. 29, No. 18, pp.1605-1606, September 1993

[60] J.H. Winters, M.A. Santoro and Z. Haas, "On the experimental measurements of

PMD effects," *Proceedings of the SPIE - The International Society for Optical Engineering*, Vol. 1784, pp. 31-40

[61] C.D. Poole, N.S. Bergano, R.E. Wagner and H.J. Schulte, "Polarization dispersion and principal states in 147-km undersea lightwave cable," *IEEE Journal of Lightwave Technology*, Vol. 6, No. 7, pp. 1185-1190, July 1988

[62] J. Bülow, W. Baumert, H. Scmuck, F. Mohr, T. Sculz, F. Küppers, W. Weiershausen, "Measurements of maximum speed of PMD fluctuation in installed field fiber," *Proc. Optical Fiber Communications Conference, OFC'99*, pp. WE4-1/83 - WE4-3/85, San Diego, CA, US, February 1999

[63] T. Okoshi, N. Fuyaka and K. Kikuchi, "New polarisation-state control device: rotatable fibre cranks," *Electronics Letters*, Vol. 21, No. 20, pp. 895-896, September 1985

[64] H. Shimizu, S. Yamazaki, T. Ono and K. Emura, "Highly practical fiber squeezer polarization controller," *IEEE Journal of Lightwave Technology*, Vol. 9, No. 10, pp. 1217-1223, October 1991

[65] C.D. Poole and D.L. Favin, "Polarization-mode dispersion measurements based on transmission spectra through a polarizer," *IEEE Journal of Lightwave Technology*, Vol. 12, No. 6, pp. 917-929, June 1994

[66] J.P. Elbers, C. Glingener, M. Düser and E. Voges, "Modelling of polarisation mode dispersion in single mode fibers," *Electronics Letters*, Vol. 33, No. 22, pp. 1894-1895, October 1997

[67] U. Brechtken-Manderscheid, *Introduction to the Calculus of Variations*, Chapman & Hall Mathematics, 1991

[68] J. Cameron, L. Chen and X. Bao, "Impact of chromatic dispersion on the system limitation due to polarization mode dispersion," *IEEE Photonics Technology Letters*, Vol. 12, No. 1, pp. 47-49, January 2000

[69] D.R. Desbruslais and P.R. Morkel, "Simulation of polarisation mode dispersion and its effects in long-haul optically amplified lightwave systems," *IEE Colloquium on 'International Transmission System'*, Digest No.1994/039, pp. 67, 6/1-6, London, UK; 15 February, 1994

[70] P.A. Williams and C.M. Wang, "Corrections to fixed analyser measurements of polarization mode dispersion," *IEEE Journal of Lightwave Technology*, Vol. 16, No. 4, pp. 534-541, June 1994

[71] B.L. Heffner, "Accurate, automated measurement of differential group delay dispersion and principal state variation using Jones matrix eigenanalysis," *IEEE Photonics Technology Letters*, Vol. 5, No. 7, pp. 814-817, July 1993

[72] B.L. Heffner, "Automated measurement of polarization mode dispersion using Jones matrix eigenanalysis," *IEEE Photonics Technology Letters*, Vol. 4, No. 9, pp. 1066-1069, September 1992

[73] T.S. Rappaport, *Wireless Communications*, New Jersey, USA, Prentice-Hall 1996

[74] C.H. Prola, J.A. Pereira, A.O. Dal Forno, R. Passy, J.P. von der Weid and N. Gisin, "PMD emulators and signal distortion in 2.48-Gb/s IM-DD lightwave systems," *IEEE Photonics Technology Letters*, Vol. 9, No. 6, pp. 842-844, June 1997

[75] J. Cameron, L. Chen and X. Bao, "Anomalous pulse-width narrowing with first-order compensation of polarization mode dispersion," to appear in *Optics Letters*

[76] J. Cameron, Private Communication, March'2000.

[77] S. Haykin, *Adaptive Filter Theory*, Third Edition, USA, Prentice-Hall 1996

[78] L. Chen, M. Yañez, X. Bao and B.R. Petersen, "Pulse narrowing in optical components with polarization mode dispersion using polarization controls," *Proc. Photonics North, International Conference on the Application of Photonic Technology*, Quebec City, Canada, June 12 to16, 2000

[79] *MATLAB, The Language of Technical Computing, Using MATLAB*, The Mathworks Inc. December 1996

[80] J. Patscher and R. Eckhardt, "Component for second-order compensation of polarisation-mode dispersion," *Electronics Letters*, Vol. 33, No. 13, pp. 1157-1159, June 1997

[81] T. Ozeki and T. Kudo, "Adaptive equalization of polarization mode-dispersion," *Proc. Optical Fiber Communications Conference, OFC'93*, pp.143 - 144,Washington D.C., US, February 1993

[82] J.H. Winters and M.A. Santoro, "Experimental equalization of polarization dispersion," *IEEE Photonics Technology Letters*, vol. 2, No. 8, pp. 591-593, August 1990

[83] D. Schlump, B. Wedding and H. Bülow, "Electronic equalisation of PMD and chromatic dispersion induced distortion after 100 km standard fibre at 10 Gbit/s," *Proc. European Conference on Optical Communications, ECOC'98*, pp. 535-535, Madrid, Spain, September 1998

[84] H. Bülow, D. Schlump, J. Weber, B. Wedding and R.Heidemann, "Electronic equalization of fiber PMD-induced distortion at 10 Gbit/s," *Proc. Optical Fiber Communications Conference, OFC'98*, pp.151 -152, San Jose, CA, US, February 22-27, 1998

[85] T. Ozeki, M. Yoshimura, T. Kudo and H. Ibe "Polarization-mode-dispersion equalization experiment using a variable equalizing optical circuit controlled by a pulse-waveform-comparison algorithm," *Proc. Optical Fiber Communications Conference, OFC'94*, pp.68 -64, February 1994

[86] S. Lee, R. Khosravani, J. Peng, V. Grubsky, D.S. Stardubov, A.E. Willner and J. Feinberg, "Adjustable compensation of polarization mode dispersion using a high-birefringent nonlinearly chirped fiber bragg grating," *IEEE Photonics Technology Letters*, Vol. 11, No. 10, pp. 1277-1279, October 1999

[87] R. Noé, D. Sandel, M. Yoshida-Dierolf, D. Hinz, C. Glingener, C. Scheerer, A. Schöpflin and G. Fischer, "Polarisation mode dispersion compensation at 20Gbit/s with fiber-based distributed equaliser," *Electronics Letters*, Vol. 34, No. 25, pp. 2421-2422, December 1998

[88] M. Yoshimura, T. Kudo and T. Ozeki, "Polarization mode dispersion equalization," *Tech. Dig. Fifth Optoelectronics Conference (OEC'94)*, pp. 258-259, Tokyo, Japan, July 12-15 1994

[89] T. Ozeki, "Optical equalizers," *Optics Letters*, Vol. 17, No. 5, pp. 375-377, March

1992

[90] L.S. Gradshteyn and I.M. Ryzhik, *Table of Integrals, Series, and Products,* Second Edition, United Kingdom Academic Press, 1994

[91] W. Shieh, "Principal states of polarization for an optical pulse," *IEEE Photonics Technology Letters*, Vol. 11, No. 6, pp. 677-679, June 1999

[92] J. Cameron, L. Chen and X. Bao, "Limitations of first order PMD compensation techniques in the presence of chromatic dispersion," *Optics Communications,* Vol. 171, pp. 15-21, November 1999

[93] J. Zhou and M.J. O'Mahony, "Optical transmission system penalties due to fiber polarization mode dispersion," *IEEE Photonics Technology Letters*, Vol. 6, No. 10, pp. 1265-1267, October 1994

[94] Y. Namihira, T.Kawazawa and H.Taga, "Polarization effects on BER degradation at 10 Gbit/s in an IM-DD 1520km optical amplifier system," *Electronics Letters*, Vol.29, No. 18, pp. 1654-1655, September 1993

[95] E. Iannone, F. Matera, A. Galtarossa, G. Gianello and M. Schiano, "Effect of polarization dispersion on the performance of IM-DD communication system," *Electronics Letters*, Vol. 5, No. 10, pp.1247-1249, October 1993

[96] P.R. Morkel, V. Syngal, D.J. Butler and R. Newman, "PMD-induced BER penalties in optically-amplified IM/DD lightwave systems," *Electronics Letters*, Vol. 30, No. 10, pp. 806-807, May 1994

[97] L. Pierre and J.-P. Thiery, "Comparison of resistance to polarisation mode dispersion of NRZ and phase-shaped binary transmission formats at 10 Gbit/s," *Electronics Letters*, Vol. 33, No. 5, pp. 402-403, February 1997

[98] D.Sandel, M. Yoshida-Dierolf, R. Noé, A.Schöpflin, E.Gottwald and G.Fischer, "Automatic polarisation mode dispersion compensation in 40Gbit/s optical transmission system," *Electronics Letters*, Vol. 34, No. 23, pp. 2258-2259, November 1998

[99] I. Riant, J. Gourhant and P. Sansonetti, "Polarization mode dispersion analysis in fiber chromatic dispersion compensators," *Proc. Optical Fiber Communications Conference, OFC'99,* pp. TuS2-1/269 - TuS2-3/271, SanDiego, CA, US, February 1999

[100] S. Lee, R. Khosravani, J. Peng, A.E. Willner, V.Grubsky, D.S. Starodubov and J.Feinberg, "High-birefringence nonlinearly-chirped fiber bragg grating for tunable compensation of polarization mode dispersion," *Proc. Optical Fiber Communications Conference, OFC'99*, pp. TuS3-1/272 - TuS3-3/274, SanDiego, CA, US, February 1999

[101] H. Ooi, Y. Akiyama and G. Ishikawa, "Automatic polarization-mode dispersion compensation in 40-Gbit/s transmission," *Proc. Optical Fiber Communications Conference, OFC'99*, pp. WE5-1/86 - WE5-3/88, San Diego, CA, US, February 1999

[102] S. Hinz, D. Sandel, M. Yoshida-Dierolf, S. Hinz, V. Mirvoda, A. Schöpflin and C. Glingener, "Polarisation mode dispersion compensation for 6 ps, 40 Gbit/s pulses using distributed equaliser in $LiNbO_3$," *Electronics Letters,* Vol. 35, No. 14, July

1999

[103] H. Bülow, "Operation of digital optical transmission system with minimal degradation due to polarisation mode dispersion," *Electronics Letters,* Vol. 3, No. 3, pp. 214-215, February 1995

[104] D.A. Watley, K.S. Farley, W.S. Lee and A.J. Hadjifotiou, "Impact of higher order polarisation mode dispersion on a 10Gb/s system over installed non-dispersive shifted fibre," *Proc. Optical Fiber Communications Conference, OFC'99,* pp.TuS1-1/266 - TuS1-3/268, SanDiego, CA, US, February 1999

[105] H. Bülow, "Limitation of optical first order PMD compensation," *Proc. Optical Fiber Communications Conference, OFC'99,* pp.WE1-1/74 -WE1-3/76, San Diego, CA, US, February 1999

[106] W. Weiershausen, R. Leppla, F. Küppers and H. Schöll, "Polarization mode dispersion in fibre transmission : theoretical approach, impact on sytems, and suppression of signal-degradation effects," *Proc. European Conference on Optical Communications, ECOC'99,* pp. II-130 to II-133, Nice, France, September 1999

[107] J.H. Winters, R.D. Gitlin and S. Kasturia, "Reducing the effects of transmission impairments in digital fiber optic systems," *IEEE Communications Magazine,* pp. 68-76, June 1993

[108] J.H. Winters and R.D. Gitlin, "Electrical signal processing techniques in long haul fiber-optic systems," *IEEE Transactions on Communications,* Vol. 38, No. 9, pp. 1439-1453, September 1990

[109] D.A. Watley, K.S. Farley, W.S. Lee, G. Bordogna, B.J. Shaw and A.P. Hadjifotiou, "Field evaluation of an optical PMD compensator using installed 10 Gbit/s system," *Proc. Optical Fiber Communications Conference, OFC'2000,* Paper: ThB6, Maryland, BA, US, February 2000

[110] H. Bülow, R. Ballentin, W. Baumert, G. Maisonneuve, G. Thielecke and T. Wehren, "Adaptive PMD mitigation at 10 Gbit/s using and electronic SiGe Equaliser IC," *Proc. European Conference on Optical Communications, ECOC'99,* pp. II-138 to II-139, Nice, France, September 1999

[111] G. Strang, *Linear Algebra and its Applications,* Third Edition, San Diego, Harcourt Brace Jovanovich, Publishers 1988

APPENDIX A

MATHEMATICAL PROOFS

Appendix A presents the proof of some of the mathematical identities and definitions used throughout the thesis. First, the proof is given for the frequency representation of the first and second moments of *t* [32] and then the functions defined in eq. 5.3 are derived.

A.1 FREQUENCY REPRESENTATION OF THE FIRST AND SECOND MOMENTS OF *t*

The denominator of eq. 3.7 is equal to the denominator of eq. 3.8 as a result of Parseval's theorem and therefore requires no proof. We begin by proving that the numerator in the frequency representation of the first moment of *t* given in eq. 3.8a equals the numerator of the first moment of *t* given by eq. 3.7. To that end, we will have to make use of the following property of the Fourier transform,

$$\Im\left\{(-jt)^n E_x(t)\right\} = \frac{d^n E_x(\omega)}{d\omega^n}, \tag{A.1}$$

where "n" is a positive integer. With the use of eq. A.1, the numerator of eq. 3.8a can be expressed as

$$j\int_{-\infty}^{\infty} E_x^*(\omega)\frac{dE_x(\omega)}{d\omega}d\omega = \int_{-\infty}^{\infty} E_x^*(\omega)\Im\left\{tE_x(t)\right\}d\omega \tag{A.2}$$

Using definition of Fourier transform given in eq. 3.5a, we can express eq. A.2 as

$$j\int_{-\infty}^{\infty} E_x^*(\omega)\frac{dE_x(\omega)}{d\omega}d\omega = \frac{1}{\sqrt{2\pi}}\int_{-\infty}^{\infty} E_x^*(\omega)\left[\int_{-\infty}^{\infty} tE_x(t)e^{-j\omega t}dt\right]d\omega . \tag{A.3}$$

Changing the order of integration in eq. A.3 we get,

$$j\int_{-\infty}^{\infty} E_x^*(\omega)\frac{dE_x(\omega)}{d\omega}d\omega = \int_{-\infty}^{\infty}\left[\frac{1}{\sqrt{2\pi}}\int_{-\infty}^{\infty} E_x^*(\omega)e^{-j\omega t}d\omega\right] tE_x(t)dt \,. \qquad (A.4)$$

We make use again of our Fourier transform definitions and express $E_x(t)$ as

$$E_x(t) = \Im^{-1}\{E_x(\omega)\} = \frac{1}{\sqrt{2\pi}}\int_{-\infty}^{\infty} E_x(\omega)e^{j\omega t}d\omega \qquad (A.5)$$

Taking the complex conjugate of eq. A.5 gives

$$E_x^*(t) = \frac{1}{\sqrt{2\pi}}\int_{-\infty}^{\infty} E_x^*(\omega)e^{-j\omega t}d\omega \,. \qquad (A.6)$$

Finally, substituting eq. A.6 into the expression within the brackets in eq. A.4 yields

$$j\int_{-\infty}^{\infty} E_x^*(\omega)\frac{dE_x(\omega)}{d\omega}d\omega = \int_{-\infty}^{\infty} E_x^*(t)tE_x(t)dt \,. \qquad (A.7)$$

The right hand side of eq. A.7 corresponds to the numerator for the first moment of *t* according to eq. 3.7. Now we proceed to prove the frequency domain expression for the second moment of *t*.

Let us define the intermediate variable $E_1(t)$ as

$$E_1(\omega) = \Im\{tE_x(t)\} = \frac{1}{\sqrt{2\pi}}\int_{-\infty}^{\infty} tE_x(t)e^{-j\omega t}dt \,. \qquad (A.8)$$

The term within the integral in the numerator of eq. 3.8b can be expanded with the use of eq. A.1 and eq. 3.5a as

$$\left|\frac{dE_x(\omega)}{d\omega}\right|^2 = \left|\Im\{(-jt)E_x(t)\}\right|^2$$

$$= \left[-\frac{j}{\sqrt{2\pi}}\int_{-\infty}^{\infty} tE_x(t)e^{-j\omega t}dt\right]\left[\frac{j}{\sqrt{2\pi}}\int_{-\infty}^{\infty} tE_x^*(t)e^{j\omega t}dt\right] \quad . \quad (A.9)$$

Taking the complex conjugate of eq. A.8 gives

$$E_1^*(\omega) = \frac{1}{\sqrt{2\pi}}\int_{-\infty}^{\infty} tE_x^*(t)e^{j\omega t}dt \quad . \quad (A.10)$$

Substituting eq. A.10 into eq. A.9 yields

$$\left|\frac{dE_x(\omega)}{d\omega}\right|^2 = \frac{1}{\sqrt{2\pi}}\int_{-\infty}^{\infty} tE_x(t)e^{-j\omega t}dt \cdot E_1^*(\omega) \; . \quad (A.11)$$

From eq. A.8 and eq. 3.5b we have

$$tE_x(t) = \Im^{-1}\{E_1(\omega)\} = \frac{1}{\sqrt{2\pi}}\int_{-\infty}^{\infty} E_1(\omega)e^{j\omega t}dt \quad (A.12)$$

Taking the complex conjugate of eq. A.12 gives

$$tE_x^*(t) = \frac{1}{\sqrt{2\pi}}\int_{-\infty}^{\infty} E_1^*(\omega)e^{-j\omega t}dt \; . \quad (A.13)$$

With the use of eq. A.11, the term in the numerator of eq. 3.8b can be written as

$$\int_{-\infty}^{\infty}\left|\frac{dE_x(\omega)}{d\omega}\right|^2 d\omega = \frac{1}{\sqrt{2\pi}}\int_{-\infty}^{\infty}\int_{-\infty}^{\infty} tE_x(t)e^{-j\omega t}dtE_1^*(\omega)d\omega \quad (A.14)$$

Changing the order of integration in eq. A.14 gives

$$\int_{-\infty}^{\infty}\left|\frac{dE_x(\omega)}{d\omega}\right|^2 d\omega = \int_{-\infty}^{\infty}\left[\frac{1}{\sqrt{2\pi}}\int_{-\infty}^{\infty} E_1^*(\omega)e^{-j\omega t}d\omega\right]tE_x(t)dt \; . \quad (A.15)$$

The expression within the brackets in eq. A.15 can be substituted by eq. A.13, doing this we

obtain

$$\int_{-\infty}^{\infty}\left|\frac{dE_x(\omega)}{d\omega}\right|^2 d\omega = \int_{-\infty}^{\infty} E_x^*(t)t^2E_x(t)dt \qquad (A.16)$$

The right hand side term in eq. A.16 accounts for the numerator of the second moment of *t* according to eq. 3.7.

A.2 Derivation of the Equation 5.3

In this section we derive each of the functions defined in eq. 5.3. Throughout the derivations the following identity [90] is used

$$\int_{-\infty}^{\infty} e^{-ax^2}dx = \sqrt{\frac{\pi}{a}} \quad . \qquad (A.17)$$

We begin by completing the square in the exponential term of eq. 5.3a,

$$\tau\sqrt{\frac{2}{\pi}}\int_{-\infty}^{\infty} e^{-2\tau^2\omega^2+j\omega\Gamma}d\omega = \tau\sqrt{\frac{2}{\pi}}\int_{-\infty}^{\infty} e^{\left\{-2\tau^2\left[\omega^2-\frac{j\Gamma}{2\tau^2}\omega+\left(\frac{j\Gamma}{4\tau^2}\right)^2-\left(\frac{j\Gamma}{4\tau^2}\right)^2\right]\right\}}d\omega \qquad (A.18a)$$

or

$$\tau\sqrt{\frac{2}{\pi}}\int_{-\infty}^{\infty} e^{-2\tau^2\omega^2+j\omega\Gamma}d\omega = \tau\sqrt{\frac{2}{\pi}}e^{-\frac{\Gamma^2}{8\tau^2}}\int_{-\infty}^{\infty} e^{-\frac{(4\tau^2\omega-j\Gamma)^2}{8\tau^2}}d\omega \quad . \qquad (A.18b)$$

The following change of variables will now be introduced in eq. A.18b

$$x = 4\tau^2\omega - j\Gamma \qquad (A.19a)$$

$$d\omega = \frac{dx}{4\tau^2} \qquad (A.19b)$$

$$a = \frac{1}{8\tau^2} \; . \qquad (A.19c)$$

Substituting eq. A.19 into eq. A.18 we obtain

$$\tau\sqrt{\frac{2}{\pi}}\int_{-\infty}^{\infty} e^{-2\tau^2\omega^2+j\omega\Gamma}\,d\omega = \tau\sqrt{\frac{2}{\pi}}e^{-\frac{\Gamma^2}{8\tau^2}}\int_{-\infty}^{\infty} e^{-ax^2}\,\frac{dx}{4\tau^2}$$

$$= \frac{1}{4\tau}\sqrt{\frac{2}{\pi}}e^{-\frac{\Gamma^2}{8\tau^2}}\int_{-\infty}^{\infty} e^{-ax^2}dx \quad . \qquad \text{(A.20)}$$

Finally, making use of eq. A.17 and eq. A.19c, eq. A.20 can be written as

$$F_1(\Gamma) = \tau\sqrt{\frac{2}{\pi}}\int_{-\infty}^{\infty} e^{-2\tau^2\omega^2+j\omega\Gamma}\,d\omega = e^{-\frac{\Gamma^2}{8\tau^2}} \quad . \qquad \text{(A.21)}$$

Completing the square in the exponential of eq. 5.3b yields

$$2\tau^3\sqrt{\frac{2}{\pi}}\int_{-\infty}^{\infty}\omega\, e^{-2\tau^2\omega^2+j\omega\Gamma}\,d\omega = 2\tau^3\sqrt{\frac{2}{\pi}}e^{-\frac{\Gamma^2}{8\tau^2}}\int_{-\infty}^{\infty}\omega\, e^{-\frac{(4\tau^2\omega-j\Gamma)^2}{8\tau^2}}\,d\omega$$

$$= \frac{\tau}{2}\sqrt{\frac{2}{\pi}}e^{-\frac{\Gamma^2}{8\tau^2}}\int_{-\infty}^{\infty}(4\tau^2\omega - j\Gamma + j\Gamma)e^{-\frac{(4\tau^2\omega-j\Gamma)^2}{8\tau^2}}\,d\omega \qquad \text{(A.22)}$$

Introducing the change of variable from eq. A.19 into eq. A.22 gives

$$2\tau^3\sqrt{\frac{2}{\pi}}\int_{-\infty}^{\infty}\omega\, e^{-2\tau^2\omega^2+j\omega\Gamma}\,d\omega = \frac{\tau}{2}\sqrt{\frac{2}{\pi}}e^{-\frac{\Gamma^2}{8\tau^2}}\int_{-\infty}^{\infty}(x+j\Gamma)e^{-ax^2}\,\frac{dx}{4\tau^2} \quad . \qquad \text{(A.23)}$$

Equation A.23 can be easily expanded as

$$2\tau^3\sqrt{\frac{2}{\pi}}\int_{-\infty}^{\infty}\omega\, e^{-2\tau^2\omega^2+j\omega\Gamma}\,d\omega = \frac{1}{8\tau}\sqrt{\frac{2}{\pi}}e^{-\frac{\Gamma^2}{8\tau^2}}\left[\int_{-\infty}^{\infty}xe^{-ax^2}dx + j\Gamma\int_{-\infty}^{\infty}e^{-ax^2}dx\right] \qquad \text{(A.24)}$$

The first integral in the right hand side of eq. A.24 is equal to zero and eqs. A. 17 and A.19c can be used to solve the second integral. The final result is thus given by

$$F_2(\Gamma) = 2\tau^3\sqrt{\frac{2}{\pi}}\int_{-\infty}^{\infty}\omega\, e^{-2\tau^2\omega^2+j\omega\Gamma}\,d\omega = \frac{j\Gamma}{2}e^{-\frac{\Gamma^2}{8\tau^2}} \qquad \text{(A.25)}$$

The procedure for deriving eq. 5.3c is similar and begins by completing the square in the exponential term,

$$4\tau^5\sqrt{\frac{2}{\pi}}\int_{-\infty}^{\infty}\omega^2 e^{-2\tau^2\omega^2+j\omega\Gamma}\,d\omega = 4\tau^5\sqrt{\frac{2}{\pi}}e^{-\frac{\Gamma^2}{8\tau^2}}\int_{-\infty}^{\infty}\omega^2 e^{-\frac{(4\tau^2\omega-j\Gamma)^2}{8\tau^2}}\,d\omega \quad . \quad (A.26)$$

From eq. 4.19a we have

$$\omega^2 = \left(\frac{x+j\Gamma}{4\tau^2}\right)^2 \quad (A.27)$$

Substituting eq. A.19 and A.27 into eq. A.26 yields

$$4\tau^5\sqrt{\frac{2}{\pi}}\int_{-\infty}^{\infty}\omega^2 e^{-\frac{(4\tau^2\omega-j\Gamma)}{8\tau^2}}\,d\omega = \tau^3\sqrt{\frac{2}{\pi}}e^{-\frac{\Gamma^2}{8\tau^2}}\int_{-\infty}^{\infty}\left(\frac{x+j\Gamma}{4\tau^2}\right)^2 e^{-ax^2}\,dx \,. \quad (A.28)$$

Expanding eq. A.28 gives

$$4\tau^5\sqrt{\frac{2}{\pi}}\int_{-\infty}^{\infty}\omega^2 e^{-2\tau^2\omega^2+j\omega\Gamma}\,d\omega = \tau^3\sqrt{\frac{2}{\pi}}e^{-\frac{\Gamma^2}{8\tau^2}}\left[\frac{1}{16\tau^4}\left(\int_{-\infty}^{\infty}x^2e^{-ax^2}\,dx-\Gamma^2\int_{-\infty}^{\infty}e^{-ax^2}\,dx\right)\right]. \quad (A.29)$$

The second integral in the right hand side of eq. A.29 can be solved by using eq. A.17 and the following identity [90] is used to solve the first integral,

$$\int_{-\infty}^{\infty}x^2e^{-ax^2}\,dx = \frac{1}{2a}\sqrt{\frac{\pi}{a}} \quad . \quad (A.30)$$

The final result is expressed as

$$F_3(\Gamma) = 4\tau^5\sqrt{\frac{2}{\pi}}\int_{-\infty}^{\infty}\omega^2 e^{-2\tau^2\omega^2+j\omega\Gamma}\,d\omega = e^{-\frac{\Gamma^2}{8\tau^2}}\left(\tau^2-\frac{\Gamma^2}{4}\right). \quad (A.31)$$

APPENDIX B
ANALYTIC EQUATIONS

This appendix presents the analytical expressions derived from each one of the procedures outlined in chapter five. Notice that, although all the eqs. presented are expressed as products of matrices, each eq. represents a scalar complex number in general.

The functions encountered as part of each eq. i.e., F_1, F_2 and F_3 are derived in appendix A and defined in eq. 5.3. Likewise the rest of the variables used are given by eqs. 5.7 and 5.8. It must be pointed out here, that no approximations were made during the derivation of any of the eqs. contained in this appendix, the results obtained from their use should therefore be exact.

$$P_{\text{ij}} = W_{1234}\begin{bmatrix} 1 & F_1(k-1) & F_1(k+m)e^{-2j\theta} & F_1(k+n)e^{-2j\theta} \\ F_1(1-k) & 1 & F_1(1+m)e^{-2j\theta} & F_1(1+n)e^{-2j\theta} \\ F_1(-m-k)e^{2j\theta} & F_1(-m-1)e^{2j\theta} & 1 & F_1(-m+n) \\ F_1(-n-k)e^{2j\theta} & F_1(-n-1)e^{2j\theta} & F_1(-n+m) & 1 \end{bmatrix} W^{+}_{1234} \quad \text{B.1a)}$$

$$P_{\text{ij}} = W_{1234}\begin{bmatrix} F_1(k-n) & F_1(k-m) & F_1(k+1)e^{-2j\theta} & F_1(2k)e^{-2j\theta} \\ F_1(1-n) & F_1(1-m) & F_1(2l)e^{-2j\theta} & F_1(1+k)e^{-2j\theta} \\ F_1(-m-n)e^{2j\theta} & F_1(-2m)e^{2j\theta} & F_1(1-m) & F_1(k-m) \\ F_1(-2n)e^{2jj} & F_1(-n-m)e^{2j\theta} & F_1(1-n) & F_1(k-n) \end{bmatrix} W^{+}_{5678} \quad \text{B.1b)}$$

$$P_{\text{ij}} = W_{5678}\begin{bmatrix} F_1(n-k) & F_1(n-1) & F_1(m+n)e^{-2j\theta} & F_1(2n)e^{-2j\theta} \\ F_1(m-k) & F_1(m-1) & F_1(2m)e^{-2j\theta} & F_1(m+n)e^{-2jj} \\ F_1(-1-k)e^{2j\theta} & F_1(-2l)e^{2j\theta} & F_1(m-1) & F_1(n-1) \\ F_1(-2k)e^{2j\theta} & F_1(-1-k)e^{2j\theta} & F_1(m-k) & F_1(n-k) \end{bmatrix} W^{+}_{1234} \quad \text{B.1c)}$$

$$P_{\text{ij}} = W_{5678}\begin{bmatrix} 1 & F_1(n-m) & F_1(n+1)e^{-2jj} & F_1(n+k)e^{-2jj} \\ F_1(m-n) & 1 & F_1(m+1)e^{-2jj} & F_1(m+k)e^{-2jj} \\ F_1(-n-1)e^{2j\theta} & F_1(-m-1)e^{2j\theta} & 1 & F_1(k-1) \\ F_1(-n-k)e^{2j\theta} & F_1(-m-k)e^{2j\theta} & F_1(1-k) & 1 \end{bmatrix} W^{+}_{5678} \quad \text{B.1d)}$$

$$P_{\text{ij}} = W_{1256}\begin{bmatrix} 1 & F_1(k-1) & F_1(k-n)e^{2j\theta} & F_1(k-m)e^{2jj} \\ F_1(1-k) & 1 & F_1(1-n)e^{2j\theta} & F_1(1-m)e^{2j\theta} \\ F_1(n-k)e^{-2j\theta} & F_1(n-1)e^{-2j\theta} & 1 & F_1(n-m) \\ F_1(m-k)e^{-2j\theta} & F_1(m-1)e^{-2j\theta} & F_1(m-n) & 1 \end{bmatrix} W^{+}_{1256} \quad \text{(B.2a)}$$

$$P_{\text{ij}} = W_{1256}\begin{bmatrix} F_1(m+k) & F_1(n+k) & F_1(1+k)e^{2j\theta} & F_1(2k)e^{2j\theta} \\ F_1(m+1) & F_1(n+1) & F_1(2l)e^{2j\theta} & F_1(k+1)e^{2j\theta} \\ F_1(m+n)e^{-2jj} & F_1(2n)e^{-2j\theta} & F_1(1+n) & F_1(k+n) \\ F_1(2m)e^{-2j\theta} & F_1(n+m)e^{-2jj} & F_1(1+m) & F_1(k+m) \end{bmatrix} W^{+}_{3478} \quad \text{(B.2b)}$$

$$P_{4,} = W_{3478}\begin{bmatrix} F_1(-k-m) & F_1(-1-m) & F_1(-m-n)e^{2jy,} & F_1(-2m)e^{2jy,} \\ F_1(-k-n) & F_1(-1-n) & F_1(-2n)e^{2jy,} & F_1(-m-n)e^{2jy,} \\ F_1(-k-1)e^{-2jy,} & F_1(-2l)e^{-2jy,} & F_1(-n-1) & F_1(-m-1) \\ F_1(-2k)e^{-2jy,} & F_1(-k-1)e^{-2jy,} & F_1(-n-k) & F_1(-m-k) \end{bmatrix} W^{+}_{1256} \quad \text{(B.2c)}$$

$$P_{4,} = W_{3478}\begin{bmatrix} 1 & F_1(n-m) & F_1(1-m)e^{2jy,} & F_1(k-m)e^{2jy,} \\ F_1(m-n) & 1 & F_1(1-n)e^{2jy,} & F_1(k-n)e^{2jy,} \\ F_1(m-1)e^{-2jy,} & F_1(n-1)e^{-2jy,} & 1 & F_1(k-1) \\ F_1(m-k)e^{-2jy,} & F_1(n-k)e^{-2jy,} & F_1(1-k) & 1 \end{bmatrix} W^{+}_{3478} \quad \text{(B.2d)}$$

$$T_{4,} = jW_{1234}\begin{bmatrix} jk & jkF_1(k-1)-F_2(k-1) \\ jlF_1(l-k)-F_2(l-k) & jl \\ -e^{2jy,}\left[jmF_1(-m-k)+F_2(-m-k)\right] & -e^{2jy,}\left[jmF_1(-m-1)+F_2(-m-1)\right] \\ -e^{2jy,}\left[jnF_1(-n-k)+F_2(-n-k)\right] & -e^{2jy,}\left[jnF_1(-n-1)+F_2(-n-1)\right] \end{bmatrix}$$

$$\begin{bmatrix} e^{-2jy,}\left[jkF_1(k+m)-F_2(k+m)\right] & e^{-2jy,}\left[jkF_1(k+n)-F_2(k+n)\right] \\ e^{-2jy,}\left[jlF_1(l+m)-F_2(l+m)\right] & e^{-2jy,}\left[jlF_1(l+n)-F_2(l+n)\right] \\ -jm & -jmF_1(-m+n)-F_2(-m+n) \\ -jnF_1(-n+m)-F_2(-n+m) & -jn \end{bmatrix} W^{+}_{1234} \quad \text{(B.3a)}$$

$$T_{4,} = jW_{5678}\begin{bmatrix} jnF_1(n-k)-F_2(n-k) & jnF_1(n-1)-F_2(n-1) \\ jmF_1(m-k)-F_2(m-k) & jmF_1(m-1)-F_2(m-1) \\ -e^{2jy,}\left[jlF_1(-1-k)+F_2(-1-k)\right] & -e^{2jy,}\left[jlF_1(-2l)+F_2(-2l)\right] \\ -e^{2jy,}\left[jkF_1(-2k)+F_2(-2k)\right] & -e^{2jy,}\left[jkF_1(-k-1)+F_2(-k-1)\right] \end{bmatrix}$$

$$\begin{bmatrix} e^{-2jy,}\left[jnF_1(n+m)-F_2(n+m)\right] & e^{-2jy,}\left[jnF_1(2n)-F_2(2n)\right] \\ e^{-2jy,}\left[jmF_1(2m)-F_2(2m)\right] & e^{-2jy,}\left[jmF_1(m+n)-F_2(m+n)\right] \\ -jlF_1(-1+m)-F_2(-1+m) & -jlF_1(-1+n)-F_2(-1+n) \\ -jkF_1(-k+m)-F_2(-k+m) & -jkF_1(-k+n)-F_2(-k+n) \end{bmatrix} W^{+}_{1234} \quad \text{(B.3b)}$$

$$T_{\psi_{\cdot}} = jW_{1234}\begin{bmatrix} jkF_1(k-n)-F_2(k-n) & jkF_1(k-m)-F_2(k-m) \\ jlF_1(1-n)-F_2(1-n) & jlF_1(1-m)-F_2(1-m) \\ -e^{2j\psi_{\cdot}}\left[jmF_1(-m-n)-F_2(-m-n)\right] & -e^{2j\psi_{\cdot}}\left[jmF_1(-2m)+F_2(-2m)\right] \\ -e^{2j\psi_{\cdot}}\left[jnF_1(-2n)-F_2(-2n)\right] & -e^{2j\psi_{\cdot}}\left[jnF_1(-n-m)+F_2(-n-m)\right] \end{bmatrix}$$

$$\begin{bmatrix} e^{-2j\psi_{\cdot}}\left[jkF_1(k+1)-F_2(k+1)\right] & e^{-2j\psi_{\cdot}}\left[jkF_1(2k)-F_2(2k)\right] \\ e^{-2j\psi_{\cdot}}\left[jlF_1(2l)-F_2(2l)\right] & e^{-2j\psi_{\cdot}}\left[jlF_1(l+k)-F_2(l+k)\right] \\ -jmF_1(-m+1)-F_2(-m+1) & -jmF_1(-m+k)-F_2(-m+k) \\ -jnF_1(-n+1)-F_2(-n+1) & -jnF_1(-n+k)-F_2(-n+k) \end{bmatrix} W^{+}_{5678} \qquad 3c)$$

$$T_{\psi_{\cdot}} = jW_{5678}\begin{bmatrix} jn & jnF_1(n-m)-F_2(n-m) \\ jmF_1(m-n)-F_2(m-n) & jm \\ -e^{2j\psi_{\cdot}}\left[jlF_1(-1-n)+F_2(-1-n)\right] & -e^{2j\psi_{\cdot}}\left[jlF_1(-1-m)+F_2(-1-m)\right] \\ -e^{2j\psi_{\cdot}}\left[jkF_1(-k-n)+F_2(-k-n)\right] & -e^{2j\psi_{\cdot}}\left[jkF_1(-k-m)+F_2(-k-m)\right] \end{bmatrix}$$

$$\begin{bmatrix} e^{-2j\psi_{\cdot}}\left[jnF_1(n+1)-F_2(n+1)\right] & e^{-2j\psi_{\cdot}}\left[jnF_1(n+k)-F_2(n+k)\right] \\ e^{-2j\psi_{\cdot}}\left[jmF_1(m+1)-F_2(m+1)\right] & e^{-2j\psi_{\cdot}}\left[jmF_1(m+k)-F_2(m+k)\right] \\ -jl & -jlF_1(-1+k)-F_2(-1+k) \\ -jkF_1(-k+1)-F_2(-k+1) & -jk \end{bmatrix} W^{+}_{5678} \qquad .3d)$$

$$T_{\psi_{\cdot}} = jW_{1256}\begin{bmatrix} jk & jkF_1(k-1)-F_2(k-1) \\ jlF_1(1-k)-F_2(1-k) & jl \\ e^{-2j\psi_{\cdot}}\left[jnF_1(n-k)-F_2(n-k)\right] & e^{-2j\psi_{\cdot}}\left[jnF_1(n-1)-F_2(n-1)\right] \\ e^{-2j\psi_{\cdot}}\left[jmF_1(m-k)-F_2(m-k)\right] & e^{-2j\psi_{\cdot}}\left[jmF_1(m-1)-F_2(m-1)\right] \end{bmatrix}$$

$$\begin{bmatrix} e^{2j\psi_{\cdot}}\left[jkF_1(k-n)-F_2(k-n)\right] & e^{2j\psi_{\cdot}}\left[jkF_1(k-m)-F_2(k-m)\right] \\ e^{2j\psi_{\cdot}}\left[jlF_1(1-n)-F_2(1-n)\right] & e^{2j\psi_{\cdot}}\left[jlF_1(1-m)-F_2(1-m)\right] \\ jn & jnF_1(n-m)-F_2(n-m) \\ jmF_1(m-n)-F_2(m-n) & jm \end{bmatrix} W^{+}_{1256} \qquad (B.4a)$$

$$T_{i,} = jW_{3478}\begin{bmatrix} -jmF_1(-m-k)-F_2(-m-k) & -jmF_1(-m-1)-F_2(-m-1) \\ -nF_1(-n-k)-F_2(-n-k) & -jnF_1(-n-1)-F_2(-n-1) \\ -e^{-2j\gamma_3}\left[jlF_1(-1-k)+F_2(-1-k)\right] & -e^{-2j\gamma_3}\left[jlF_1(-2l)+F_2(-2l)\right] \\ -e^{-2j\gamma_3}\left[jkF_1(-2k)+F_2(-2k)\right] & -e^{-2j\gamma_3}\left[jkF_1(-1-k)+F_2(-1-k)\right] \end{bmatrix}$$

$$\begin{bmatrix} -e^{2j\gamma_3}\left[jmF_1(-m-n)+F_2(-m-n)\right] & -e^{2j\gamma_3}\left[jmF_1(-2m)+F_2(-2m)\right] \\ -e^{2j\gamma_3}\left[jnF_1(-2n)+F_2(-2n)\right] & -e^{2j\gamma_3}\left[jnF_1(-n-m)+F_2(-n-m)\right] \\ -jlF_1(-1-n)+F_2(-1-n) & -jlF_1(-1-m)+F_2(-1-m) \\ -jkF_1(-k-n)+F_2(-k-n) & -jkF_1(-k-m)+F_2(-k-m) \end{bmatrix} W^{+}_{1256} \quad \text{(B.4b)}$$

$$T_{i,} = jW_{1256}\begin{bmatrix} jkF_1(k+m)-F_2(k+m) & jkF_1(k+n)-F_2(k+n) \\ jlF_1(l+m)-F_2(l+m) & jlF_1(l+n)-F_2(l+n) \\ e^{-2j\gamma_3}\left[jnF_1(n+m)-F_2(n+m)\right] & e^{-2j\gamma_3}\left[jnF_1(2n)-F_2(2n)\right] \\ e^{-2j\gamma_3}\left[jmF_1(2m)-F_2(2m)\right] & e^{-2j\gamma_3}\left[jmF_1(m+n)-F_2(m+n)\right] \end{bmatrix}$$

$$\begin{bmatrix} e^{2j\gamma_3}\left[jkF_1(k+1)-F_2(k+1)\right] & e^{2j\gamma_3}\left[jkF_1(2k)-F_2(2k)\right] \\ e^{2j\gamma_3}\left[jlF_1(2l)-F_2(2l)\right] & e^{2j\gamma_3}\left[jlF_1(1+k)-F_2(1+k)\right] \\ jnF_1(n+1)-F_2(n+1) & jnF_1(n+k)-F_2(n+k) \\ jmF_1(m+1)-F_2(m+1) & jmF_1(m+k)-F_2(m+k) \end{bmatrix} W^{+}_{3478} \quad \text{(B.4c)}$$

$$T_{i,} = jW_{3478}\begin{bmatrix} -jm & -jmF_1(n-m)-F_2(n-m) \\ -jnF_1(m-n)-F_2(m-n) & -jn \\ -e^{-2j\gamma_3}\left[jlF_1(m-1)+F_2(m-1)\right] & -e^{-2j\gamma_3}\left[jlF_1(n-1)+F_2(n-1)\right] \\ -e^{-2j\gamma_3}\left[jkF_1(m-k)+F_2(m-k)\right] & -e^{-2j\gamma_3}\left[jkF_1(n-k)+F_2(n-k)\right] \end{bmatrix}$$

$$\begin{bmatrix} -e^{2j\gamma_3}\left[jmF_1(1-m)+F_2(1-m)\right] & -e^{2j\gamma_3}\left[jmF_1(k-m)+F_2(k-m)\right] \\ -e^{2j\gamma_3}\left[jnF_1(1-n)+F_2(1-n)\right] & -e^{2j\gamma_3}\left[jnF_1(k-n)+F_2(k-n)\right] \\ -jl & -jlF_1(k-1)-F_2(k-1) \\ -jkF_1(1-k)-F_2(1-k) & -jk \end{bmatrix} W^{+}_{3478} \quad \text{(B.4d)}$$

$$S_{\phi_1} = w_{1234}\begin{bmatrix} k^2+\tau^2 & lkF_1(k-l)+j(l-k)F_2(k-l)+F_3(k-l) \\ klF_1(l-k)+j(k-l)F_2(l-k)+F_3(l-k) & l^2+\tau^2 \\ \left[-kmF_1(-m-k)+j(m+k)F_2(-m-k)+F_3(-m-k)\right]e^{2j\pi_1} & \left[-lmF_1(-m-l)+j(l+m)F_2(-m-l)+F_3(-m-l)\right]e^{2j\pi_1} \\ \left[-knF_1(-n-k)+j(n+k)F_2(-n-k)+F_3(-n-k)\right]e^{2j\pi_1} & \left[-lnF_1(-n-l)+j(l+n)F_2(-n-l)+F_3(-n-l)\right]e^{2j\pi_1} \end{bmatrix}$$

$$\begin{bmatrix} \left[-mkF_1(m+k)-j(m+k)F_2(m+k)+F_3(m+k)\right]e^{-2j\pi_1} & \left[-nkF_1(n+k)-j(k+n)F_2(n+k)+F_3(n+k)\right]e^{-2j\pi_1} \\ \left[-mlF_1(m+l)-j(m+l)F_2(m+l)+F_3(m+l)\right]e^{-2j\pi_1} & \left[-nlF_1(n+l)-j(n+l)F_2(n+l)+F_3(n+l)\right]e^{-2j\pi_1} \\ m^2+\tau^2 & nmF_1(n-m)+j(m-n)F_2(n-m)+F_3(n-m) \\ mnF_1(m-n)+j(n-m)F_2(m-n)+F_3(m-n) & n^2+\tau^2 \end{bmatrix} w^*_{1234} \qquad \text{(B.5a)}$$

$$S_{\phi_2} = w_{1234}\begin{bmatrix} nkF_1(-n+k)+j(n-k)F_2(-n+k)+F_3(-n+k) & mkF_1(-m+k)+j(m-k)F_2(-m+k)+F_3(-m+k) \\ nlF_1(-n+l)+j(n-l)F_2(-n+l)+F_3(-n+l) & mlF_1(-m+l)+j(m-l)F_2(-m+l)+F_3(-m+l) \\ \left[-mnF_1(-n-m)+j(n+m)F_2(-n-m)+F_3(-n-m)\right]e^{2j\pi_2} & \left[-m^2F_1(-2m)+2jmF_2(-2m)+F_3(-2m)\right]e^{2j\pi_2} \\ \left[-n^2F_1(-2n)+2jnF_2(-2n)+F_3(-2n)\right]e^{2j\pi_2} & \left[-mnF_1(-m-n)+j(m+n)F_2(-m-n)+F_3(-m-n)\right]e^{2j\pi_2} \end{bmatrix}$$

$$\begin{bmatrix} \left[-lkF_1(l+k)-j(k+l)F_2(l+k)+F_3(l+k)\right]e^{-2j\pi_2} & \left[-k^2F_1(2k)-2jkF_2(2k)+F_3(2k)\right]e^{-2j\pi_2} \\ \left[-l^2F_1(2l)-2jlF_2(2l)+F_3(2l)\right]e^{-2j\pi_2} & \left[-klF_1(k+l)-j(l+k)F_2(k+l)+F_3(k+l)\right]e^{-2j\pi_2} \\ lmF_1(l-m)+j(m-l)F_2(l-m)+F_3(l-m) & kmF_1(k-m)+j(m-k)F_2(k-m)+F_3(k-m) \\ lnF_1(l-n)+j(n-l)F_2(l-n)+F_3(l-n) & knF_1(k-n)+j(n-k)F_2(k-n)+F_3(k-n) \end{bmatrix} w^*_{5678} \qquad \text{(B.5b)}$$

$$S_{\varphi_1} = w_{5678}\begin{bmatrix} knF_1(-k+n)+j(k-n)F_2(-k+n)+F_3(-k+n) & nlF_1(n-l)+j(l-n)F_2(n-l)+F_3(n-l) \\ kmF_1(-k+m)+j(k-m)F_2(-k+m)+F_3(-k+m) & mlF_1(m-l)+j(l-m)F_2(m-l)+F_3(m-l) \\ \left[-klF_1(-k-l)+j(k+l)F_2(-k-l)+F_3(-k-l)\right]e^{2j\pi_1} & \left[-l^2F_1(-2l)+2jlF_2(-2l)+F_3(-2l)\right]e^{2j\pi_1} \\ \left[-k^2F_1(-2k)+2jkF_2(-2k)+F_3(-2k)\right]e^{2j\pi_1} & \left[-lkF_1(-l-k)+j(l+k)F_2(-l-k)+F_3(-l-k)\right]e^{2j\pi_1} \end{bmatrix}$$

$$\begin{bmatrix} \left[-mnF_1(m+n)-j(m+n)F_2(m+n)+F_3(m+n)\right]e^{-2j\pi_1} & \left[-n^2F_1(2n)-2njF_2(2n)+F_3(2n)\right]e^{-2j\pi_1} \\ \left[-m^2F_1(2m)-2jmF_2(2m)+F_3(2m)\right]e^{-2j\pi_1} & \left[-mnF_1(m+n)-j(m+n)F_2(m+n)+F_3(m+n)\right]e^{-2j\pi_1} \\ lmF_1(m-l)+j(l-m)F_2(m-l)+F_3(m-l) & lnF_1(n-l)+j(l-n)F_2(n-l)+F_3(n-l) \\ mkF_1(m-k)+j(k-m)F_2(m-k)+F_3(m-k) & knF_1(n-k)+j(k-n)F_2(n-k)+F_3(n-k) \end{bmatrix} w_{1234} \quad \text{(B.5c)}$$

$$S_{\varphi_2} = w_{5678}\begin{bmatrix} n^2+\tau^2 & mnF_1(-m+n)+j(m-n)F_2(-m+n)+F_3(-m+n) \\ mnF_1(m-n)+j(n-m)F_2(m-n)+F_3(m-n) & m^2+\tau^2 \\ \left[-nlF_1(-n-l)+j(n+l)F_2(-n-l)+F_3(-n-l)\right]e^{2j\pi_2} & \left[-mlF_1(-m-l)+j(m+l)F_2(-m-l)+F_3(-m-l)\right]e^{2j\pi_2} \\ \left[-knF_1(-n-k)+j(n+k)F_2(-n-k)+F_3(-n-k)\right]e^{2j\pi_2} & \left[-mkF_1(-m-k)+j(m+k)F_2(-m-k)+F_3(-m-k)\right]e^{2j\pi_2} \end{bmatrix}$$

$$\begin{bmatrix} \left[-lnF_1(n+l)-j(n+l)F_2(n+l)+F_3(n+l)\right]e^{-2j\pi_2} & \left[-knF_1(k+n)-j(n+k)F_2(k+n)+F_3(k+n)\right]e^{-2j\pi_2} \\ \left[-lmF_1(l+m)-j(l+m)F_2(l+m)+F_3(l+m)\right]e^{-2j\pi_2} & \left[-kmF_1(k+m)-j(k+m)F_2(k+m)+F_3(k+m)\right]e^{-2j\pi_2} \\ l^2+\tau^2 & klF_1(k-l)+j(l-k)F_2(k-l)+F_3(k-l) \\ lkF_1(l-k)+j(k-l)F_2(l-k)+F_3(l-k) & k^2+\tau^2 \end{bmatrix} w'_{5678} \quad \text{(B.5d)}$$

$$S_{x_1} = w_{1256}\begin{bmatrix} k^2+\tau^2 & klF_1(k-l)+j(l-k)F_2(k-l)+F_3(k-l) \\ lkF_1(l-k)+j(k-l)F_2(l-k)+F_3(l-k) & l^2+\tau^2 \\ \left[nkF_1(n-k)+j(k-n)F_2(n-k)+F_3(n-k)\right]e^{-2j\eta_1} & \left[nlF_1(n-l)+j(l-n)F_2(n-l)+F_3(n-l)\right]e^{-2j\eta_1} \\ \left[mkF_1(m-k)+j(k-m)F_2(m-k)+F_3(m-k)\right]e^{-2j\eta_1} & \left[mlF_1(m-l)+j(l-m)F_2(m-l)+F_3(m-l)\right]e^{-2j\eta_1} \end{bmatrix}$$

$$\begin{bmatrix} \left[nkF_1(k-n)+j(n-k)F_2(k-n)+F_3(k-n)\right]e^{2j\eta_1} & \left[mkF_1(k-m)+j(m-k)F_2(k-m)+F_3(k-m)\right]e^{2j\eta_1} \\ \left[nlF_1(l-n)+j(n-l)F_2(l-n)+F_3(l-n)\right]e^{2j\eta_1} & \left[mlF_1(l-m)+j(m-l)F_2(l-m)+F_3(l-m)\right]e^{2j\eta_1} \\ n^2+\tau^2 & mnF_1(n-m)+j(m-n)F_2(n-m)+F_3(n-m) \\ nmF_1(m-n)+j(n-m)F_2(m-n)+F_3(m-n) & m^2+\tau^2 \end{bmatrix} w^*_{1256} \qquad \text{(B.6a)}$$

$$S_{x_1} = w_{3478}\begin{bmatrix} -mkF_1(-m-k)+j(m+k)F_2(-m-k)+F_3(-m-k) & -mlF_1(-m-l)+j(m+l)F_2(-m-l)+F_3(-m-l) \\ -nkF_1(-n-k)+j(n+k)F_2(-n-k)+F_3(-n-k) & -nlF_1(-n-l)+j(n+l)F_2(-n-l)+F_3(-n-l) \\ \left[-lkF_1(-l-k)+j(l+k)F_2(-l-k)+F_3(-l-k)\right]e^{-2j\eta_1} & \left[-l^2F_1(-2l)+2jlF_2(-2l)+F_3(-2l)\right]e^{-2j\eta_1} \\ \left[-k^2F_1(-2k)+2jkF_2(-2k)+F_3(-2k)\right]e^{-2j\eta_1} & \left[-klF_1(-k-l)+j(k+l)F_2(-k-l)+F_3(-k-l)\right]e^{-2j\eta_1} \end{bmatrix}$$

$$\begin{bmatrix} \left[-mnF_1(-m-n)+j(m+n)F_2(-m-n)+F_3(-m-n)\right]e^{2j\eta_1} & \left[-m^2F_1(-2m)+2jmF_2(-2m)+F_3(-2m)\right]e^{2j\eta_1} \\ \left[-n^2F_1(-2n)+j2nF_2(-2n)+F_3(-2n)\right]e^{2j\eta_1} & \left[-mnF_1(-n-m)+j(m+n)F_2(-n-m)+F_3(-n-m)\right]e^{2j\eta_1} \\ -lnF_1(-l-n)+j(l+n)F_2(-l-n)+F_3(-l-n) & -mlF_1(-m-l)+j(m+l)F_2(-m-l)+F_3(-m-l) \\ -knF_1(-k-n)+j(k+n)F_2(-k-n)+F_3(-k-n) & -kmF_1(-m-k)+j(m+k)F_2(-m-k)+F_3(-m-k) \end{bmatrix} w^*_{1256} \qquad \text{(B.6b)}$$

$$S_{x_1} = w_{1256}\begin{bmatrix} -mkF_1(m+k) - j(m+k)F_2(m+k) + F_3(m+k) & -knF_1(k+n) - j(k+n)F_2(k+n) + F_3(k+n) \\ -mlF_1(m+l) - j(m+l)F_2(m+l) + F_3(m+l) & -lnF_1(l+n) - j(l+n)F_2(l+n) + F_3(l+n) \\ \left[-mnF_1(m+n) - j(m+n)F_2(m+n) + F_3(m+n)\right]e^{-2j\pi_3} & \left[-n^2F_1(2n) - 2jnF_2(2n) + F_3(2n)\right]e^{-2j\pi_3} \\ \left[-m^2F_1(2m) - 2jmF_2(2m) + F_3(2m)\right]e^{-2j\pi_3} & \left[-mnF_1(m+n) - j(m+n)F_2(m+n) + F_3(m+n)\right]e^{-2j\pi_3} \end{bmatrix}$$

$$\begin{bmatrix} \left[-klF_1(k+l) - j(k+l)F_2(k+l) + F_3(k+l)\right]e^{2j\pi_3} & \left[-k^2F_1(2k) - 2jkF_2(2k) + F_3(2k)\right]e^{2j\pi_3} \\ \left[-l^2F_1(2l) - 2jlF_2(2l) + F_3(2l)\right]e^{2j\pi_3} & \left[-klF_1(k+l) - j(k+l)F_2(k+l) + F_3(k+l)\right]e^{2j\pi_3} \\ -lnF_1(l+n) - j(l+n)F_2(l+n) + F_3(l+n) & -knF_1(k+n) - j(k+n)F_2(k+n) + F_3(k+n) \\ -mlF_1(m+l) - j(m+l)F_2(m+l) + F_3(m+l) & -mkF_1(m+k) - j(m+k)F_2(m+k) + F_3(m+k) \end{bmatrix} w'_{3478} \qquad \text{(B.6c)}$$

$$S_{x_4} = w_{3478}\begin{bmatrix} m^2+\tau^2 & mnF_1(n-m) + j(m-n)F_2(n-m) + F_3(n-m) \\ mnF_1(m-n) + j(n-m)F_2(m-n) + F_3(m-n) & n^2+\tau^2 \\ \left[lmF_1(m-l) + j(l-m)F_2(m-l) + F_3(m-l)\right]e^{-2j\pi_3} & \left[nlF_1(n-l) + j(l-n)F_2(n-l) + F_3(n-l)\right]e^{-2j\pi_3} \\ \left[kmF_1(m-k) + j(k-m)F_2(m-k) + F_3(m-k)\right]e^{-2j\pi_3} & \left[knF_1(n-k) + j(k-n)F_2(n-k) + F_3(n-k)\right]e^{-2j\pi_3} \end{bmatrix}$$

$$\begin{bmatrix} \left[mlF_1(l-m) + j(m-l)F_2(l-m) + F_3(l-m)\right]e^{2j\pi_3} & \left[kmF_1(k-m) + j(k-m)F_2(k-m) + F_3(k-m)\right]e^{2j\pi_3} \\ \left[nlF_1(l-n) + j(n-l)F_2(l-n) + F_3(l-n)\right]e^{2j\pi_3} & \left[knF_1(k-n) + j(n-k)F_2(k-n) + F_3(k-n)\right]e^{2j\pi_3} \\ l^2+\tau^2 & klF_1(k-l) + j(l-k)F_2(k-l) + F_3(k-l) \\ klF_1(l-k) + j(k-l)F_2(l-k) + F_3(l-k) & k^2+\tau^2 \end{bmatrix} w'_{3478} \qquad \text{(B.6d)}$$

APPENDIX C

ZERO PMD

Appendix C presents the trivial case in which the optical fiber under study does not have any PMD. The rms-pulsewidth of a signal at the output of such a fiber is shown to be the same as the rms-pulsewidth at the input irrespective of the choice of the input and output states of polarization. In order to prove that, the analytic three segment model from fig. 5.1 is used.

C.1 THE ZERO PMD CASE

To begin the rms-pulsewidth analysis we assign the following values to the fusion angles of our three segment model in fig. 5.1, $\theta_1 = \pi/2$, $\theta_2 = 0^o$. The DGDs introduced by each section will be, $\tau_1 = \tau_2 = \Delta$ and $\tau_3 = 0$. Under these conditions the DGD of the first segment will be cancelled by the second segment and $\mathbf{T_L}(\omega)$ in eq. 5.6b will become frequency independent. Substituting these values into eq. 5.6b yields

$$\mathbf{T_L} = \begin{bmatrix} 0 & -1 \\ 1 & 0 \end{bmatrix} = \mathbf{R}(\pi/2)\,, \tag{C.1}$$

where $\mathbf{R}(\pi/2)$ represents a 90^o rotation matrix [111]. Substituting $\mathbf{T_L}$ into eq. 3.3 and using eq. 5.2, the electric field and its derivative at the output of PA in fig. 5.1 will be given by

$$E_x(\omega) = \boldsymbol{\chi}^+ \mathbf{T_L} \boldsymbol{\varphi} E_{in}(\omega) = \boldsymbol{\chi}^+ \mathbf{R}(\pi/2) \boldsymbol{\varphi} E_{in}(\omega) \tag{C.2a}$$

$$\frac{dE_x(\omega)}{d\omega} = -\boldsymbol{\chi}^+ \mathbf{R}(\pi/2) \boldsymbol{\varphi} 2\tau^2 \sqrt{\tau}\left(\frac{2}{\pi}\right)^{1/4} e^{-(\tau\omega)^2}\,. \tag{C.2b}$$

Thus, the power of the output signal will be

$$P_x = \int_{-\infty}^{\infty} |E_x(\omega)|^2 d\omega = \left|\boldsymbol{\chi}^+ \mathbf{R}(\pi/2) \boldsymbol{\varphi}\right|^2 \tag{C.3}$$

From equations 3.8, 5.3 and C.2, the first two moments of *t* can be expressed as

$$\langle t \rangle = \frac{j\left|\boldsymbol{\chi}^+ \mathbf{R}(\pi/2) \boldsymbol{\varphi}\right|^2}{P_x} F_2(0) = jF_2(0) = 0 \tag{C.4a}$$

$$\langle t^2 \rangle = \frac{\left|\boldsymbol{\chi}^+ \mathbf{R}(\pi/2) \boldsymbol{\varphi}\right|^2}{P_x} F_3(0)\tau^2 = \tau^2 \tag{C.4b}$$

Therefore, eq. 3.6 gives an output rms-pulsewidth, $\sigma_x = \tau$, for all χ and ϕ. As a result, we can conclude that, when the PMD of an optical fiber has been completely cancelled out, the rms-pulsewidth of the output signal will always equal that of the input signal, regardless of the choice of the transmission and reception states of polarization.

APPENDIX D

WAVELENGTH DIVISION MULTIPLEXING (WDM)

Here we consider a Wavelength Division Multiplexing (WDM) system consisting of five channels, the central channel having a carrier wavelength, λ_3, of 1.55 μm and with 100 Ghz of spacing between each channel. For every channel the pulse-shape used for a bit "1" is given by eq. 5.1 with τ = 25ps. The system under study is similar to that from fig. 3.1 and is depicted in fig. D.1. The carrier angular frequencies and wavelengths of every channel are summarized in table D.1.

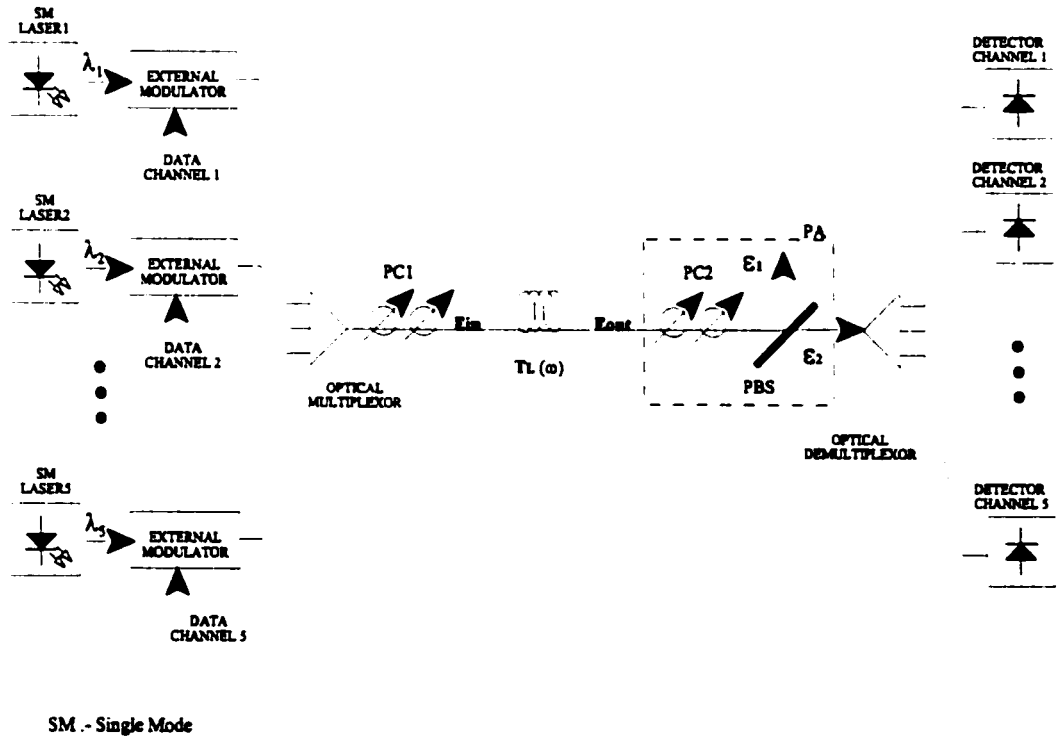

SM .- Single Mode

Fig. D.1 Five channel WDM system.

All the channels in the WDM array are transmitted in the same state of polarization (determined by PC1) and received in the same state of polarization (determined by PC2).

Channel No.	λ (μm)	ω (rad/ps)
1	1.5516	1214.0
2	1.5508	1214.6
3	1.5500	1215.3
4	1.5492	1215.9
5	1.5484	1216.5

Table D.1 Carrier frequencies and wavelengths.

The fiber simulated had a mean DGD of 30 ps and consisted of 500 segments of Hi-Bi fiber. The input and output states of polarization used were selected through the searching procedure depicted in fig. 3.4. The figure of merit used was empirically fixed at 10^{-14}. The carrier frequency used for the optimization of the input and output states of polarization was that of the central channel, i.e., $\omega_0 = \omega_3 = 1215.3$ rad/ps ($\lambda_3 = 1.55$ μm).

Finally, the same bit sequence was used as the transmitted data for every channel, namely "0001101100100111", which contains all the possible three bit sequences. Fig. D.2 shows the input data sequence for every channel. Fig. D.3 shows the normalized received bit sequence in every channel and table D.2 summarizes the results.

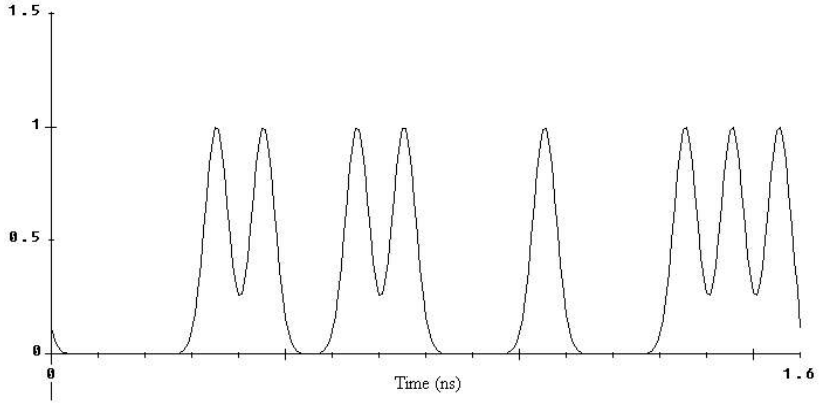

Fig. D.2 Transmitted bit sequence for every channel.

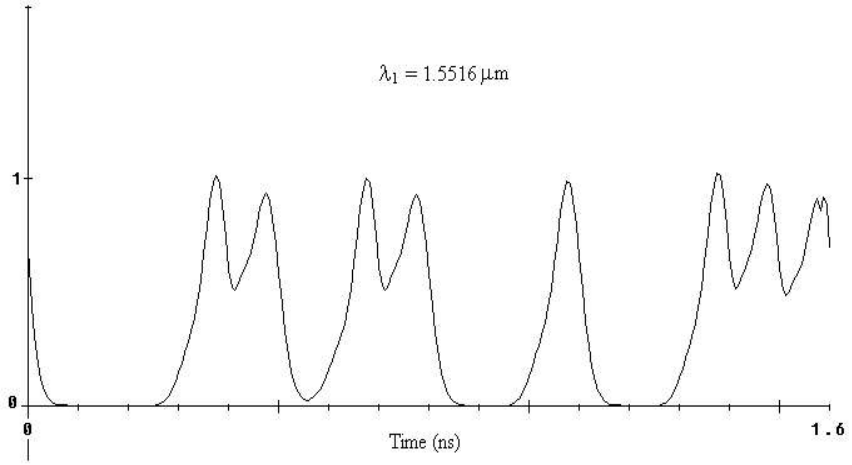

Fig. D.3a Output bit sequence for the first channel.

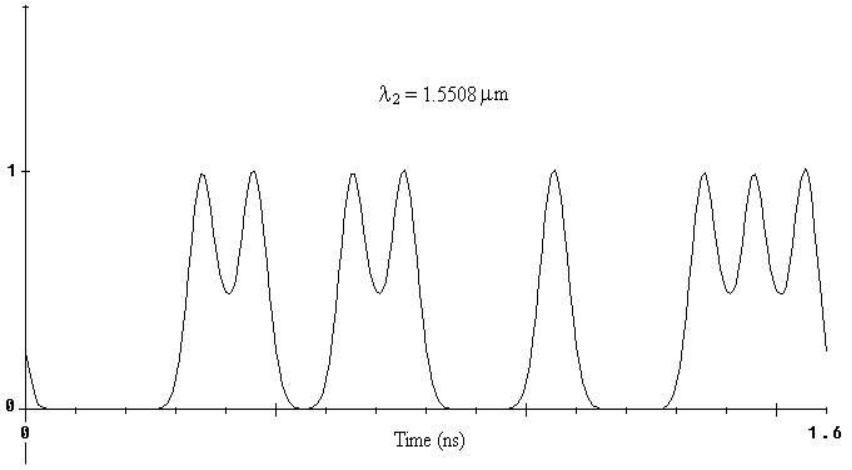

Fig. D.3b Output bit sequence for the second channel.

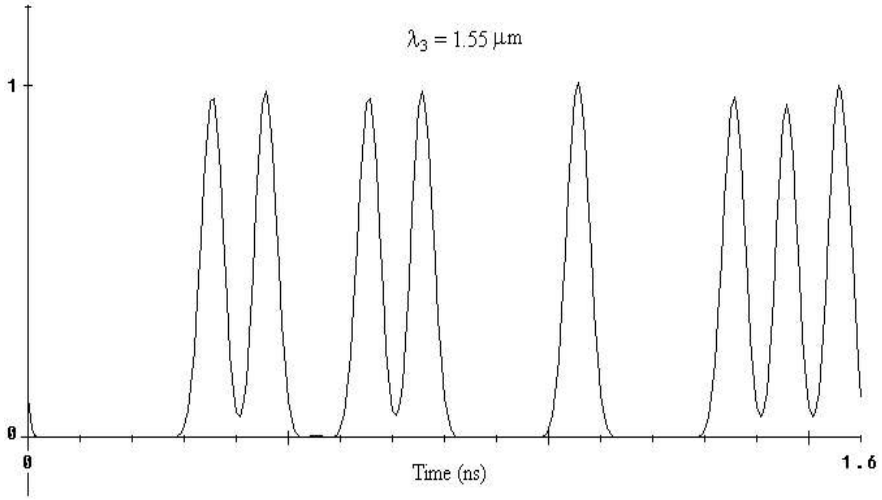

Fig. D.3c Output bit sequence for the third channel.

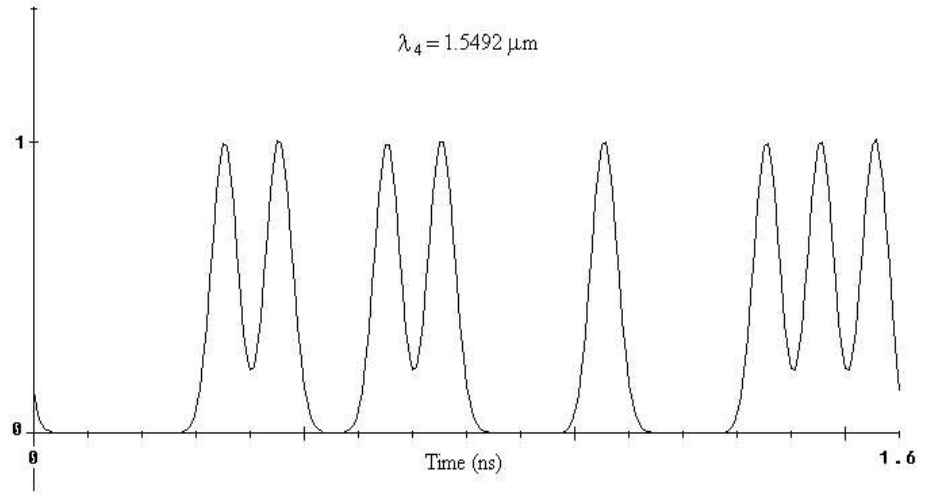

Fig. D.3d Output bit sequence for the fourth channel.

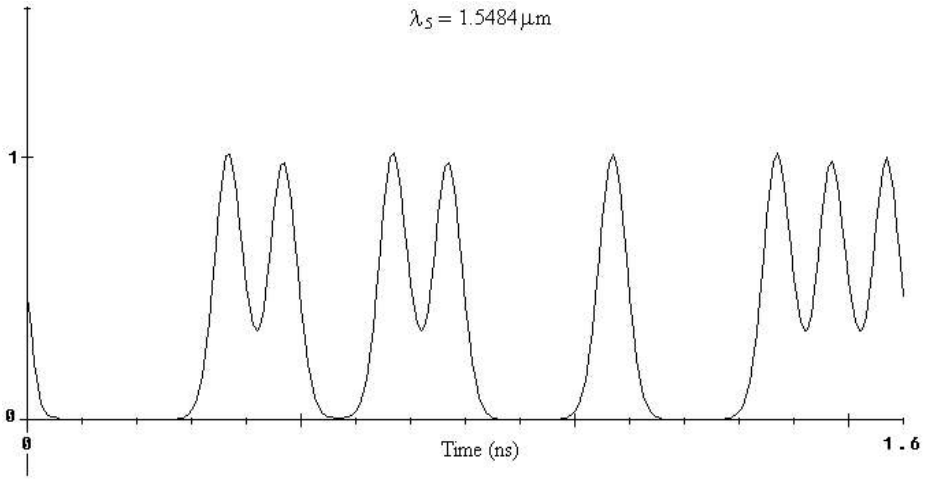

Fig. D.3e Output bit sequence for the fifth channel.

<DGD>=30ps	Channel 1	Channel 2	Channel 3	Channel 4	Channel 5
σ_x (ps)	32.6	28.4	18.4	23.4	27.2
P_x (%)	21.3	25.9	8.4	46.4	60.8

Table D.2 Fractional power and rms-pulsewidths for the five channel system of fig. D.1

Although a pulsewidth reduction has been achieved in the central channel, the neighbouring channels show diversified results. Whilst the fourth channel benefits from the optimization of the central channel by exhibiting pulsewidth compression and high power

levels, the first channel undergoes pulsewidth broadening and exhibits low power levels. Thus, in this case, the optimization of the input and output states of polarization would have to be done individually for each channel in order to avoid an irregular performance of the system.

The bandwidth of the input and output states of polarization[1] calculated by mean of the algorithm in fig, 3.4 depends in general, on the DGD of the fiber under study and the rms-pulsewidth of the input signal. The calculation of such a bandwidth through simulation is necessary before definitive conclusions can be drawn regarding the feasibility of optimizing the input and output states of polarization only for the central channel of a WDM system. The calculation of such a bandwidth is however, not a simple one due to the statistical nature of PMD and the high dimensionality of the searching procedure. A large population of fibers would have to be simulated and for each fiber a large number of initial search points would need to be used to ensure the convergence to an absolute minimum value of the rms-pulsewidth. This should be a topic of further research.

[1] The bandwidth over which the optimized states of polarization remain nearly constant.

APPENDIX E
SOURCE CODE

Appendix E presents the Matlab source code used for the implementation of the searching procedure depicted in fig. 3.4, which deals with the simultaneous optimization of both, input and output states of polarization, in order to minimize the rms-pulsewidth of the output signal. The more general case of an optical fiber made up by an arbitrary number of segments of Hi-Bi fiber is solved by the program Nsegm.m which also calculates the broadband frequency response for a WDM system with an arbitrary number of channels. The frequency response is saved in ascii format in two files, one named "`NUMO_500S.txt`" which contains the normalized magnitude of the frequency response and the other, "`NUMQ_500S.txt`" which contains phase response. The input signal is given by eq. 5.1. The rms-pulsewidth of the input signal and the value for the figure of merit used during the optimization procedure can be changed by changing the values of the variables "tau" and "fom" respectively.

The search in itself is carried out by a subroutine called "OptimizeN.m", which in turns makes use of additional subroutines called "phifuncN.m" and "chifuncN.m". The purpose of these two subroutines is the calculation of $\mathbf{S}_{\omega}$, $\mathbf{T}_{\omega}$, $\mathbf{P}_{\omega}$ and $\mathbf{S}_{\omega'}$, $\mathbf{T}_{\omega'}$, $\mathbf{P}_{\omega'}$ respectively through numerical approximation. An additional functions such as, "Fw.m" and "canonize.m"required for numerical interpolation and state of polarization representation are also included. Finally the "TimeDomain.m" program permits the visualization in time domain of the signal at the output of the fiber.

NSegm (avgdgd,k,cw,BW,deltaw,Nch)

```
% NSegm Numerically searches for the narrowing polarization states of
% an optical fiber made up by "k" sections of Hi-Bi fiber.
% It also calculates the broadband frequency response of the fiber
% for a WDM system in which the input and output states of polarization
% used were optimized for the central channel.

% avgdgd -> The Average Differential group delay, DGD, of the fiber in
%           picoseconds, ps.
% k      -> The number of fiber segments (wave plates) that make up the
%           fiber.
% cw     -> The carrier wavelength of the signal in micrometers.
% BW     -> The Bandwidth of the channel centered @ cw and signal %
%         centered @ 0 Hz, (it must be given in GHz).
% deltaw -> The Frequency resolution, in GHz.
% Nch    -> Number of WDM channels on one side of wc, the WDM array is
%           assumed to be symmetric.
%
% Mauricio Yañez, last revision : May'20th of 2000


close all;
warning off;
echo off;
avgdgd = avgdgd*1e-12;cw = cw*1e-6;
wc = 2*pi*3e8/cw;
BW = BW*1e9;
deltaw = deltaw*1e9;
n = ceil (BW/deltaw);      % "n" is the number of samples in frequency.
deltaw = 2*pi*(BW/n);      % deltaw takes its final value.
W = -2*pi*BW/2 : deltaw : 2*pi*BW/2-deltaw;
tau = 25*1e-12;
Ein = sqrt(tau)*(2/pi)^0.25*exp(-(tau*W).^2);
MaxDelay = avgdgd*sqrt(3)/sqrt(8*k/(3*pi));
delay = MaxDelay*rand(1,k);
theta = 2*pi*rand(1,k);
TL = zeros (2,2,n);TL1 = zeros (2,2,n);TL2 = zeros (2,2,n);
%%%%%%%%%%%%%%%%%%%%%%%%% Building the Fiber within BW %%%%%%%%%%%%%%%%%%
f = 1;
for w = wc-(2*pi*BW/2) : deltaw : wc+(2*pi*BW/2)-deltaw,
  T = eye (2);T1 = eye (2);
  for i=1:k,
      T = T*[cos(theta(i)) sin(theta(i)); -sin(theta(i))
      cos(theta(i))]*[exp(j*w*delay(i)/2) 0; 0 exp(-j*w*delay(i)/2)];
      T1 = T1*[cos(theta(i)) sin(theta(i)); -sin(theta(i))
      cos(theta(i))]*[exp(j*(w+deltaw/2)*delay(i)/2) 0; 0
      exp(-j*(w+deltaw/2)*delay(i)/2)];
  end
  TL  (:,:,f) = T1;           % TL will now fall in the middle point of
  TL1 (:,:,f) = T*Ein(f);     % the differential.
  TL2 (:,:,f) = T'*Ein(f);
  f = f + 1;
end
W = W + deltaw/2;
Ein = sqrt(tau)*(2/pi)^0.25*exp(-(tau*W).^2); % Ein will now fall in
[FX,FY,TL1] = gradient (TL1,deltaw);          % the middle point
[FX,FY,TL2] = gradient (TL2,deltaw);          % of the differential.
%%%%%%%%%%%%%%%%%%%%%%%%% The Search begins now %%%%%%%%%%%%%%%%%%%%%%%%%
```

```
nn = 60; fom = 1e-14;
Ptmp = zeros (1,nn); Sigmtmp = zeros (1,nn);
rnd_alpha1 = 2*pi*rand(1,nn); rnd_gamma1 = 2*pi*rand(1,nn);
rnd_alpha2 = 2*pi*rand(1,nn); rnd_gamma2 = 2*pi*rand(1,nn);
Phi_guess(:,1:nn) = [exp(-
j*rnd_gamma1).*cos(rnd_alpha1);exp(j*rnd_gamma1).*sin(rnd_alpha1)];
Chi_guess(:,1:nn) = [exp(-
j*rnd_gamma2).*cos(rnd_alpha2);exp(j*rnd_gamma2).*sin(rnd_alpha2)];
h = waitbar (0,'Searching,...');
for i=1:nn,
    [Phi_guess(:,i),Chi_guess(:,i),Sigmtmp(i),Ptmp(i)] = optimizeN ...
    (TL,TL1,TL2,Ein,W,Phi_guess(:,i),Chi_guess(:,i),tau,fom);
    waitbar (i/nn);
end
close (h);
minSgm = min (Sigmtmp);
ix = pdesubix (Sigmtmp,minSgm);
P = Ptmp (ix);
Phi1 = Phi_guess (:,ix); Chi1 = Chi_guess (:,ix);
[dummy,dummy,gamma,A] = canonize (Chi1);
Chi2 = [exp(-j*gamma)*A(2);-exp(j*gamma)*A(1)];
[dummy,dummy,gamma,A] = canonize (Phi1);
Phi2 = [exp(-j*gamma)*A(2);-exp(j*gamma)*A(1)];
TimeDomain (TL,Ein,deltaw,Phi1,Chi1,2e-12,25+minSgm,P);
%%%%%%%%%%%%%%%%%%%% Recreating HF for minSgm & Saving Data %%%%%%%%%%%
n1 = 64;              %n1 is the number of samples taken from H(w)
                      %within channel spacing.
n2 = 2*(Nch+1)*n1;    %n2 is the total number of samples taken from
                      %H(w).
BW = 100e9;           %BW is the channel interspacing now !
BW = (Nch+1)*BW;  deltaw = 2*pi*(2*BW)/n2;
TL = zeros (2,2,n2);HL = zeros (1,n2);
f = 1;                %Re-building the Fiber for the WDM System.
h = waitbar (0,'Re-building the fiber for the WDM System');
for w = wc-(2*pi*BW) : deltaw : wc+(2*pi*BW)-deltaw,
   T = eye (2);
   for i=1:k,
      T = T*[cos(theta(i)) sin(theta(i)); -sin(theta(i))
      cos(theta(i))]*[exp(j*w*delay(i)/2) 0; 0 exp(-j*w*delay(i)/2)];
   end
   TL (:,:,f) = T;
   f = f + 1;
   waitbar ((f-1)/length(wc-(2*pi*BW) : deltaw : wc+(2*pi*BW)-deltaw));
end
close (h);
Chia = Chi1(1);Chib = Chi1(2);Phia = Phi1(1);Phib = Phi1(2);
HL (:) = (TL(1,1,:)*conj(Chia)+TL(2,1,:)*conj(Chib))*Phia + ...
         (TL(1,2,:)*conj(Chia)+TL(2,2,:)*conj(Chib))*Phib;
Lambda = 2*pi*3e8./(wc-(2*pi*BW) : deltaw : wc+(2*pi*BW)-deltaw);
Lambda = Lambda*1e9;                        % Lambda is now in nm.
Phase = 180*unwrap(angle(HL))/pi;
HF = abs(HL); HF = HF/max(HF);
NUMO = [Lambda',HF'];
NUMQ = [Lambda',Phase'];
save NUMO_500S.txt NUMO -ascii
save NUMQ_500S.txt NUMQ -ascii
save Nsegm
```

```
function [PhiFinal,ChiFinal,Sigmeff,PFinal] = OptimizeN
(TL,TL1,TL2,Ein,W,Phi,Chi,tau,fom)
% NEWoptimizeN Finds the Input & Output States of Polarization for
% pulse narrowing on a fiber made up by multiple segments.
% This function numerically optimizes the launching and reception
% angles for a fiber optic with PMD. Optimization criteria is the
% maximum pulse narrowing.

deltaw = W(2) - W(1);
PhiFinal = Phi; ChiFinal = Chi; Sigmout_min = tau*1e12;
Sphi = zeros (2,2);Pphi = zeros (2,2);Tphi = zeros (2,2);
Schi = zeros (2,2);Pchi = zeros (2,2);Tchi = zeros (2,2);
[Tphi,Sphi,Pphi] = phifuncN (TL,TL1,TL2,Ein,W,Phi);
P =  abs(Chi'*Pphi*Chi); PFinal = P;
TT = Chi'*Tphi*Chi;
T2 = Chi'*Sphi*Chi;
MPhi = Sphi/P - Pphi*Chi*Chi'*Sphi/P^2 - 2*Tphi*Chi*Chi'*Tphi/P^2 +...
       2*TT*Pphi*Chi*Chi'*Tphi/P^3;
[CHI,etha] = eig(MPhi);
Sigmout1 = 1e12*sqrt(abs((CHI(:,1)'*Sphi*CHI(:,1))/...
           (CHI(:,1)'*Pphi*CHI(:,1))-((CHI(:,1)'*Tphi*CHI(:,1))/...
           (CHI(:,1)'*Pphi*CHI(:,1)))^2));
Sigmout2 = 1e12*sqrt(abs((CHI(:,2)'*Sphi*CHI(:,2))/...
           (CHI(:,2)'*Pphi*CHI(:,2)) -((CHI(:,2)'*Tphi*CHI(:,2))/...
           (CHI(:,2)'*Pphi*CHI(:,2)))^2));
[Kchi,Chi,gamma2,A2,Sigmout] = decide (Sigmout1,Sigmout2,CHI);
FOM = 1 ; iter = 1; SigmOut = zeros (1,500); PP = zeros (1,500);
while FOM > fom,
   [Tchi,Schi,Pchi] = chifuncN (TL,TL1,TL2,Ein,W,Chi);
   P =  abs(Phi'*Pchi*Phi);
   if Sigmout < Sigmout_min
      Sigmout_min = Sigmout;PFinal = P;
      PhiFinal = Phi; ChiFinal = Chi;
   end
   TT = Phi'*Tchi*Phi;
   T2 = Phi'*Schi*Phi;
   MChi = Schi/P - Pchi*Phi*Phi'*Schi/P^2 - ...
         2*Tchi*Phi*Phi'*Tchi/P^2 + 2*TT*Pchi*Phi*Phi'*Tchi/P^3;
   [PHI,lambda] = eig(MChi);
   Phiold = Phi;
   Sigmout1 = 1e12*sqrt(abs((PHI(:,1)'*Schi*PHI(:,1))/...
              (PHI(:,1)'*Pchi*PHI(:,1)) - ((PHI(:,1)'*Tchi*PHI(:,1))/...
              (PHI(:,1)'*Pchi*PHI(:,1)))^2));
   Sigmout2 = 1e12*sqrt(abs((PHI(:,2)'*Schi*PHI(:,2))/...
              (PHI(:,2)'*Pchi*PHI(:,2)) - ((PHI(:,2)'*Tchi*PHI(:,2))/...
              (PHI(:,2)'*Pchi*PHI(:,2)))^2));
   [Kphi,Phi,gamma1,A1,Sigmout] = decide (Sigmout1,Sigmout2,PHI);
   FOM1 = abs(Phiold'*Phi);
   [Tphi,Sphi,Pphi] = phifuncN (TL,TL1,TL2,Ein,W,Phi);
   P =  abs(Chi'*Pphi*Chi);
   if Sigmout < Sigmout_min
      Sigmout_min = Sigmout;PFinal = P;
      PhiFinal = Phi; ChiFinal = Chi;
   end
   TT = Chi'*Tphi*Chi;
   T2 = Chi'*Sphi*Chi;
   MPhi = Sphi/P - Pphi*Chi*Chi'*Sphi/P^2 - ...
          2*Tphi*Chi*Chi'*Tphi/P^2 + 2*TT*Pphi*Chi*Chi'*Tphi/P^3;
```

```
   [CHI,etha] = eig(MPhi);
   Chiold = Chi;
   Sigmout1 = 1e12*sqrt(abs((CHI(:,1)'*Sphi*CHI(:,1))/...
             (CHI(:,1)'*Pphi*CHI(:,1)) - ((CHI(:,1)'*Tphi*CHI(:,1))/...
             (CHI(:,1)'*Pphi*CHI(:,1)))^2));
   Sigmout2 = 1e12*sqrt(abs((CHI(:,2)'*Sphi*CHI(:,2))/...
             (CHI(:,2)'*Pphi*CHI(:,2)) -((CHI(:,2)'*Tphi*CHI(:,2))/...
             (CHI(:,2)'*Pphi*CHI(:,2)))^2));
   [Kchi,Chi,gamma2,A2,Sigmout] = decide (Sigmout1,Sigmout2,CHI);
   SigmOut(iter) = Sigmout; PP(iter) = P;
   iter = iter+1;
   FOM2 = abs(Chiold'*Chi);
   FOM = abs(1-FOM1) + abs (1-FOM2);
   TimeDomain (TL,Ein,deltaw,Phi,Chi,2e-12,Sigmout,P);
end
P =  abs(Chi'*Pphi*Chi);
if Sigmout < Sigmout_min
   Sigmout_min = Sigmout;PFinal = P;
   PhiFinal = Phi; ChiFinal = Chi;
end
Sigmeff = Sigmout_min - tau*1e12;
SigmOut = SigmOut (1:iter-1);
PP = PP (1:iter-1);
```

```
function [Tphi,Sphi,Pphi] = phifuncN (TL,TL1,TL2,Ein,W,Phi);
% This function calculates Tphi,Sphi,Pphi by using numerical
% approximations


N = length (W); Ktmp = zeros (1,N);
Phi1 = Phi (1); Phi2 = Phi(2);
%%%%%%%%%%%%%%%%%%%%%%%%%%%%%%%%%%%% Calculating Pphi %%%%%%%%%%%%%%%%%%%%
Ktmp (:) = (TL(1,1,:)*Phi1+TL(1,2,:)*Phi2).*...
           (conj(TL(1,1,:))*conj(Phi1)+conj(TL(1,2,:))*conj(Phi2));
           Ktmp = Ktmp.*(Ein.^2);
X11 = quad8 ('Fw',W(1),W(N),[],[],Ktmp,W);
Ktmp (:) = (TL(1,1,:)*Phi1+TL(1,2,:)*Phi2).*...
           (conj(TL(2,1,:))*conj(Phi1)+conj(TL(2,2,:))*conj(Phi2));
           Ktmp = Ktmp.*(Ein.^2);
X12 = quad8 ('Fw',W(1),W(N),[],[],Ktmp,W);
Ktmp (:) = (TL(2,1,:)*Phi1+TL(2,2,:)*Phi2).*...
           (conj(TL(1,1,:))*conj(Phi1)+conj(TL(1,2,:))*conj(Phi2));
           Ktmp = Ktmp.*(Ein.^2);
X21 = quad8 ('Fw',W(1),W(N),[],[],Ktmp,W);
Ktmp (:) = (TL(2,1,:)*Phi1+TL(2,2,:)*Phi2).*...
           (conj(TL(2,1,:))*conj(Phi1)+conj(TL(2,2,:))*conj(Phi2));
           Ktmp = Ktmp.*(Ein.^2);
X22 = quad8 ('Fw',W(1),W(N),[],[],Ktmp,W);
Pphi = [X11  X12; X21 X22];
%%%%%%%%%%%%%%%%%%%%%%%%%%%%%%%%%%%% Calculating Tphi %%%%%%%%%%%%%%%%%%%%
Ktmp (:) = j*(TL1(1,1,:)*Phi1+TL1(1,2,:)*Phi2).*...
           (conj(TL(1,1,:))*conj(Phi1)+conj(TL(1,2,:))*conj(Phi2));
           Ktmp = Ktmp.*Ein;
X11 = quad8 ('Fw',W(1),W(N),[],[],Ktmp,W);
Ktmp (:) = j*(TL1(1,1,:)*Phi1+TL1(1,2,:)*Phi2).*...
           (conj(TL(2,1,:))*conj(Phi1)+conj(TL(2,2,:))*conj(Phi2));
           Ktmp = Ktmp.*Ein;
X12 = quad8 ('Fw',W(1),W(N),[],[],Ktmp,W);
Ktmp (:) = j*(TL1(2,1,:)*Phi1+TL1(2,2,:)*Phi2).*...
           (conj(TL(1,1,:))*conj(Phi1)+conj(TL(1,2,:))*conj(Phi2));
           Ktmp = Ktmp.*Ein;
X21 = quad8 ('Fw',W(1),W(N),[],[],Ktmp,W);
Ktmp (:) = j*(TL1(2,1,:)*Phi1+TL1(2,2,:)*Phi2).*...
           (conj(TL(2,1,:))*conj(Phi1)+conj(TL(2,2,:))*conj(Phi2));
           Ktmp = Ktmp.*Ein;
X22 = quad8 ('Fw',W(1),W(N),[],[],Ktmp,W);
Tphi = [X11  X12; X21 X22];
%%%%%%%%%%%%%%%%%%%%%%%%%%%%%%%%%%%% Calculating Sphi %%%%%%%%%%%%%%%%%%%%
Ktmp (:) = (TL1(1,1,:)*Phi1+TL1(1,2,:)*Phi2).*...
           (TL2(1,1,:)*conj(Phi1)+TL2(2,1,:)*conj(Phi2));
X11 = quad8 ('Fw',W(1),W(N),[],[],Ktmp,W);
Ktmp (:) = (TL1(1,1,:)*Phi1+TL1(1,2,:)*Phi2).*...
           (TL2(1,2,:)*conj(Phi1)+TL2(2,2,:)*conj(Phi2));
X12 = quad8 ('Fw',W(1),W(N),[],[],Ktmp,W);
Ktmp (:) = (TL1(2,1,:)*Phi1+TL1(2,2,:)*Phi2).*...
           (TL2(1,1,:)*conj(Phi1)+TL2(2,1,:)*conj(Phi2));
X21 = quad8 ('Fw',W(1),W(N),[],[],Ktmp,W);
Ktmp (:) = (TL1(2,1,:)*Phi1+TL1(2,2,:)*Phi2).*...
           (TL2(1,2,:)*conj(Phi1)+TL2(2,2,:)*conj(Phi2));
X22 = quad8 ('Fw',W(1),W(N),[],[],Ktmp,W);
Sphi = [X11  X12; X21 X22];
```

```
function [Tchi,Schi,Pchi] = chifuncN (TL,TL1,TL2,Ein,W,Chi);
% This function calculates Tchi,Schi,Pchi by using numerical
% approximations


N = length (W); Ktmp = zeros (1,N);
Chi1 = Chi (1); Chi2 = Chi(2);
%%%%%%%%%%%%%%%%%%%%%%%%%%%%%%%%%% Calculating Pchi %%%%%%%%%%%%%%%%%%%%
Ktmp (:) = (conj(TL(1,1,:))*Chi1+conj(TL(2,1,:))*Chi2).*...
           (TL(1,1,:)*conj(Chi1)+TL(2,1,:)*conj(Chi2));
           Ktmp = Ktmp.*(Ein.^2);
X11 = quad8 ('Fw',W(1),W(N),[],[],Ktmp,W);
Ktmp (:) = (conj(TL(1,1,:))*Chi1+conj(TL(2,1,:))*Chi2).*...
           (TL(1,2,:)*conj(Chi1)+TL(2,2,:)*conj(Chi2));
           Ktmp = Ktmp.*(Ein.^2);
X12 = quad8 ('Fw',W(1),W(N),[],[],Ktmp,W);
Ktmp (:) = (conj(TL(1,2,:))*Chi1+conj(TL(2,2,:))*Chi2).*...
           (TL(1,1,:)*conj(Chi1)+TL(2,1,:)*conj(Chi2));
           Ktmp = Ktmp.*(Ein.^2);
X21 = quad8 ('Fw',W(1),W(N),[],[],Ktmp,W);
Ktmp (:) = (conj(TL(1,2,:))*Chi1+conj(TL(2,2,:))*Chi2).*...
           (TL(1,2,:)*conj(Chi1)+TL(2,2,:)*conj(Chi2));
           Ktmp = Ktmp.*(Ein.^2);
X22 = quad8 ('Fw',W(1),W(N),[],[],Ktmp,W);
Pchi = [X11  X12; X21 X22];
%%%%%%%%%%%%%%%%%%%%%%%%%%%%%%%%%% Calculating Tchi %%%%%%%%%%%%%%%%%%%%
Ktmp (:) = j*(TL1(1,1,:)*conj(Chi1)+TL1(2,1,:)*conj(Chi2)).*...
           (conj(TL(1,1,:))*Chi1+conj(TL(2,1,:))*Chi2);
           Ktmp = Ktmp.*Ein;
X11 = quad8 ('Fw',W(1),W(N),[],[],Ktmp,W);
Ktmp (:) = j*(TL1(1,2,:)*conj(Chi1)+TL1(2,2,:)*conj(Chi2)).*...
           (conj(TL(1,1,:))*Chi1+conj(TL(2,1,:))*Chi2);
           Ktmp = Ktmp.*Ein;
X12 = quad8 ('Fw',W(1),W(N),[],[],Ktmp,W);
Ktmp (:) = j*(TL1(1,1,:)*conj(Chi1)+TL1(2,1,:)*conj(Chi2)).*...
           (conj(TL(1,2,:))*Chi1+conj(TL(2,2,:))*Chi2);
           Ktmp = Ktmp.*Ein;
X21 = quad8 ('Fw',W(1),W(N),[],[],Ktmp,W);
Ktmp (:) = j*(TL1(1,2,:)*conj(Chi1)+TL1(2,2,:)*conj(Chi2)).*...
           (conj(TL(1,2,:))*Chi1+conj(TL(2,2,:))*Chi2);
           Ktmp = Ktmp.*Ein;
X22 = quad8 ('Fw',W(1),W(N),[],[],Ktmp,W);
Tchi = [X11  X12; X21 X22];
%%%%%%%%%%%%%%%%%%%%%%%%%%%%%%%%%% Calculating Schi %%%%%%%%%%%%%%%%%%%%
Ktmp (:) = (TL1(1,1,:)*conj(Chi1)+TL1(2,1,:)*conj(Chi2)).*...
           (TL2(1,1,:)*Chi1+TL2(1,2,:)*Chi2);
X11 = quad8 ('Fw',W(1),W(N),[],[],Ktmp,W);
Ktmp (:) = (TL1(1,2,:)*conj(Chi1)+TL1(2,2,:)*conj(Chi2)).*...
           (TL2(1,1,:)*Chi1+TL2(1,2,:)*Chi2);
X12 = quad8 ('Fw',W(1),W(N),[],[],Ktmp,W);
Ktmp (:) = (TL1(1,1,:)*conj(Chi1)+TL1(2,1,:)*conj(Chi2)).*...
           (TL2(2,1,:)*Chi1+TL2(2,2,:)*Chi2);
X21 = quad8 ('Fw',W(1),W(N),[],[],Ktmp,W);
Ktmp (:) = (TL1(1,2,:)*conj(Chi1)+TL1(2,2,:)*conj(Chi2)).*...
           (TL2(2,1,:)*Chi1+TL2(2,2,:)*Chi2);
X22 = quad8 ('Fw',W(1),W(N),[],[],Ktmp,W);
Schi = [X11  X12; X21 X22];
```

```
function  abc = Fw (w,Ktmp,W)
% This function is required for numerical integration.

abc = interp1 (W,Ktmp,w,'*cubic');



function [K,x,gamma,A] = canonize (v)
%CANONIZE Returns a complex vector on its canonical form.

A = zeros(1,2);
n1 = v(1); n2 = v(2);
A(1) = abs(n1); A(2) = abs(n2);
theta1 = angle (n1); theta2 = angle (n2);
gamma = (theta2-theta1)/2;
K = exp(j*(theta2+theta1)/2);
x = [A(1)*exp(-j*gamma) ; A(2)*exp(j*gamma)];
```

```
function  dummy1 = TimeDomain (TL,Ein,deltaw,Phi,Chi,deltaT,sigmeff,p)
% TimeDomain Shows the Time Domain for of a signal, Ein, being
% transmitted through an Optical fiber with a transfer Matrix TL,
% launched and received at states of polarization Phi & Chi.
% Ein and TL are in the frequency Domain !
% deltaT and deltaw are the time and frequency resolutions.


n = length(Ein);p = p*100;
Phi1 = Phi(1);Phi2 = Phi(2);
Chi1 = Chi(1);Chi2 = Chi(2);
Eout = zeros (1,n);
Eout (:) = ((TL(1,1,:)*conj(Chi1)+TL(2,1,:)*conj(Chi2))*Phi1 + ...
           (TL(1,2,:)*conj(Chi1)+TL(2,2,:)*conj(Chi2))*Phi2); Eout =
Eout.*Ein;
ts = 2*pi/deltaw;       %Be aware that Ein is in the frequency domain !
n1 = ts/deltaT;         %n1 is the required number of samples for a
                        %resolution of deltaT.
n2 = length(Eout);      %n2 is the actual numbre of samples taken from
                        %Eout(w)
if n1>=n2               %The IFFT will use "n" points to meet deltaT.
   n = 2^(max(nextpow2(n1),nextpow2(n2)));
end
deltaT = ts/n;          %deltaT is now the real IFFT time resolution.
nn = floor (100e-12/deltaT); %Readjusting the time vector to 200 ps.
t = -deltaT*(nn):deltaT:deltaT*(nn-1); t = t*1e12;
if mod (n2,2) == 0, i = n2/2;
else i = (n2+1)/2-1; end
Ein = fftshift(Ein);
ein (1:i) = Ein(1:i);
ein (i+1:i+n-n2) = zeros (1,n-n2);
ein (i+n-n2+1:n) = Ein(i+1:n2);
ein = ifftshift(ifft (ein));  %ein is now in the time domain !
Pin = abs(ein.*conj(ein));
K = max(Pin);
Pin = Pin/K;
ix = pdesubix (Pin,1);        %Relocating Pin around its center.
Pin = Pin (ix-nn:ix+nn-1);
Eout = fftshift(Eout);
eout (1:i) = Eout(1:i);
eout (i+1:i+n-n2) = zeros (1,n-n2);
eout (i+n-n2+1:n) = Eout(i+1:n2);
eout = ifftshift(ifft (eout));   %eout is now in the time domain !
Pout = abs(eout.*conj(eout));
Pout = Pout/max(Pout);
ix = pdesubix (Pout,max(Pout));  %Relocating Pout around its center.
Pout = Pout (ix-nn:ix+nn-1);
figure (100)
plot (t,Pin,'w'); xlabel ('Time (ps)'); ylabel ('Normalized Optical
Power');
hold;
plot (t,Pout,'w:','Erasemode','xor');
if sigmeff ~= 0
   title (strcat('\sigma_{x} = ',num2str(sigmeff,4),'ps, P_{x} = ',
   num2str(p,4),'%'));
else
   title (strcat('P_{x} = ',num2str(p,4),'%'));
end
```

```
legend ('Input Pulse','Output Pulse');
drawnow
hold;
```